AD

USAAMRDL TECHNICAL REPORT 71-38

GROUND TEST EVALUATION OF THE SIKORSKY ACTIVE TRANSMISSION ISOLATION SYSTEM

By

Paul W. von Hardenberg
Paul B. Saltanis

September 1971

EUSTIS DIRECTORATE
U. S. ARMY AIR MOBILITY RESEARCH AND DEVELOPMENT LABORATORY
FORT EUSTIS, VIRGINIA

CONTRACT DAAJ02-69-C-0101
SIKORSKY AIRCRAFT
DIVISION OF UNITED AIRCRAFT CORPORATION
STRATFORD, CONNECTICUT

R

125

DISCLAIMERS

The findings in this report are not to be construed as an official Department of the Army position unless so designated by other authorized documents.

When Government drawings, specifications, or other data are used for any purpose other than in connection with a definitely related Government procurement operation, the United States Government thereby incurs no responsibility nor any obligation whatsoever; and the fact that the Government may have formulated, furnished, or in any way supplied the said drawings, specifications, or other data is not to be regarded by implication or otherwise as in any manner licensing the holder or any other person or corporation, or conveying any rights or permission, to manufacture, use, or sell any patented invention that may in any way be related thereto.

Trade names cited in this report do not constitute an official endorsement or approval of the use of such commercial hardware or software.

DISPOSITION INSTRUCTIONS

Destroy this report when no longer needed. Do not return it to the originator.

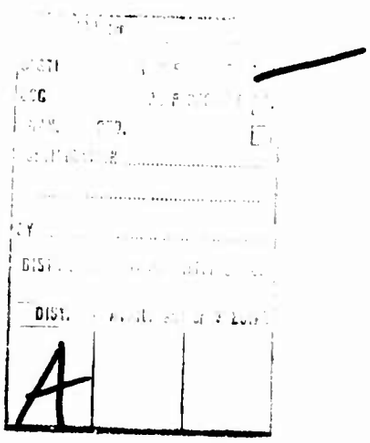

Unclassified
Security Classification

DOCUMENT CONTROL DATA - R & D

(Security classification of title, body of abstract and indexing annotation must be entered when the overall report is classified)

1. ORIGINATING ACTIVITY (Corporate author)	2a. REPORT SECURITY CLASSIFICATION
Sikorsky Aircraft Division of United Aircraft Corporation Stratford, Connecticut	Unclassified
	2b. GROUP

3. REPORT TITLE

GROUND TEST EVALUATION OF THE SIKORSKY ACTIVE TRANSMISSION ISOLATION SYSTEM

4. DESCRIPTIVE NOTES (Type of report and inclusive dates)

Final Technical Report

5. AUTHOR(S) (First name, middle initial, last name)

Paul W. von Hardenberg
Paul B. Saltanis

6. REPORT DATE	7a. TOTAL NO. OF PAGES	7b. NO. OF REFS
September 1971	124 125	10

8a. CONTRACT OR GRANT NO.	9a. ORIGINATOR'S REPORT NUMBER(S)
DAAJ02-69-C-0101	
b. PROJECT NO.	USAAMRDL Technical Report 71-38
c. Task 1F162204A14608	9b. OTHER REPORT NO(S) (Any other numbers that may be assigned this report)
d.	SER-50682

10. DISTRIBUTION STATEMENT

Approved for public release; distribution unlimited.

11. SUPPLEMENTARY NOTES	12. SPONSORING MILITARY ACTIVITY
	Eustis Directorate U.S. Army Air Mobility R&D Laboratory Fort Eustis, Virginia

13. ABSTRACT

Active isolation of a full-scale CH-53A helicopter fuselage was successfully demonstrated during hangar shake tests. Overall reductions of approximately 70 percent in fuselage response to main rotor 6p excitations were achieved, while sensitivity to 1p in-plane excitation was increased by only 13 percent. These isolation levels were achieved with a design constrained by the geometry of the CH-53A fuselage. Analytical studies indicate that further reductions in vibratory response could be achieved if fuselage and isolation system design were integrated.

The frequency response of the system to vibratory forces at the rotor along all three axes was measured, and the sensitivity of isolation to variation in system characteristics was determined. The transient response to the application of a sudden longitudinal moment was also observed. It was concluded that significant vibration response reductions can be achieved over the complete range of excitation frequency above the isolator resonances. Satisfactory correlation of transient test results with a simplified analytical model substantiates the analysis, which predicts that the active isolation system will achieve deflection design goals for control systems and engine installations. In addition, it was shown that substantial variations in isolator damping, stiffness, and gain from basic design values do not significantly affect 6p isolation.

Stability analyses were limited to isolator modes and aircraft mechanical stability. The analytical prediction of isolator mode stability was substantiated by test. Examination of the aircraft dynamic characteristics revealed that the mechanical stability of the CH-53A remains virtually unchanged with incorporation of the active isolation system.

In view of the successful test results, it is recommended that the active isolator development program be continued with the design, fabrication, and test of a flight demonstration vehicle. Further analyses should include an investigation of overall flight vehicle dynamics and a load spectrum survey to establish effects on isolation and transient response characteristics. The projected weight of a production CH-53A active isolation system is 1.1 percent of the total aircraft weight, with negligible hydraulic power requirements.

DD FORM 1 NOV 68 1473 REPLACES DD FORM 1473, 1 JAN 64, WHICH IS OBSOLETE FOR ARMY USE.

Unclassified
Security Classification

Unclassified
Security Classification

14. KEY WORDS	LINK A		LINK B		LINK C	
	ROLE	WT	ROLE	WT	ROLE	WT
Helicopter Vibration Control Active Vibration Isolation						

Unclassified
Security Classification

9684-71

DEPARTMENT OF THE ARMY
U. S. ARMY AIR MOBILITY RESEARCH & DEVELOPMENT LABORATORY
EUSTIS DIRECTORATE
FORT EUSTIS, VIRGINIA 23604

This report was prepared by Sikorsky Aircraft Division of United Aircraft Corporation under the terms of Contract DAAJ02-69-C-0101. It contains the results of a full-scale ground vibration test of an active rotor isolation system performed on a six-bladed CH-53A helicopter.

The isolation system consists of three unidirectional, hydropneumatic isolators installed at the transmission/airframe interface. The isolators are oriented in the vertical direction, but isolation is provided in both the vertical and inplane directions. Rigid links with control rod-ends connecting the transmission to the airframe provide torsional restraint. In this system, the crux of inplane isolation is placement of the isolators at a preselected waterline, in effect placing the rotor hub at the center of percussion of the upper body (rotor and transmission). That is, inplane rotor forces appearing as shear forces at the hub do not cause inplane reactions at the isolators. Instead, the upper body pivots about a horizontal axis at the waterline of the isolators, and vertical forces developed in the isolators form a couple that restrains the rotation.

The objective of this contractual effort was to experimentally demonstrate, for the steady-state flight condition of an articulated rotor system, the feasibility of rotor isolation. System evaluation considered amount of isolation afforded, relative displacement, isolator stability, ground resonance, power requirements, isolator size and weight, and fail-safe aspects.

Excellent isolation and displacement control were attained. At the predominant rotor excitation frequency (6/rev), average isolation in the vertical and inplane directions was 68% and 71%, respectively. At the 1/rev excitation frequency, an average amplification of 13% was experienced. Estimated relative displacement to an acceleration of 1g to 3g in 0.6 second is 0.24 inch. The very low corresponding isolation system power required (15 hp) could be derived from the 3,000-psi onboard hydraulic system.

Within the scope of this effort, feasibility of the isolation system was demonstrated for new helicopter designs. A new design offers the maximum design freedom for isolator placement and weight savings. The projected 370-pound system weight (1.1% GW) is possible only through considerable airframe structure and transmission housing modification.

The quasi-focusing technique used to achieve inplane isolation is adequate for articulated rotor systems because hub shear forces are the only significant source of excitation. However, for semirigid and rigid rotor configuration, hub moment excitations are of concern. More importantly, isolation of these hub moments may prove to be very difficult because isolation of hub moments cannot be effectively reduced by isolator waterline placement alone. Isolator focusing, possibly including kinematic linkages, may be required. Feasibility for helicopters with appreciably fewer rotor blades (closer proximity of 1/rev and blade-passage frequency) is questionable.

This program was conducted under the technical direction of Mr. Joseph H. McGarvey of the Reliability and Maintainability Division of this Directorate.

Task 1F162204A14608
Contract DAAJ02-69-C-0101
USAAMRDL Technical Report 71-38
September 1971

GROUND TEST EVALUATION OF THE SIKORSKY ACTIVE TRANSMISSION ISOLATION SYSTEM

Sikorsky Engineering Report No. 50682

By

Paul W. von Hardenberg
Paul B. Saltanis

Prepared By

Sikorsky Aircraft
Division of United Aircraft Corporation
Stratford, Connecticut

for

EUSTIS DIRECTORATE
U. S. ARMY AIR MOBILITY RESEARCH AND DEVELOPMENT LABORATORY
Fort Eustis, Virginia

ABSTRACT

Active isolation of a full-scale CH-53A helicopter fuselage was successfully demonstrated during hangar shake tests. Overall reductions of approximately 70 percent in fuselage response to main rotor 6p excitations were achieved, while sensitivity to 1p in-plane excitation was increased by only 13 percent. These isolation levels were achieved with a design constrained by the geometry of the CH-53A fuselage. Analytical studies indicate that further reductions in vibratory response could be achieved if fuselage and isolation system design were integrated.

The frequency response of the system to vibratory forces at the rotor along all three axes was measured, and the sensitivity of isolation to variation in system characteristics was determined. The transient response to the application of a sudden longitudinal moment was also observed. It was concluded that significant vibration response reductions can be achieved over the complete range of excitation frequency above the isolator resonances. Satisfactory correlation of transient test results with a simplified analytical model substantiates the analysis, which predicts that the active isolation system will achieve deflection design goals for control systems and engine installations. In addition, it was shown that substantial variations in isolator damping, stiffness, and gain from basic design values do not significantly affect 6p isolation.

Stability analyses were limited to isolator modes and aircraft mechanical stability. The analytical prediction of isolator mode stability was substantiated by test. Examination of the aircraft dynamic characteristics revealed that the mechanical stability of the CH-53A remains virtually unchanged with incorporation of the active isolation system.

In view of the successful test results, it is recommended that the active isolator development program be continued with the design, fabrication, and test of a flight demonstration vehicle. Further analyses should include an investigation of overall flight vehicle dynamics and a load spectrum survey to establish effects on isolation and transient response characteristics. The projected weight of a production CH-53A active isolation system is 1.1 percent of the total aircraft weight, with negligible hydraulic power requirements.

FOREWORD

This research program demonstrating the feasibility of an active rotor/transmission isolation system was performed by Sikorsky Aircraft, Division of United Aircraft Corporation, Stratford, Connecticut, under Contract DAAJ02-69-C-0101 (Task 1F162204A14608) for the U. S. Army Air Mobility Research and Development Laboratory (USAAMRDL), Fort Eustis, Virginia. The study was begun on 1 July 1969 and completed on 31 October 1970.

The program was conducted under the technical direction of Mr. J. McGarvey, Contracting Officer's Representative, USAAMRDL.

Principal Sikorsky personnel in this program were Messrs. P. W. von Hardenberg, Project Manager, and P.B. Saltanis, Research Engineer. The work was done under the direction of Mr. E. S. Carter, Chief of Aeromechanics Branch. Acknowledgement is given to Messrs. A. S. Jacobson, Research Engineer, and K. H. Wallischeck, Hydraulics Engineer, who participated in the design effort.

BLANK PAGE

TABLE OF CONTENTS

	PAGE
ABSTRACT	iii
FOREWORD	v
LIST OF ILLUSTRATIONS	viii
LIST OF TABLES	xi
LIST OF SYMBOLS	xii
INTRODUCTION	1
APPARATUS AND INSTRUMENTATION	4
BASIC DATA AND DESIGN	10
GROUND TEST EVALUATION	29
MECHANICAL STABILITY	62
WEIGHT, POWER, AND FAIL-SAFE REQUIREMENTS	63
SEMIRIGID AND RIGID ROTOR CONSIDERATIONS	67
CONCLUSIONS	70
RECOMMENDATIONS	71
LITERATURE CITED	72
APPENDIX.PRELIMINARY DESIGN ANALYSIS	73
DISTRIBUTION	111

LIST OF ILLUSTRATIONS

Figure		Page
1	Isolation System Schematic	3
2	Ground Test Apparatus	5
3	Major Measurement System Components	7
4	Test Vehicle Accelerometer Locations	8
5	Shake Test Console Schematic	9
6	Vertical Transmissibility to Vertical Excitation	12
7	Lateral and Roll Transmissibilities to Lateral Excitation	13
8	Longitudinal and Roll Transmissibilities to Longitudinal Excitation	14
9	Transfer Function Roots	15
10	Transient Load and Response	16
11	Isolator Assembly Drawing	21
12	Complete and Disassembled Isolator	23
13	Installation Sketch	25
14	Attachment Hardware and System Installation	27
15	Pilot Vertical Isolated/Hard Response to Vertical Excitation	34
16	Representative Isolated/Hard Response to Vertical Excitation	35
17	Analytical/Experimental Transmissibility to Vertical Excitation	37
18	Pilot Lateral Isolated/Hard Response to Lateral Excitation	40
19	Representative Isolated/Hard Response to Lateral Excitation	41
20	Main Rotor and Transmission Base Response to Lateral Excitation	43
21	Analytical/Experimental Transmissibility to Lateral Excitation	44
22	Pilot Vertical Isolated/Hard Response to Longitudinal Excitation	45
23	Representative Isolated/Hard Response to Longitudinal Excitation	46
24	Analytical/Experimental Transmissibility to Longitudinal Excitation	48

Figure		Page
25	Effect of Changes in Damping, Stiffness and Gain.	55
26	Transient Test Apparatus.	59
27	Analytical/Experimental Transient Response Time History. . . .	60
28	Peak Deflection Versus Step Load Applied for All Test Conditions.	61
29	Top View of Production and Prototype Frame and Beam Rearrangement.	66
30	Effect of Isolator Waterline Location on Transmissibilities. .	68
31	Longitudinal and Pitch Transmissibilities to Pitch Excitation.	69
32	Lateral and Roll Transmissibilities to Roll Excitation. . . .	70
33	Active Transmission Isolator Concept Shown Qualitatively. . .	76
34	Illustrative Breakdown of Isolator Impedance Components . . .	77
35	Description of Coordinate System and Mathematical Models.	78
36	Air Spring With Damping.	80
37	Functional Schematic With Notation.	83
38	Vertical Rigid-Body Model.	84
39	In-Plane Mathematical Model(Longitudinal-Pitch).	86
40	Effect of Isolator Waterline Location on Lateral Isolation.	89
41	CH-53A Vertical Transient Loads and Response.	93
42	CH-53A Vertical Transmissibility.	94
43	CH-53A Lateral and Roll Transmissibility.	95
44	CH-53A Longitudinal and Pitch Transmissibilities.	96
45	CH-53A Transfer Function Roots.	97
46	CH-53A Isolator Conceptual Hardware Sketch.	98
47	CH-53A Isolator Installation Sketch.	99
48	UH-1D Vertical Transient Load and Response.	102
49	UH-1D Vertical Transmissibility.	103
50	UH-1D Lateral and Roll Transmissibilities.	104
51	UH-1D Longitudinal and Pitch Transmissibilities.	105
52	HLH Vertical Transient Load and Response	107
53	HLH Vertical Transmissibility	108

Figure		Page
54	HLH Lateral and Roll Transmissibilities	109
55	HLH Longitudinal and Pitch Transmissibilities	110

LIST OF TABLES

TABLE		PAGE
I	Basic Data	17
II	Experimental Isolator Weight Breakdown	24
III	6P Comparison	31
IV	1P Comparison	32
V	6P Isolator Measurements	50
VI	1P Isolator Measurements	51
VII	Comparison of Test and Analysis - 1P and 6P Isolator Displacements	52
VIII	Estimated Weight for Test, Prototype, and Production System	65
IX	CH-53A Design Data, Geometric and Inertia Properties	92
X	UH-1D Isolator Parameters, Geometric and Inertia Properties	101
XI	HLH Isolator Parameters, Geometric and Inertia Properties	106

LIST OF SYMBOLS

A	Air volume reaction surface area for general air spring
$A_{a,b}$	Air volume reaction surface area for low and high pressure sides of isolator element
a	Longitudinal distance between shaft centerline and isolator element location
a_i	Vertical transfer function numerator polynomial coefficients
B	Air damping coefficient for general air spring
$B_{a,b}$	Air damping coefficients on low and high pressure sides of isolator element
b	Lateral distance between shaft centerline and isolator element location
b_j	Vertical transfer function denominator polynomial coefficients
C_v	Isolator element viscous damping coefficient
C_2	Feedback element linkage ratio
c_i	Vertical transmissibility numerator polynomial coefficients
$D(s)$	Isolator impedance denominator polynomial
$D_{mz}(s)$	Vertical transmissibility denominator polynomial
$D_z(s)$	Vertical transfer function denominator polynomial
$D_\theta(s)$	Pitch to longitudinal force transfer function denominator polynomial
d_j	Isolator element impedance denominator polynomial coefficients
e_i	Longitudinal transmissibility to longitudinal force numerator polynomial coefficients
F_I	Isolator element piston force
$F_{a,b}$	Air volume reaction forces for low and high pressure sides of isolator element
F_{vd}	Isolator element viscous damping force
F_x	Longitudinal rotor head input force
F_z	Vertical rotor head input force
f_j	Longitudinal transmissibility to longitudinal force denominator polynomial coefficients
$G_{a,b}$	Servovalve flow gains for low and high pressure sides of isolator element
g_i	Pitch transmissibility to longitudinal force numerator polynomial coefficients

h_j	Pitch transmissibility to longitudinal force denominator polynomial coefficients
$I_{1x,2x}$	Moments of inertia of upper and lower bodies in the roll direction
$I_{1y,2y}$	Moments of inertia of upper and lower bodies in the pitch direction
$K_{a,b}$	Air spring impedance of low and high pressure sides of isolator element
$K_I(s)$	Isolator element impedance polynomial expression
ℓ_1	Distance between upper body cg and isolator location
ℓ_2	Distance between lower body cg and isolator location
ℓ_3	Distance between rotor head cg and upper body mass
m_1	Upper body mass
m_2	Lower body mass
$N(s)$	Isolator impedance numerator polynomial
$N_{mz}(s)$	Vertical transmissibility numerator polynomial
$N_z(s)$	Vertical transfer function numerator polynomial
$N_\theta(s)$	Pitch to longitudinal force transfer function numerator polynomial
n	Number of blades
n_i	Isolator element impedance numerator polynomial coefficients
P	Mean operating pressure of air in general air spring
$P_{a,b}$	Operating air pressures for low and high pressure sides of isolator element
P_d	Isolator element drain pressure
P_h	Pressure of isolator element high pressure source
$q_{a,b}$	Flow rates of servovalve for low and high pressure sides of isolator element
r_i	Pitch to longitudinal force transfer function numerator polynomial coefficients
$S_{a,b}$	Piston area for low and high pressure sides of isolator element
s	Derivative operator, where $s = \frac{d}{dt}$
s_j	Pitch to longitudinal force transfer function denominator polynomial coefficients
T_m	Transmissibility in the pitch direction

T_{mx}	Transmissibility in the longitudinal direction
T_{mz}	Transmissibility in the vertical direction
T_z	Isolator vertical deflection transfer function
$T_{\theta r}$	Isolator pitch deflection transfer function
T_∞	Asymptotic value of in-plane transmissibility as input frequency approaches infinity
V_c	Volume contained between diaphragm and air restriction for general air spring
$V_{ca,b}$	Volume contained between diaphragm and air restriction for low and high pressure sides of isolator element
V_t	Volume contained between housing and air restriction for general air spring
$V_{ta,b}$	Volume contained between housing and air restriction for low and high pressure sides of isolator element
X_I	Relative axial displacement across isolator element
$x_{1,2}$	Longitudinal displacements of upper and lower body cg's in isolated configuration
$x_{1r,2r}$	Longitudinal displacements of upper and lower body cg's in rigid configuration
Y	Deflection across servovalve
$y_{1,2}$	Lateral displacement of upper and lower body cg's in isolated configuration
Z	Displacement across general air spring
$Z_{a,b}$	Air spring displacements on low and high pressure sides of isolator element
$z_{1,2}$	Vertical displacements of upper and lower body cg's in isolated configuration
$z_{1r,2r}$	Vertical displacements of upper and lower body cg's in rigid configuration
γ	Ratio of specific heats
Δz	Vertical deflection across isolation system
θ_r	Pitch displacement across isolation system
$\theta_{1,2}$	Pitch displacements of upper and lower body cg's in isolated configuration
$\phi_{1,2}$	Roll displacement of upper and lower body cg's in isolated configuration

INTRODUCTION

BACKGROUND

Consideration of helicopter vibration is required to insure that the vehicle is free of damaging fatigue loads and that the crew's performance is not degraded. Helicopters usually have one predominant source of excitation: the main rotor. Excitation is at a discrete frequency, or frequencies, associated with the number of blades times the rotational speed of the rotor. The problem then is one of separating the elastic fuselage frequencies from the main rotor excitation frequencies plus exploiting the advantages of altering the fuselage mode shapes. Prediction and definition of these modes, even experimentally, are complex and control is even more difficult, usually requiring significant structural changes or weight penalties. Satisfactory results are often limited to particular fuselage locations, with other areas showing no improvement or even increased response.

An effective method of providing vibration control is structural detuning of the transmission/rotor head. Further, using the flexible approach results in two fundamental advantages. First, with a flexible detuned transmission/rotor head, all of the resulting flexible fuselage modes that significantly contribute to the final forced response have a minimal amount of rotor motion; thus, their participation from a normal modes viewpoint is minimized. Second, since the flexibility incorporated between the transmission and fuselage is an order of magnitude more than the fuselage flexibilities, it becomes the only significant structural parameter controlling the fuselage dynamics; this directly improves the accuracy of the design prediction.

ACTIVE TRANSMISSION ISOLATION

Incorporation of flexibility between the transmission and fuselage to provide isolation from main rotor excitation, combined with active elements to control deflections, has long been recognized as a direct approach to reduce airframe vibration levels. Analytic feasibility of isolating an entire fuselage from vertical and in-plane main rotor excitations occurring at np and higher frequencies has been demonstrated under Sikorsky-funded research and development. The results of these precontract efforts are presented in the appendix.

The isolation system developed for this program is composed of three self-contained hydropneumatic active isolation units which do not employ any external signal conditioning devices and are designed to operate from available in-flight hydraulic power supply sources. Figure 1 shows a schematic representation of the transmission fuselage attachments. The upper body, consisting of the transmission and rotor head, is attached by three vertical isolators and rigid in-plane restraints to the lower body, or fuselage. This method of attachment constrains the relative motions of the upper and lower bodies to those composed of vertical motions of the isolators. These are vertical, pitch, and roll motions of the upper body relative to the lower. As substantiated within this report, no in-plane isolators are required to obtain fuselage isolation from in-plane forces.

This report presents the accomplishments of a program of design, fabrication, and evaluation of a full-scale test vehicle to demonstrate the feasibility of this concept. Test apparatus, isolator hardware, and installation are described, and results of the ground test evaluation are presented. Feasibility of weight, size, power, and fail-safe requirements for a production system is established.

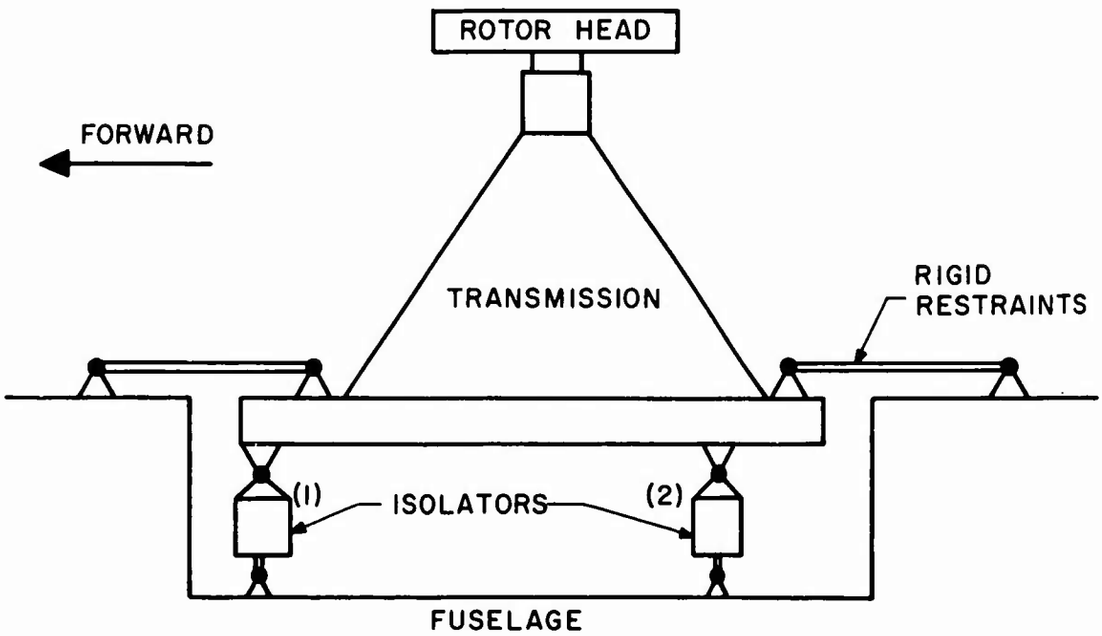

Figure 1. Isolation System Schematic.

APPARATUS AND INSTRUMENTATION

APPARATUS

The ground test apparatus employed to evaluate the isolation system installed in the test vehicle consisted of a suspension system to simulate free flight and a rotor head mounted shaker, shown in Figure 2. In addition, hydraulic power supplies were used to operate the shaker and activate the isolators.

The structural static CH-53A test vehicle was weighed and ballasted to a gross weight of 35,000 pounds with a neutral center-of-gravity mass distribution. Concentrated weights were used to dynamically simulate the tail rotor and intermediate gearbox, which were not installed in the test vehicle. The engines were not installed or simulated to simplify the test evaluation. Production CH-53A engines were installed on passive isolators, resulting in engine rigid-body modes (8 to 10 Hz) which are in the proximity of the isolator modes (5 to 11 Hz).

The bungee suspension system labeled in Figure 2 lifted the entire test vehicle off the deck to simulate free flight. The flexibility of the bungee results in low rigid-body test vehicle mode frequencies, the highest being the vertical, confirmed by test to be 1.0 Hz. This effectively eliminates contributions from these modes to test vehicle response at 1p, 3.1 Hz, or in the lowest frequency mode.

A dummy rotor head was employed to simulate the mass of the head and blades and to provide attachments to the suspension system and shaker. The shaker consists of two counterrotating eccentric masses with adjustable unbalance which produce a unidirectional sinusoidal excitation proportional to the speed of rotation squared. The shaker was hydraulically driven from a large commercial pump, with a manually operated flow bypass control valve used to adjust speed.

An independent hydraulic system was maintained for the isolation system. This system consisted of a vari-drive electric motor driving a 6 gpm aircraft-type piston pump operating at 3000 psi. A bypass valve to the fluid reservoir was used to maintain constant supply pressure. Pressure relief and electrically actuated cutoff valves were incorporated for safety. Pump output was filtered, and its temperature was monitored and maintained within normal operating range with a return-line oil cooler.

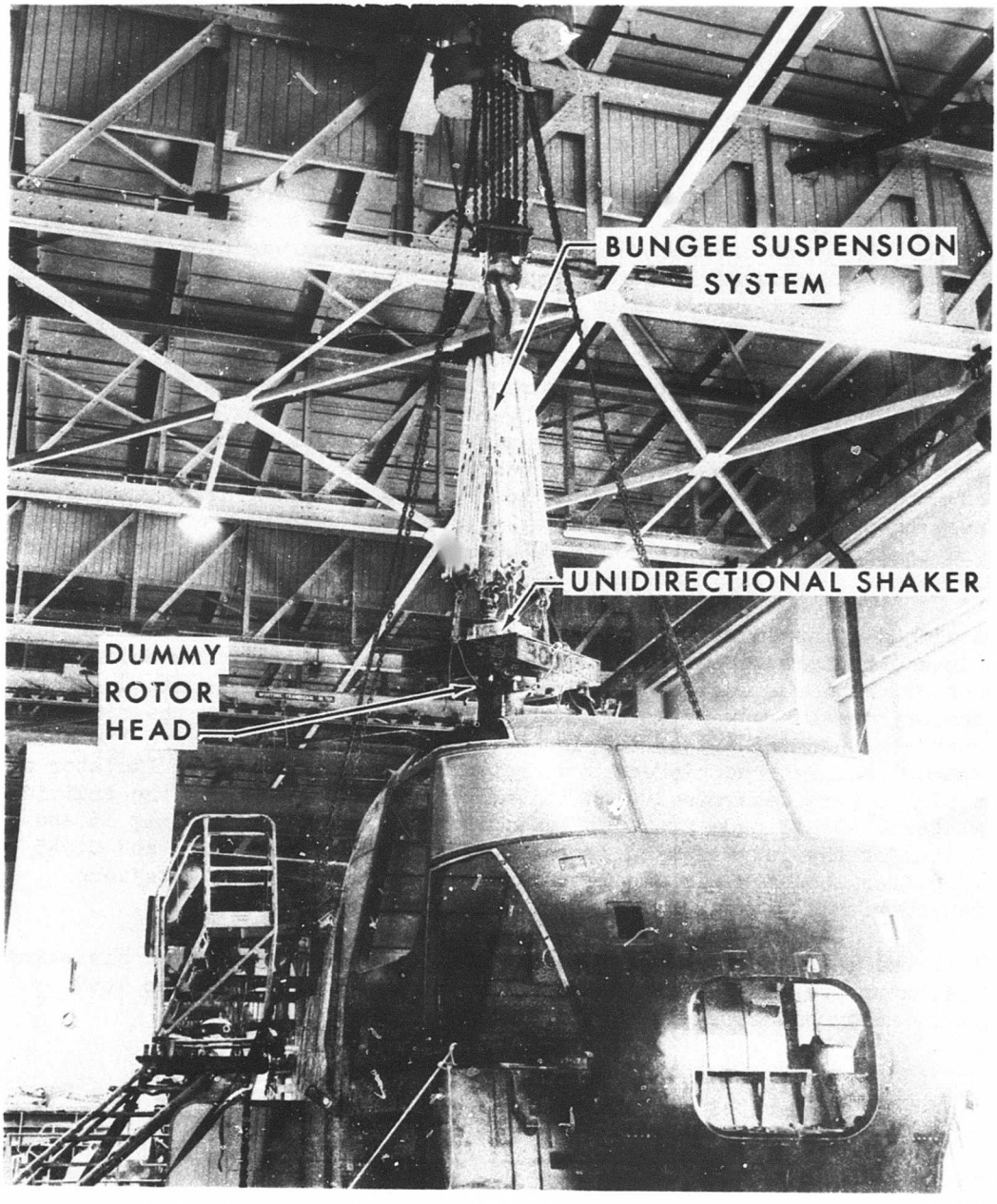

Figure 2. Ground Test Apparatus.

INSTRUMENTATION

Two measurement systems were employed to satisfy the requirements of three tests. The first system, involving a normalizing unit and X-Y-Y' plotter output display, was designed to evaluate a broad range of frequency response of the test vehicle with and without the isolators activated. The second system, utilizing a direct-writing oscillograph, was used to obtain additional isolation data at two discrete test frequencies. The second system was also used to obtain real-time histories of several parameters when a step-input load was applied to the test vehicle. The major instrumentation components are shown in Figure 3.

The first measurement system was used to directly record quasi-steady-state test vehicle accelerations. These accelerations were normalized to the test vehicle input excitation as the input frequency was slowly varied. Selected accelerometer locations and their orientation with respect to the test vehicle are illustrated by the arrows in the structural arrangement shown in Figure 4. The acceleration transducers were calibrated, fixed in position, and wired to the Sikorsky designed and fabricated shake test console shown schematically in Figure 5. Each acceleration transducer was manually selected at the switchboard; its signal was preamplified, filtered, normalized to G/1000 pounds of excitation force, and plotted together with its phase versus frequency on an X-Y-Y' plotter. These plots were obtained for any desired location by slowly varying the shaker frequency through the range of interest. Increased resolution in the G/1000 pound scale of these plots could be obtained by altering the preamplifier gain setting.

The second measurement system was used to obtain additional isolator data at 1p and 6p test vehicle excitation frequencies. Steady isolator measurements of pressures were made with bourdon-type gages, while steady-state vibratory pressures were determined with diaphragm pressure transducers. Pressure transducer output was amplified and filtered to remove the steady component and was recorded on a direct-writing oscillograph. Isolator displacements were determined with linear potentiometers across the individual isolators. Oscillograph output sensitivities were approximately 15 and 45 psi/in. for the low and high isolator pressures respectively, and 0.045 in./in. for isolator displacements. Isolator flow requirements were measured with a glass tube flowmeter.

The second measurement system was also used to obtain real-time histories of isolator pressures and displacements resulting from the step load inputs. A dynamometer was used to measure the applied loads.

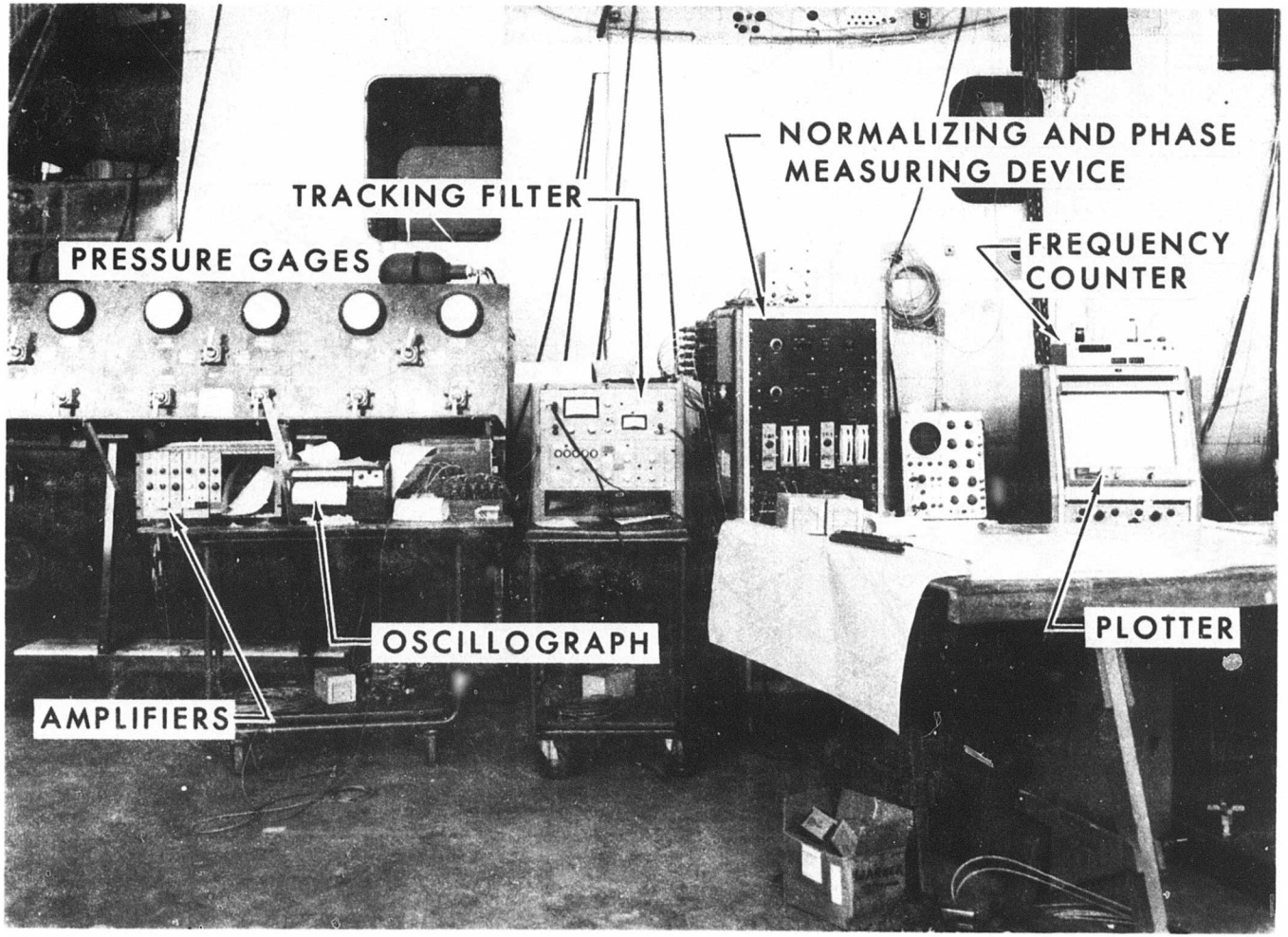

Figure 3. Major Measurement System Components.

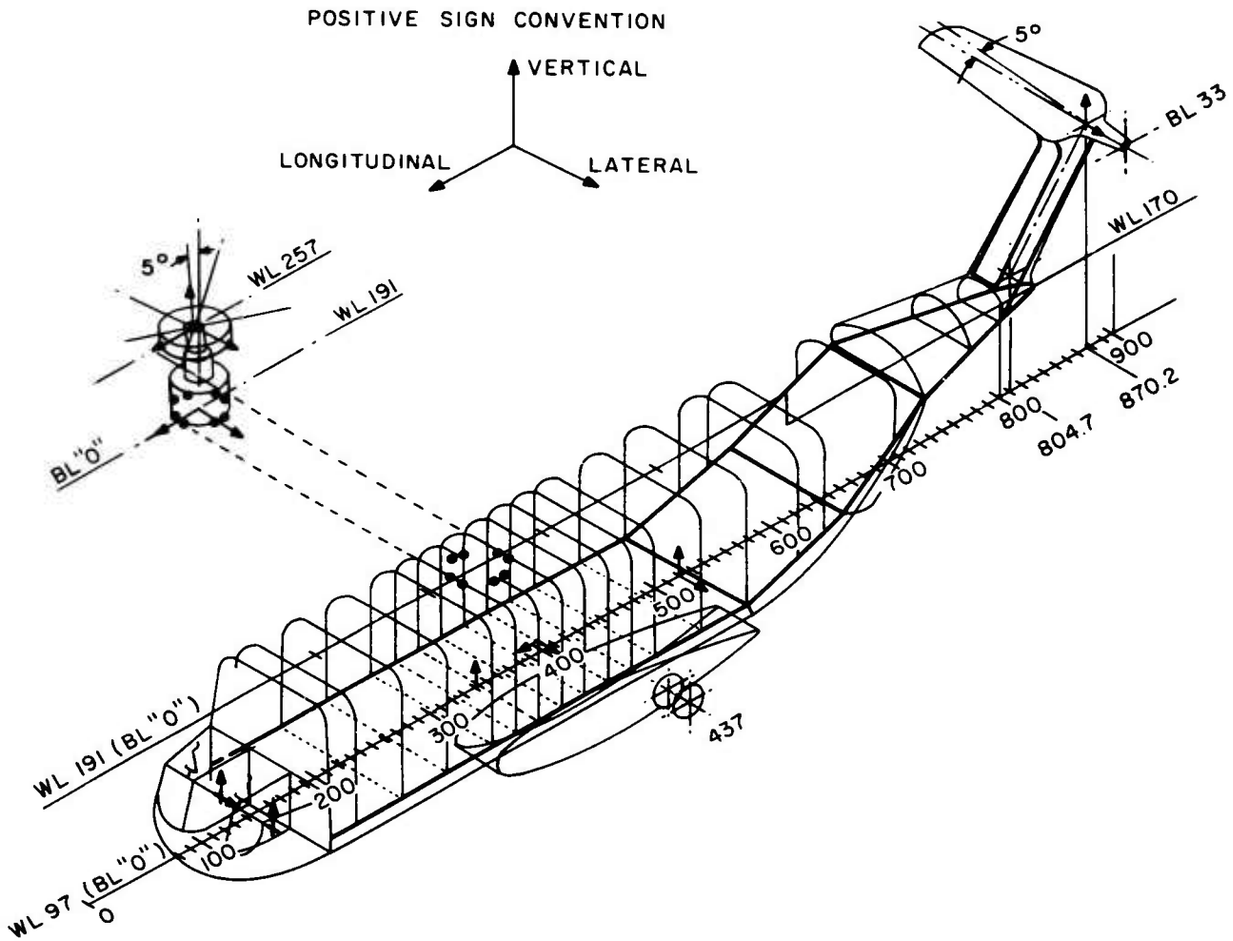

Figure 4. Test Vehicle Accelerometer Locations.

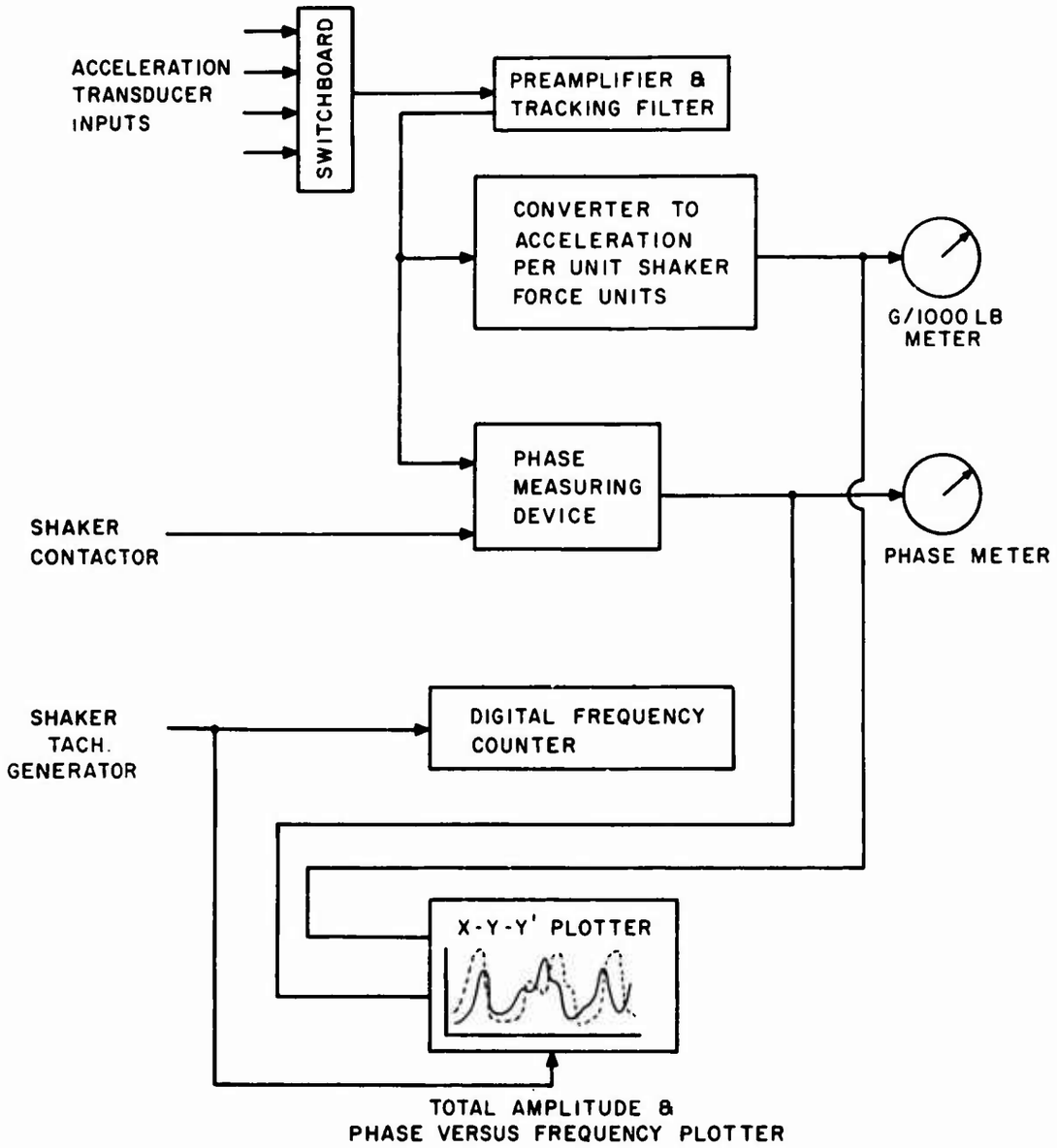

Figure 5. Shake Test Console Schematic.

BASIC DATA AND DESIGN

BASIC DATA

A preliminary analysis, conducted prior to this contract, and funded by Sikorsky Aircraft (see appendix), was reevaluated to determine final isolation system transmissibilities, transient response, and stability characteristics. This latter effort terminated in what was considered to be basic data for the test hardware. During this effort, it was decided to avoid the possibility of introducing low-frequency instabilities from rotor and/or pilot coupling by designing all isolator rigid-body mode frequencies above 1p. This provides better overall system confidence until a more detailed investigation can be performed. Further, system isolation transmissibilities were not severely compromised.

The system's performance was analyzed and predicted using a mathematical model consisting of two rigid masses attached by a linear description of the isolation system. The upper body is the transmission and rotor system and the lower body is the fuselage. Isolation potential of the system is evaluated using transmissibility, defined as the magnitude ratio of the isolated fuselage response to the unisolated. The isolation performance, the basis of the transient load requirements and the results, and the design implications of actual isolation system nonlinearities are discussed below.

The system's isolation potential to vertical and in-plane rotor excitations is shown as transmissibility versus frequency plots in Figures 6 through 8. A vertical rotor-head excitation will produce only vertical response of the fuselage cg, while an in-plane excitation produces both an in-plane displacement and a rotation of the cg. The vertical transmissibility at CH-53A 6p, 18.5 Hz, is 0.79. Lateral translational and rotational 6p transmissibilities to lateral excitation are 0.23 and 0.18 respectively. For longitudinal excitation, the 6p transmissibilities are 0.10 and 0.11.

Transfer function roots associated with vertical, longitudinal, and lateral excitation are presented in Figure 9. Note that all the roots are in the left half of the complex plane, demonstrating that the isolation system is stable. The most lightly damped roots correspond to the isolator rigid-body modes defined by the peaks in the transmissibility curves.

Transient load response of the isolation system was evaluated by analytically applying a vertical load to the rotor head corresponding to a +1G to +3G vehicle acceleration in a period of 0.6 second. This load has been used to size the isolation system presented. Figure 10 shows the resultant time response of the relative deflection across the isolation system. The maximum relative deflection has a magnitude of 0.15 inch.

Allowable transient response for a production design would be based on control system and possibly engine output shaft displacement requirements. Control system displacement coupling can be avoided by proper arrangement of the linkages across the isolation system. Assuming that the engine is attached to the fuselage rather than cantilevered to the transmission,

shaft alignment criteria would have to be met. Using 0.75 degree, a typical production tolerance for a high-speed shaft, the isolation system's corresponding allowable relative deflection would be 0.21 inch. This permits some latitude in the selection of the servovalve gain setting. For example, reducing the gain from 200 to 100 would increase the deflection from 0.15 to 0.24 inch and provide a greater stability margin.

Basic data for the isolator design is presented in Table I. The appendix contains a discussion of the contribution of each of these parameters to isolator performance. A brief description of these parameters follows. One-third of the fuselage weight is supported by each isolator's difference in pressure across its piston. The subscript b denotes the high pressure side. These pressures are supplied by a hydraulic servovalve with flow gains $G_{a,b}$ to provide isolator centering. Piston motion is transferred to compression of the primary air volumes $V_{ca,b}$ through the hydraulic fluid to provide the spring rate required for isolation. While volumes $V_{ta,b}$ together with airflow restrictions $B_{a,b}$ are incorporated for damping, fluid damping is also provided by orifices.

The piston and fluid damping value presented in Table I represents a desired isolator viscous damping coefficient. However, piston sliding friction and orifice fluid restrictions are nonlinear forms of damping which can be represented as the equivalent to a viscous damper with the same energy dissipation at a particular amplitude of steady-state operation. The equivalent viscous damping associated with sliding friction is inversely proportional to the isolator piston velocity, the predominate factor at low levels of excitation. Solving for the isolator forced displacement at 6p with the linear analysis and determining the equivalent damping supplied by various values of sliding friction showed that 10 pounds of friction would contribute to approximately 10% of total damping. Ten pounds was then selected as the design goal. The remainder of the equivalent damping value was obtained by sizing orifices which have a velocity squared characteristic.

Isolator locations were selected considering the frequencies of the isolator rigid-body modes and the internal reaction forces at the rigid in-plane restraints. The ratio of the vertical to the lateral and longitudinal rigid-body mode frequencies is determined by the isolator plan spacing. The selection presented in Table I was chosen to maintain the in-plane isolator modes above 1p while limiting the vertical stiffness to provide vertical isolation. Internal reaction forces through rigid in-plane restraints attached at the base of the transmission do not significantly affect fuselage isolation.

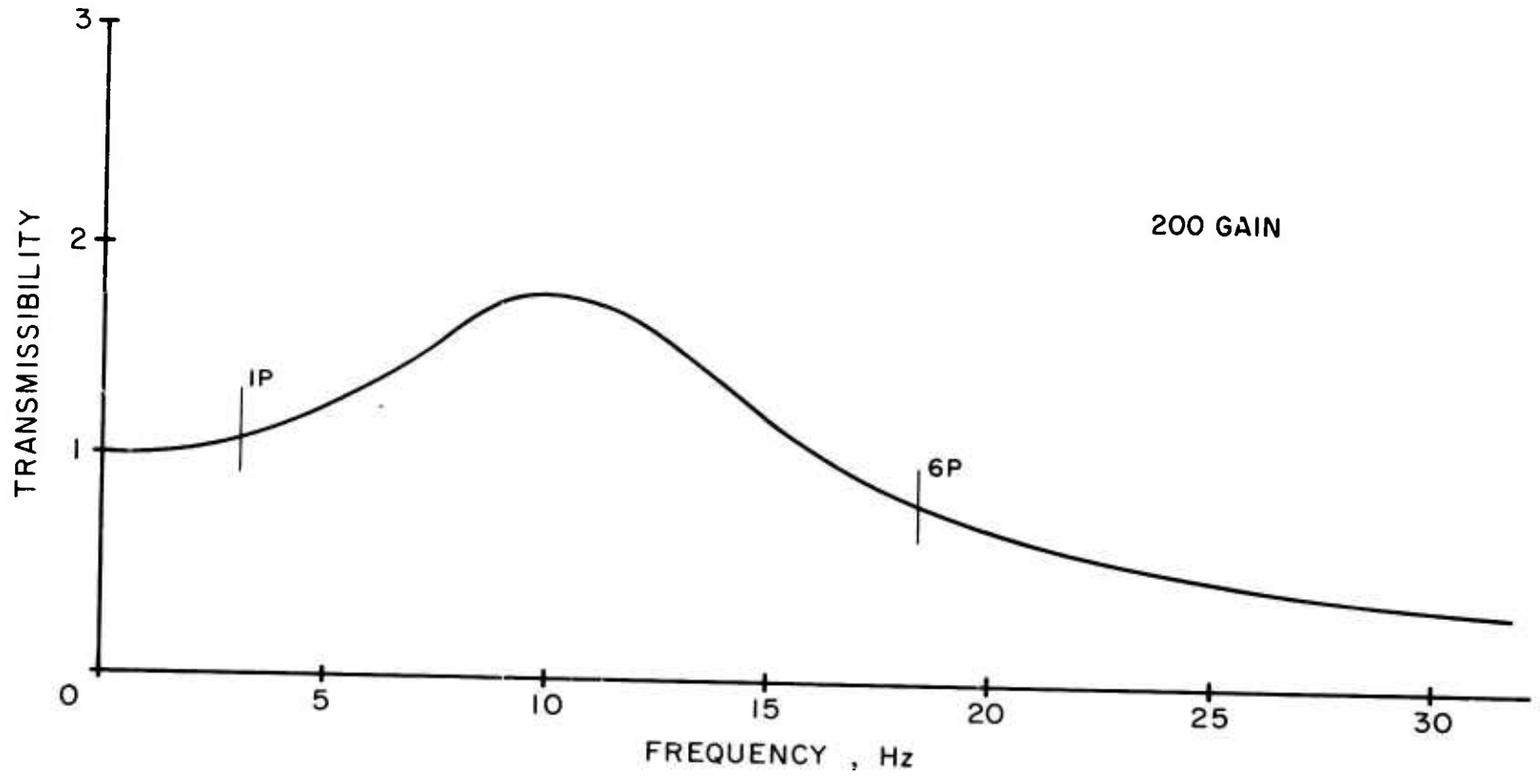

Figure 6. Vertical Transmissibility to Vertical Excitation.

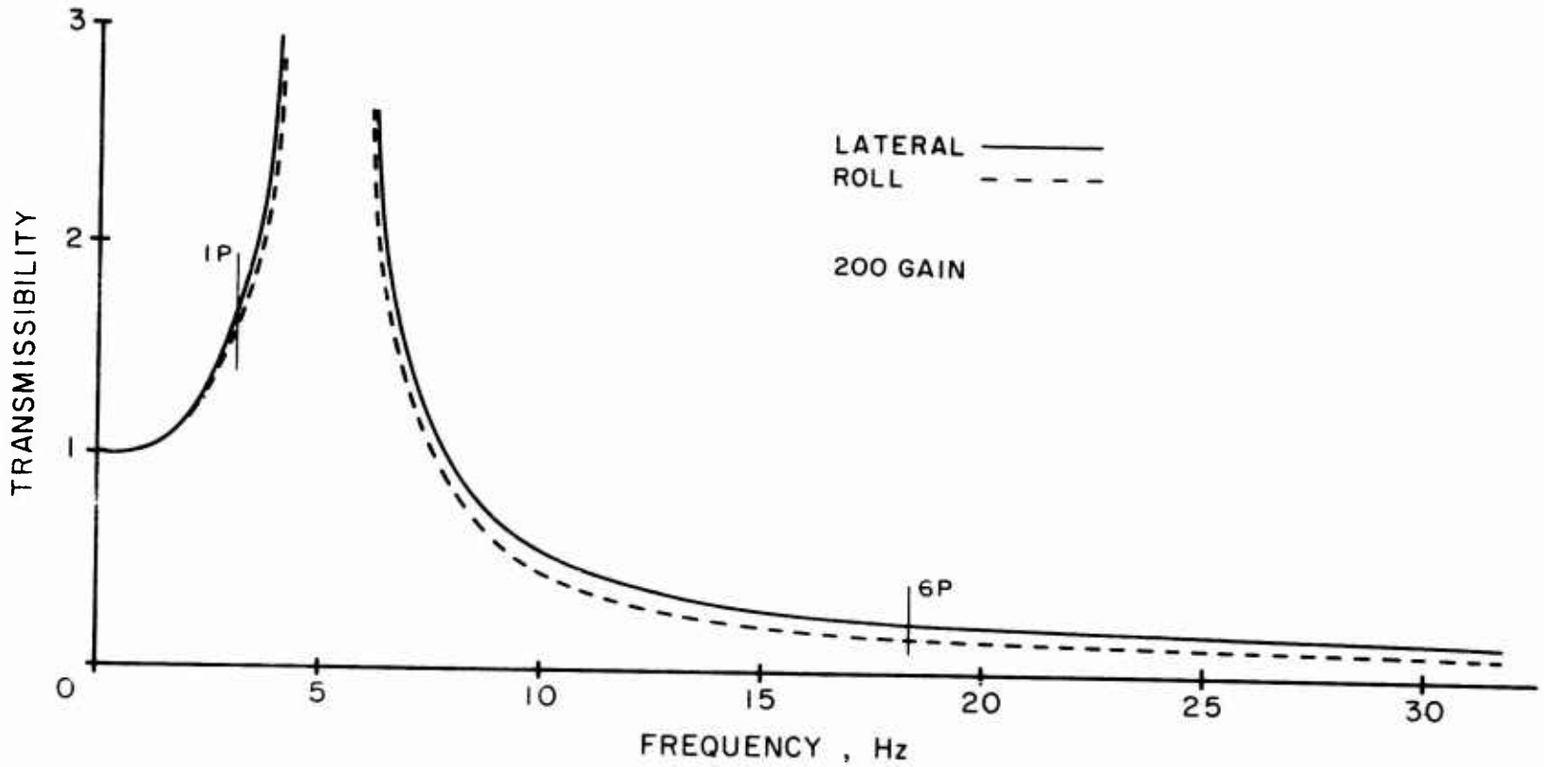

Figure 7. Lateral and Roll Transmissibilities to Lateral Excitation.

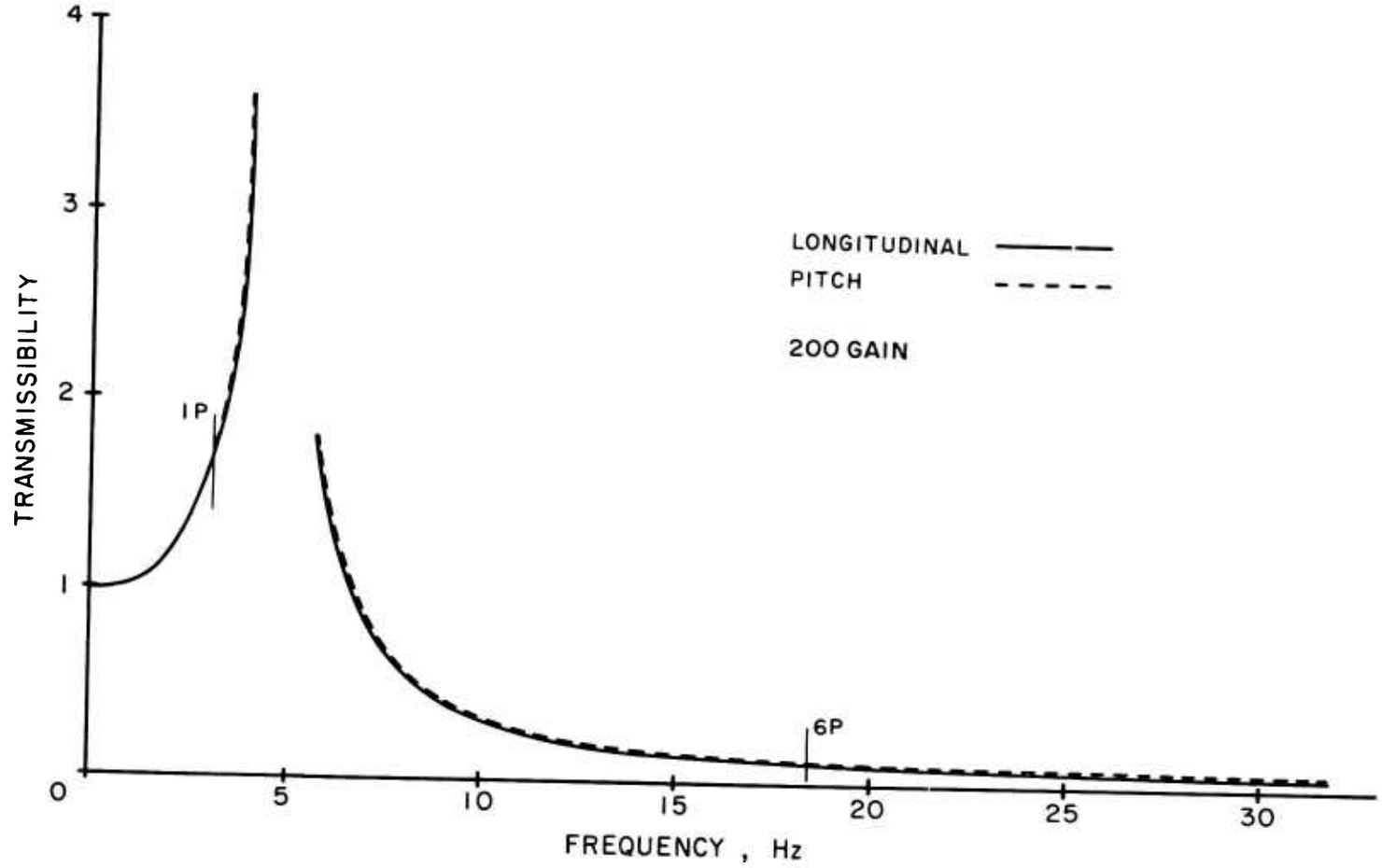

Figure 8. Longitudinal and Pitch Transmissibilities to Longitudinal Excitation.

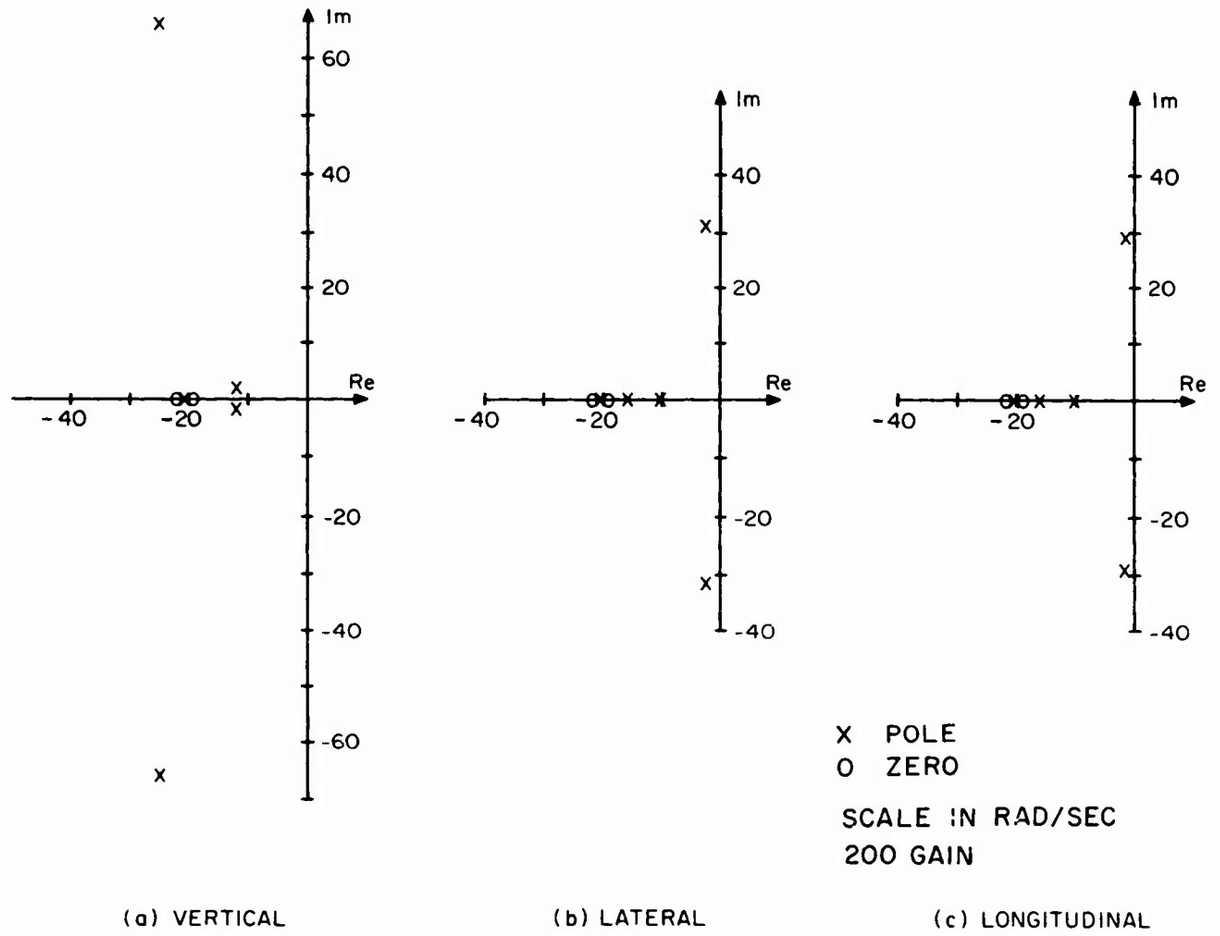

Figure 9. Transfer Function Roots.

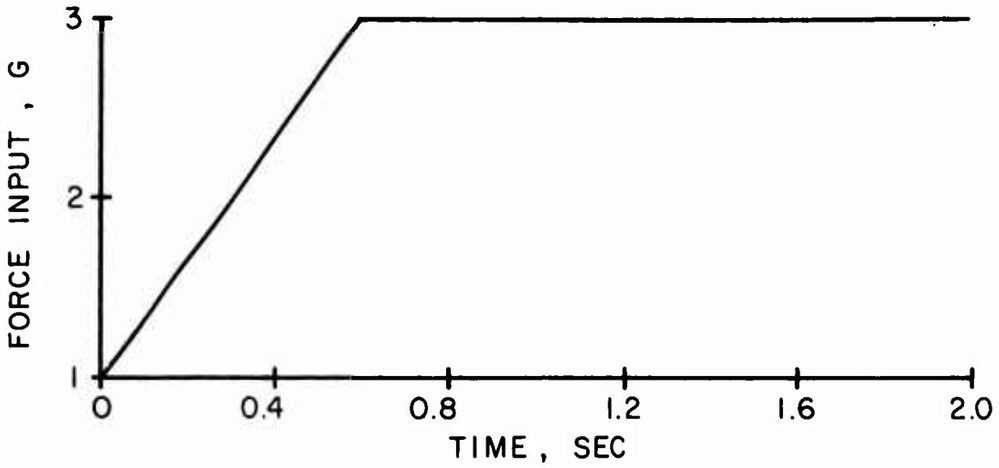

(a) DESIGN LOAD

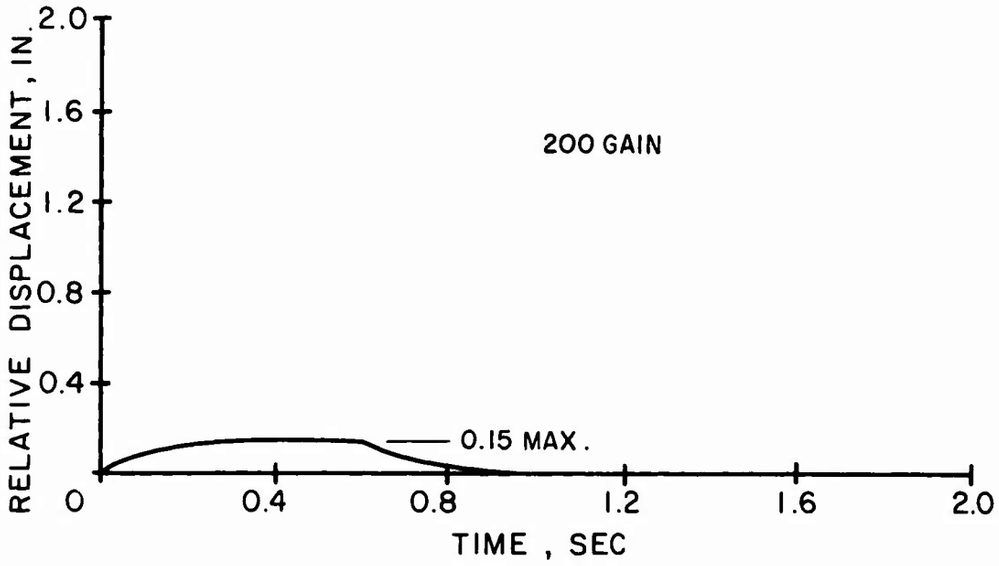

(b) RESPONSE

Figure 10. Transient Load and Response.

TABLE I. BASIC DATA		
Piston Areas ($in.^2$)	S_a	14.2
	S_b	12.1
Air Volumes ($in.^3$)	Total	45
	V_{cb}	16
	V_{ca}	6
	V_{tb}	16
	V_{ta}	7
Piston and Fluid Damping (lb sec/in.)	C_v	285
Air Damping ($in.^5$/lb sec)	B_a	.16
	B_b	.11
Steady Operating Air Pressures (psi)	P_a	303
	P_b	1100
Valve Feedback Gains ($in.^2$/sec)	G_a	200 *
	G_b	200 *
Isolator Spacing (in.)	a	16.5
	b	25.2
Lengths (in.)	ℓ_1	47
	ℓ_2	49
	ℓ_3	19
* Testing has shown 100 to be a better choice.		

DESIGN

Isolator and test vehicle installation hardware was designed to the basic data specifications developed. The design philosophy included fabrication of an isolator with readily adjustable settings for ground test evaluation. In addition, it was decided that the nonisolated fuselage would be an evaluation of the test vehicle with the isolation system installed, but deactivated. Therefore, any possible effects of irrelevant hardware changes would not be introduced into the effect of activating the isolation system.

An isolator assembly drawing is presented in Figure 11; Figure 12 presents photos of complete and disassembled isolators. Primary air volumes are contained with diaphragms in the cavities formed by the -4 bodies and the -5 and -6 caps. Secondary air volumes are shown attached to the main unit in Figure 12 (a), with lines containing capillary flow restrictions. A modified CH-53A main rotor servovalve with enlarged ports and modified quiescent pressure characteristics, together with the adjustable ratio linkage shown, provide the centering capability of the isolator. Fluid damping is provided by the -8 orifices leading to the air cavities on both sides of the piston. Low friction seals and bearings are utilized to minimize friction on the piston shaft, while the piston rings shown in the assembly drawing were replaced by a lapped fit to meet the basic data specification of 10 pounds of sliding friction. Table II presents a detailed weight breakdown of each total isolator weight of 96.5 pounds.

The test vehicle attachment hardware and the system installation are shown in an assembly drawing, Figure 13, and photos, Figure 14. The transmission was bolted to a large steel plate, with the isolators suspending the fuselage through holes cut in the skin of the cabin ceiling. The lower attachment was an I-beam frame, weighing approximately 700 pounds, bolted to the lower caps of the fuselage frames. The high weight of the steel plate, approximately 1200 pounds, was offset by using a transmission without gears. This permitted the upper body to have the proper mass and center of gravity. Installation attachments were overdesigned to avoid introducing local flexibilities into the load path between the transmission and the basic fuselage. System installation was largely dictated by the location of the existing CH-53A test vehicle structural members (see Figure 13). The isolators' spacing dimensions a and b had to be compatible with the locations of the frame and longitudinal beams. Further, the pitch axis of rotation had to be located 2.4 inches aft of the desired aircraft station (station midway between the upper body cg and the rotor head where inertial and applied forces are considered to act, respectively), resulting in a small amount of pitch/vertical coupling. The transmission base was restrained in-plane to fuselage frames by four in-plane rigid rods. These rods are of equal length and are attached symmetrically about station 342 (midway between the main transmission frames) and the fuselage centerline. Again, see Figure 13. The rod arrangement introduces second-order counterclockwise yawing of the transmission plate (looking down) when the transmission plate is given small (vibratory or transient amplitudes) vertical, pitch, or roll displacements. This is due to second-order projected dimension changes of the rigid rods, and the transmission plate for the rotational

cases, in the section A-A view of the installation. Although these items are not considered problems, they should be given consideration in a new design, and should be reduced or avoided if possible.

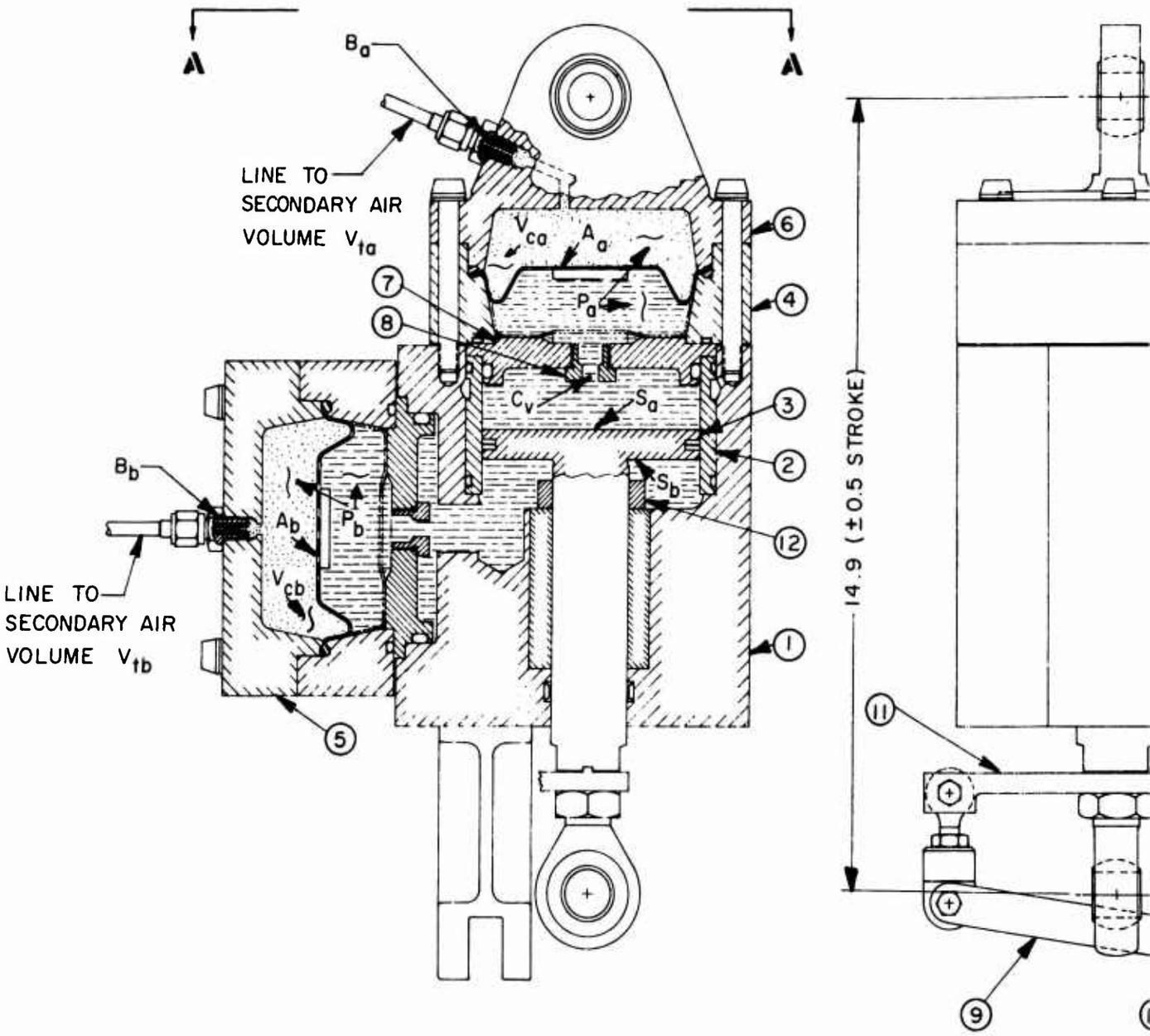

GAIN	$1/C_2$
50	12
100	6
200	3

Figure 11. Isolator Assembly Drawing.

Preceding page blank

A

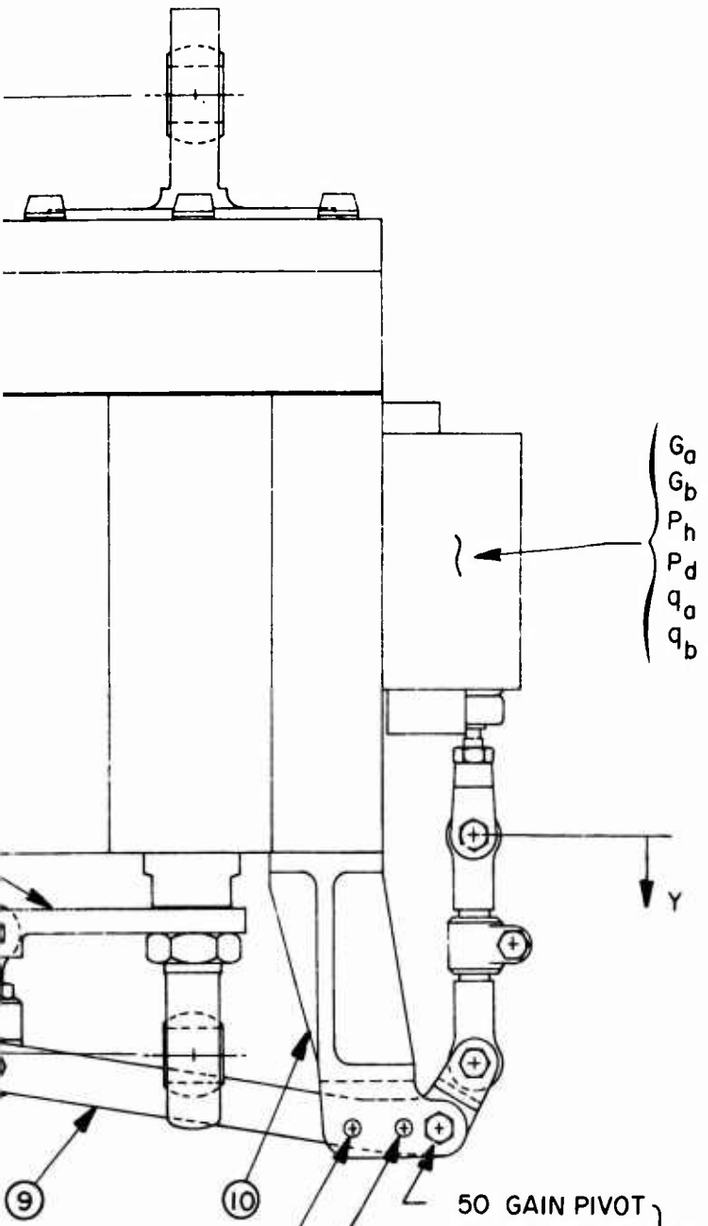

GAIN	$1/C_2$
50	12
100	6
200	3

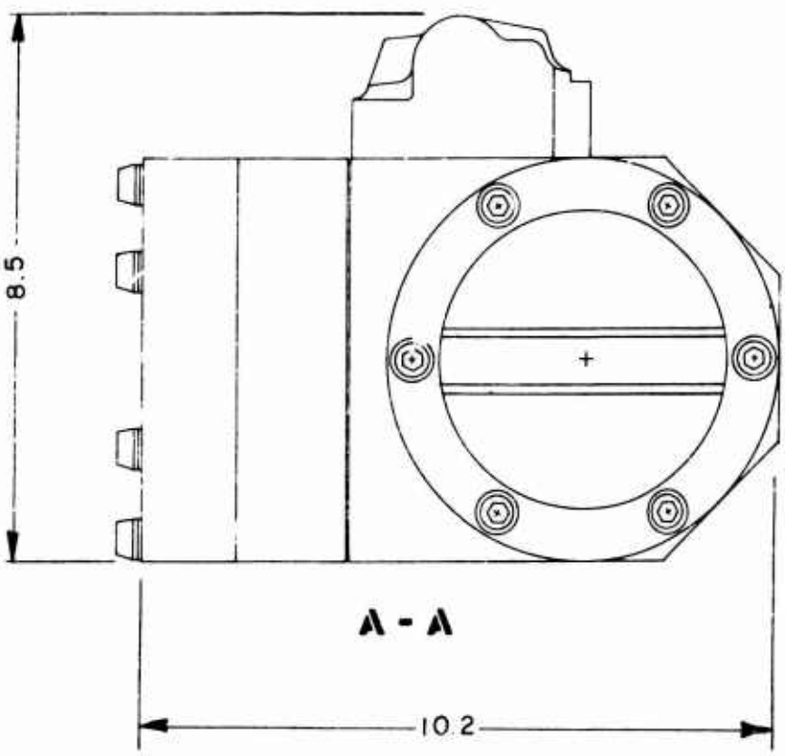

NUMBER	COMPONENT	NO. REQ'D.
1	HOUSING	1
2	SLEEVE	1
3	PISTON	1
4	BODY	2
5	CAP	1
6	CAP	1
7	ORIFICE PLATE	2
8	ORIFICE	2
9	LINK	1
10	BRACKET	1
11	ARM	1
12	PISTON STOP	1

B

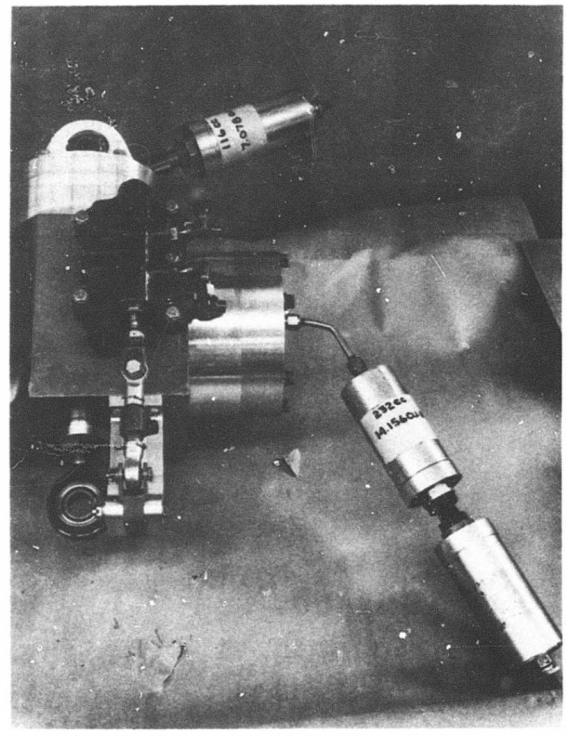

(a) Complete

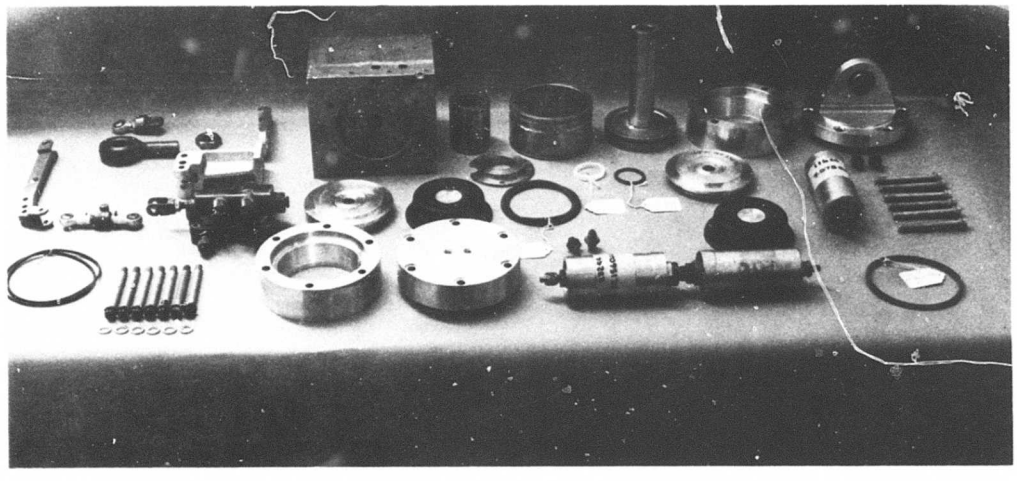

(b) Disassembled

Figure 12. Complete and Disassembled Isolator.

TABLE II. EXPERIMENTAL ISOLATOR WEIGHT BREAKDOWN

Component	Dash Number	Weight - lb
Housing	1	55.8
Sleeve	2	2.7
Piston	3	4.0
Body (2)	4	5.5
Cap	5	4.0
Cap	6	3.3
Orifice and plate (2)	7,8	1.9
Cap bolts	-	1.5
Valve housing	-	3.0
Valve linkage	9, 10, 11	2.6
Piston stop	12	0.8
Ball bushing	-	1.3
Secondary air volumes	-	5.8
Fittings	-	1.7
Oil	-	2.4
Diaphragms, seals	-	0.2
Total		96.5

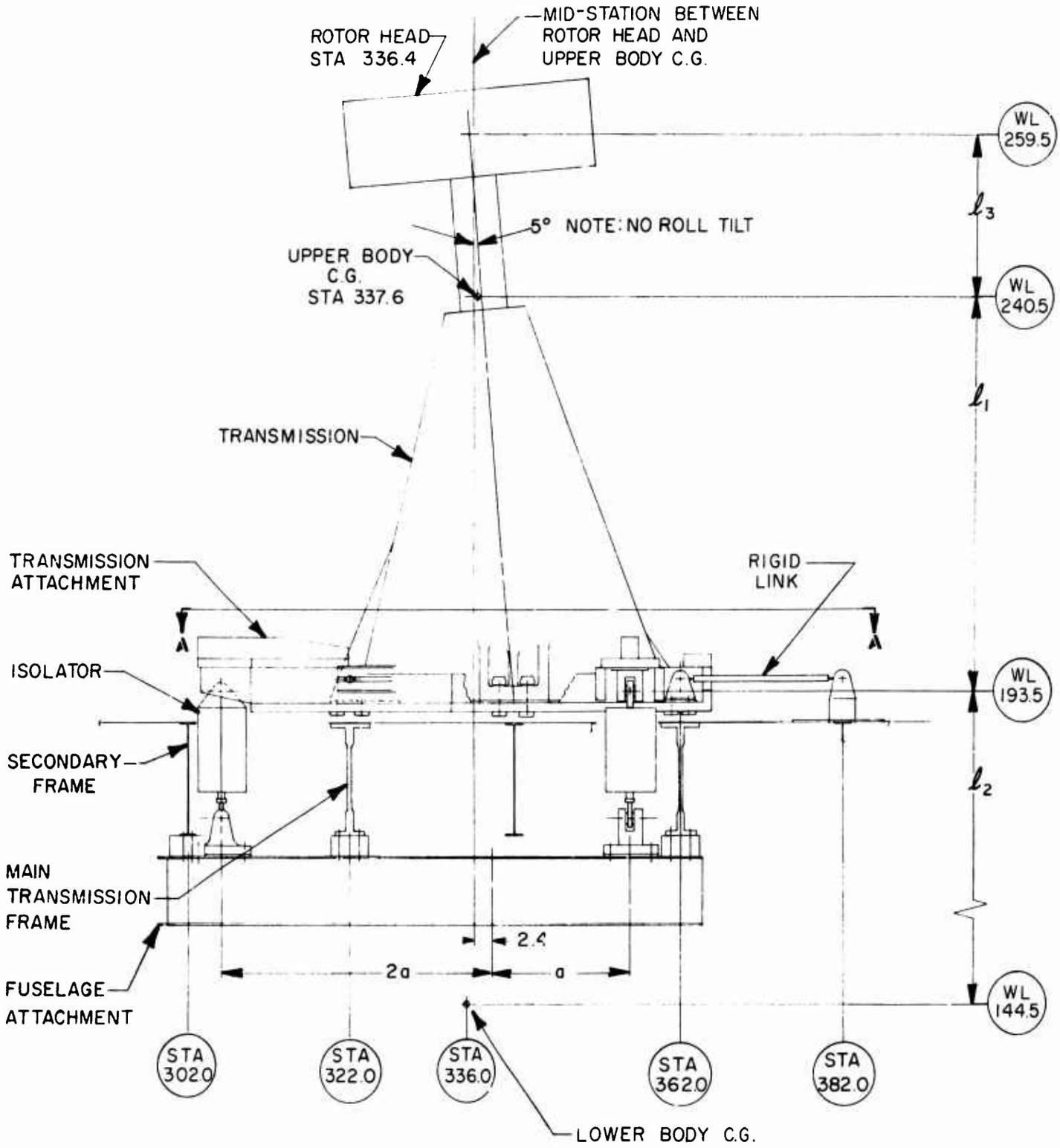

Figure 13. Installation Sketch.

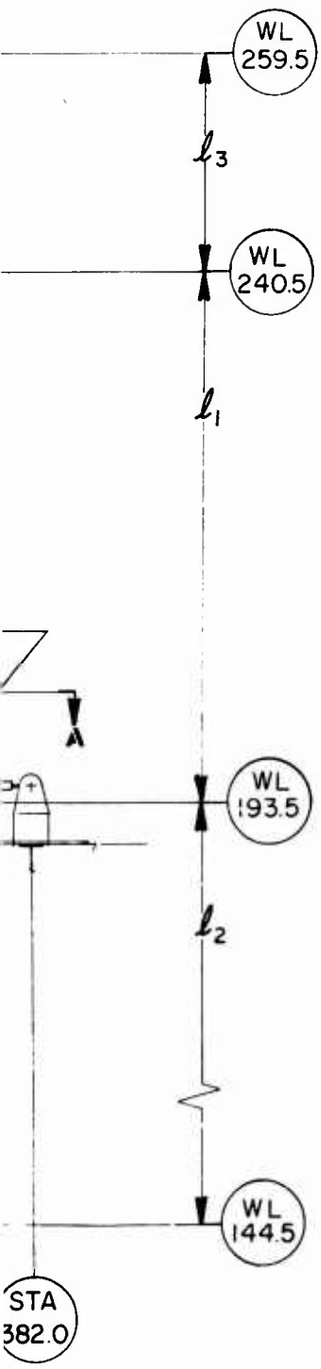
WL 259.5
ℓ_3
WL 240.5
ℓ_1
A
WL 193.5
ℓ_2
WL 144.5
STA 382.0

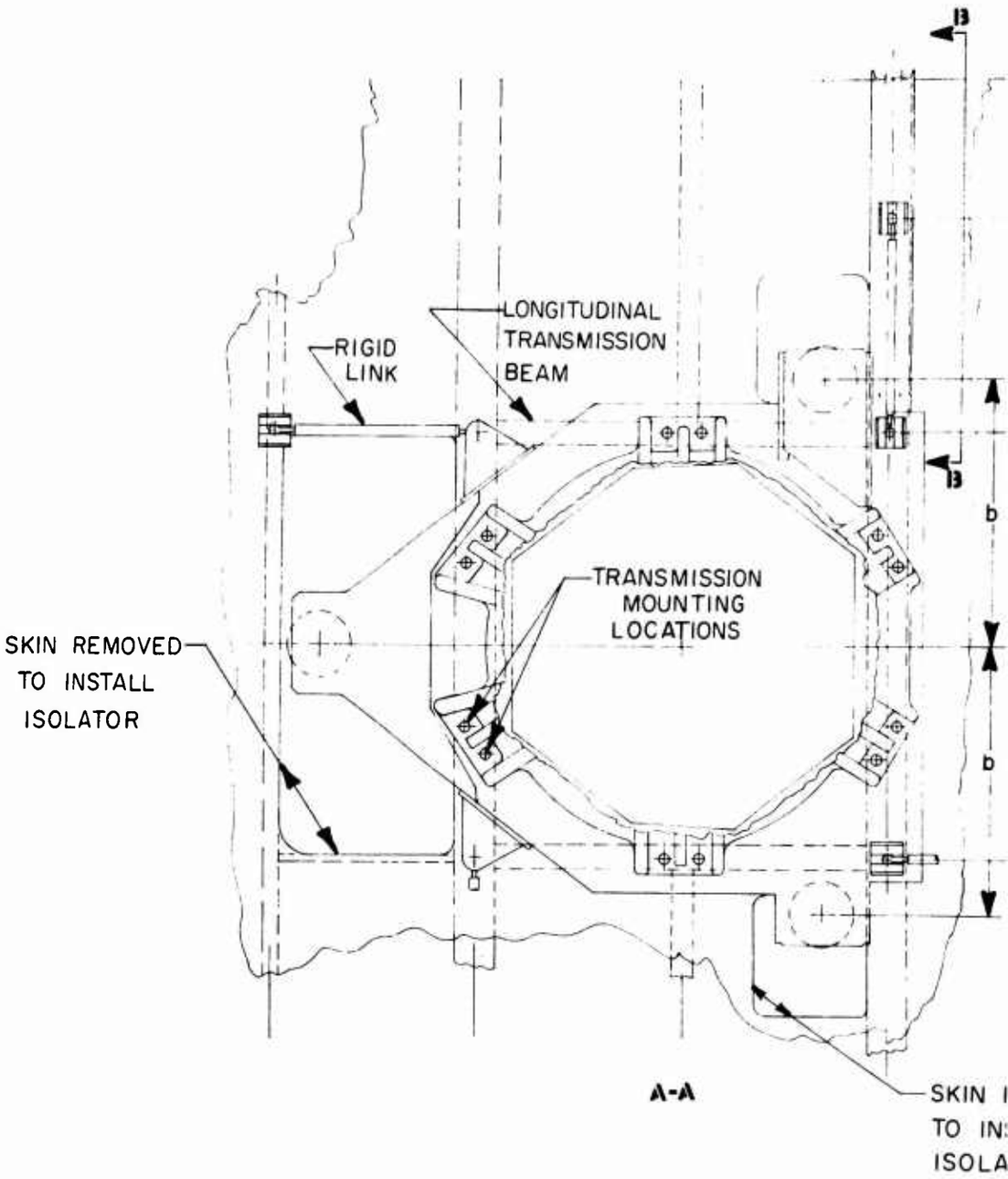
B
RIGID LINK
LONGITUDINAL TRANSMISSION BEAM
B
b
TRANSMISSION MOUNTING LOCATIONS
b
SKIN REMOVED TO INSTALL ISOLATOR
A-A
SKIN
TO IN
ISOLA

B

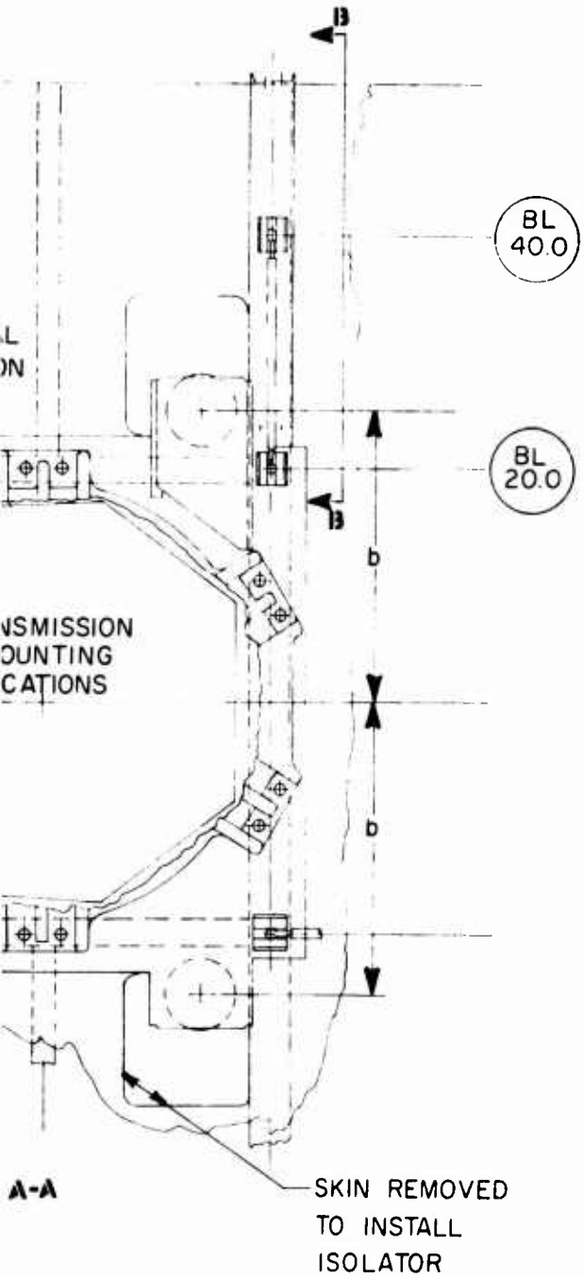
B
BL 40.0
BL 20.0
B
b
b
NSMISSION
OUNTING
CATIONS
A-A
SKIN REMOVED
TO INSTALL
ISOLATOR

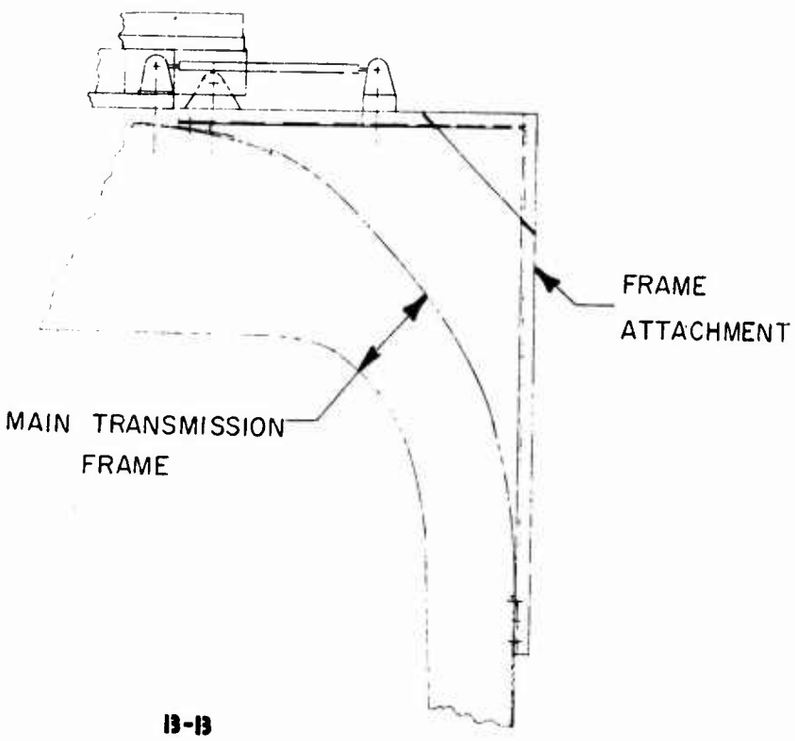
FRAME
ATTACHMENT
MAIN TRANSMISSION
FRAME
B-B

26

C

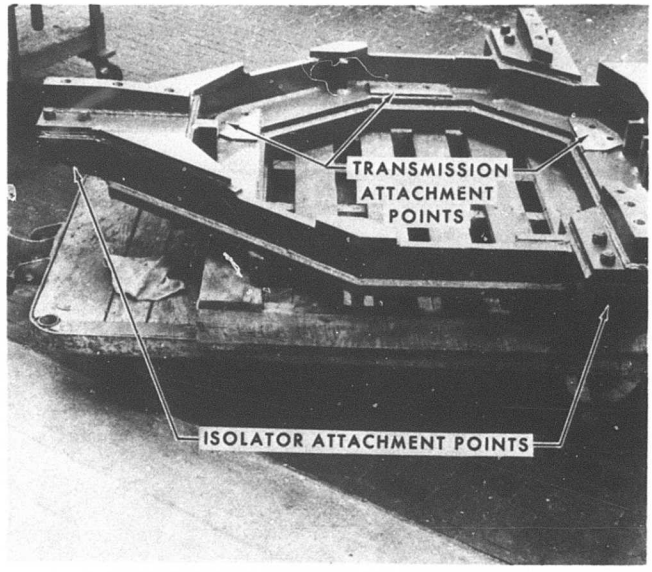

(a) Transmission Attachment

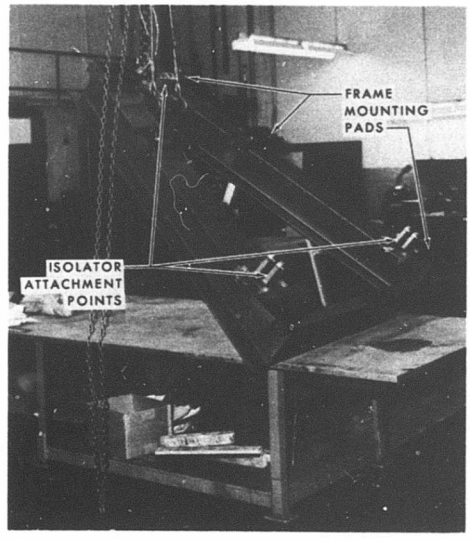

(b) Fuselage Attachment

Figure 14. Attachment Hardware and System Installation.

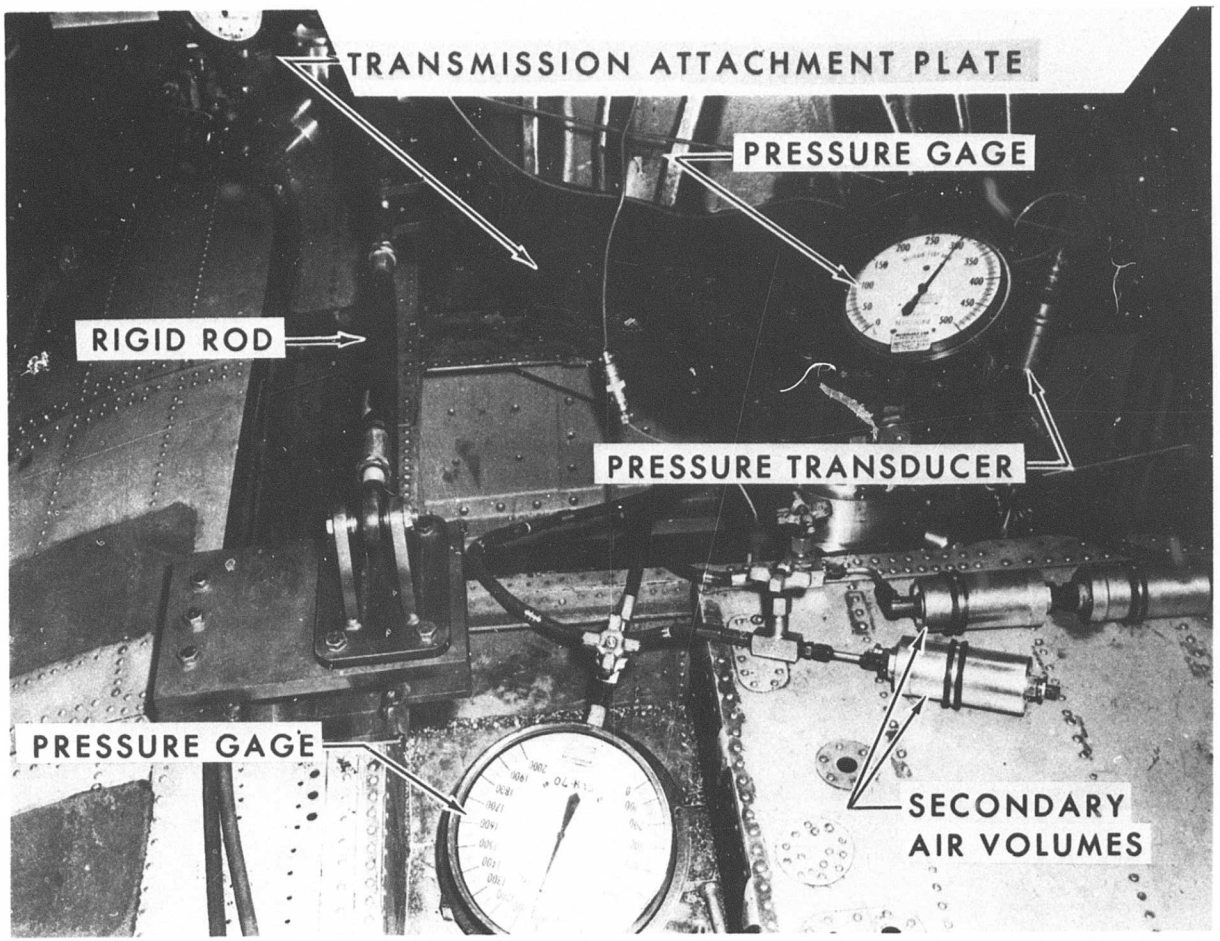

(c) Isolation System Installation - Top View

Figure 14. Concluded.

GROUND TEST EVALUATION

SYSTEM CHECKOUT

The isolators and installations underwent a preliminary checkout phase before the commencement of system test evaluation. Prior to test vehicle installation, isolator components were bench tested. After the system was installed, a final check was made of design parameters and general functional behavior of the overall system and support equipment.

Laboratory bench tests were performed to verify that internal air volumes and dimensions were in agreement with design data. Dry breakout friction was measured and found to be within 8 to 10 pounds for all three isolators, which meets the design goal of 10 pounds. The isolators were subjected to proof tests and inspected for air and oil leakage. Isolator centering was found to be precise, with no noticeable dead band.

Subsequent to installation, the test vehicle was suspended, resulting in a 1G steady isolator loading. Design spring rates were established by calculations using measurements of the isolator volumes, precharge and operating pressures. Higher operating pressures on both sides of the piston were noted. This was attributed to increased internal leakage across the lapped piston that was not previously accounted for, since this modification was made subsequent to the design analysis. Servovalve gain was reduced from 200 to 100 after excessive surging was noted in the isolator supply system when the test excitation frequency was coincident with the isolator natural frequencies. Gain predominantly affects stability and has no significant effect on 1p and 6p transmissibilities. This was confirmed by analyses and later by tests.

The hard-mounted configuration was checked to insure that no relative motion existed across the bottomed isolators. Also, the rigid restraints and attachment fittings were checked to insure that they represented a non-flexible load path from the transmission to the fuselage.

STEADY-STATE EVALUATION

The steady-state isolator evaluation was made by comparing frequency response sweeps from the isolated and hard-mounted test vehicle configurations. These sweeps were conducted from 150 to 1700 cpm (2.5 to 28.3 Hz) with a main rotor unidirectional excitation of 850 pounds at the 6p frequency for the vertical, lateral and longitudinal directions.

To negate local variations in response sensitivities resulting from changes in the fuselage mode shapes and natural frequencies. the response at the 1p and 6p frequencies was averaged over all the fuselage locations. Further averaging at the 6p frequency was achieved by using center and ±5% frequency data. The latter was not necessary at the 1p frequency since the shape and frequency of the first mode, the prime contributor to 1p response throughout the ±5% frequency range, is essentially unaltered by the isolation system.

Table III presents a comparison of the isolated and hard fuselage sensitivities and the average fuselage transmissibilities for each of the rotor-head excitations at the 6p frequency. Average transmissibilities of 0.32 for vertical excitation and 0.29 for both longitudinal and lateral excitation were obtained. These results show the large fuselage vibration reductions possible through active isolation. They also demonstrate the practicality of providing isolation to vertical and in-plane rotor-head excitations with only three vertical isolators and rigid in-plane restraints.

Table IV similarly presents the results of the 1p transmissibilities. It is demonstrated that less than a 15% increase in 1p fuselage sensitivity results with the introduction of the active isolation system. Absence of significantly increased 1p response is important for considerations of crew comfort and structural integrity of the helicopter should accidental partial blade loss occur.

These results are further discussed in the following sections. A more generalized review of the entire frequency range is provided, in addition to a discussion pertaining to analytical/test correlation.

TABLE III. 6P COMPARISON

Fuselage Location	Vertical Excitation			Longitudinal Excitation			Lateral Excitation		
	Isolated G/1000 lb	Hard G/1000 lb	Isolated / Hard	Isolated G/1000 lb	Hard G/1000 lb	Isolated / Hard	Isolated G/1000 lb	Hard G/1000 lb	Isolated / Hard
Pilot Vertical	.024	.053	[illegible]	.030	.107	.28	.026	.109	.24
Pilot Lateral	.003	.033	[illegible]	.025	.056	.45	.023	.100	.23
Copilot Vertical	.024	.082	[illegible]	.018	.074	.24	.044	.157	.28
C.G. Vertical	.031	.089	.35	.012	.073	.16	.001	.010	.10
C.G. Lateral	.019	.053	.36	.012	.051	.23	.065	.136	.48
C.G. Longitudinal	.014	.040	.35	.025	.062	.40	.002	.017	.12
Aft Cabin Vertical	.072	.210	.34	.035	.157	.22	-	-	-
Aft Cabin Lateral	-	-	-	-	-	-	.029	.083	.35
Tail Rotor Gearbox Vert.	.019	.081	.23	.030	.090	.33	.000	.031	.00
Tail Rotor Gearbox Lat.	.008	.037	.22	.017	.034	.50	.000	.019	.00
Average Transmissibility	$\frac{\Sigma \text{ Isolated}}{\Sigma \text{ Hard}} = .32$			$\frac{\Sigma \text{ Isolated}}{\Sigma \text{ Hard}} = .29$			$\frac{\Sigma \text{ Isolated}}{\Sigma \text{ Hard}} = .29$		

TABLE IV. 1P COMPARISON

Fuselage Location	Vertical Excitation			Longitudinal Excitation			Lateral Excitation		
	Isolated G/1000 lb	Hard G/1000 lb	Isolated / Hard	Isolated G/1000 lb	Hard G/1000 lb	Isolated / Hard	Isolated G/1000 lb	Hard G/1000 lb	Isolated / Hard
Pilot Vertical	.080	.072	1.11	.012	.018	0.66	.040	.040	1.00
Pilot Lateral	.056	.048	1.17	.008	.004	2.00	.052	.040	1.30
Copilot Vertical	.080	.068	1.17	.012	.018	0.67	.028	.028	1.00
C.G. Vertical	.044	.056	.79	.012	.012	1.00	.028	.028	1.00
C.G. Lateral	.060	.040	1.50	.006	.006	1.00	.040	.036	1.11
C.G. Longitudinal	.044	.048	.92	.030	.024	1.25	.024	.024	1.00
Aft Cabin Vert.	.068	.056	1.21	-	-	-	-	-	-
Aft. Cabin Lateral	-	-	-	-	-	-	.028	.020	1.40
Tail Rotor Gearbox Vert.	.100	.100	1.00	.224	.188	1.19	.028	.024	1.17
Tail Rotor Gearbox Lat.	.048	.048	1.00	.010	.008	1.25	.088	.076	1.16
Average Transmissibility	$\frac{\Sigma \text{ Isolated}}{\Sigma \text{ Hard}} = 1.08$			$\frac{\Sigma \text{ Isolated}}{\Sigma \text{ Hard}} = 1.13$			$\frac{\Sigma \text{ Isolated}}{\Sigma \text{ Hard}} = 1.13$		

Fuselage Isolation to Vertical Excitation

Frequency sweeps of the pilot vertical response in both the hard and isolated configurations are shown in Figure 15. Also shown is a sweep recorded at five times the output sensitivity through the 6p range. Comparison of these curves shows that the isolation system attenuates fuselage response from approximately 800 cpm (13.33 Hz) through the higher frequencies. This characteristic isolation is more apparent in other representative fuselage locations shown in Figure 16.

The main rotor head is of particular interest, since it is the in-flight excitation driving point and its impedance characteristics are most important in determining the resulting overall fuselage response. The transmission mode of the hard-mounted test vehicle, occurring in the 900- to 1000-cpm region, is the most significant contributor to the 6p, 1110 cpm fuselage response (note that the frequency of this mode is lower than the production CH-53A aircraft due to the weight of added support structure). Activation of the isolation system effectively attenuates this mode and introduces another vertical transmission mode at 670 cpm. This mode is much simpler, essentially involving only the transmission plus rotor mass and the stiffness of the isolation system. Thus, from approximately 800 cpm through the higher frequencies, the overall fuselage is shown to be effectively isolated. Also note that no significant increase in rotorhead response is observed by activating the isolation system.

Experimental fuselage transmissibilities compared to analytical predictions are shown in Figure 17. The analytic transmissibility curve presented corresponds to the actual isolation system gain and pressures tested. (These changes resulted in negligible 1p and 6p transmissibility differences from those based on original design values.) The experimental points plotted were obtained by an averaging technique. For each 100-cpm frequency bandwidth of the experimental sweeps, the average response was determined and then averaged over all the fuselage locations. The transmissibilities obtained were then plotted at the corresponding center frequency.

Figure 17 shows that the experimental points deviate from the analytic results at approximately 12 Hz and converge to a line that appears asymptotic to the analytic curve at higher frequencies. The generally lower experimental points shown are a result of the contribution of the hard-mounted fuselage response which is not considered in the analysis. Note the scatter over the frequency range. Although the absolute value is noticeably greater at the lower frequencies, the percentage variation is fairly constant. One of the low-frequency experimental points is questionable because of the high gradients observed in the lowest test vehicle mode frequency at 240 cpm, 4.0 Hz. The peak response was difficult to reproduce for all the sweeps recorded and used for this evaluation.

Figure 17 shows that the 1p experimental value compares very closely to the analytical curve. Therefore, the two-mass analysis accurately predicts the small 1p increase in fuselage sensitivity obtained and conservatively predicts a transmissibility to vertical excitation in the 6p region of interest.

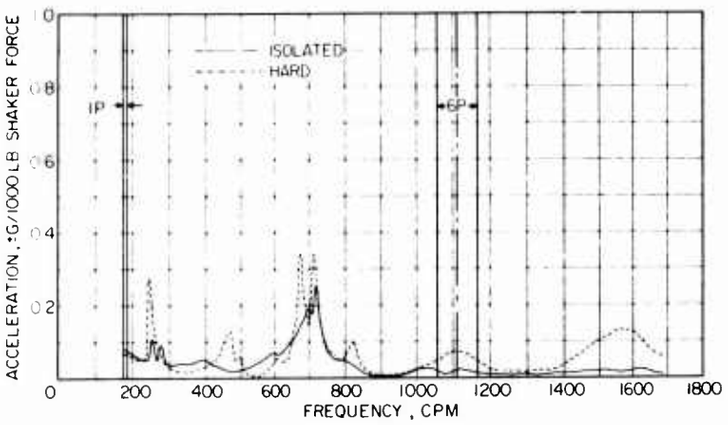

(a) Complete Sweep

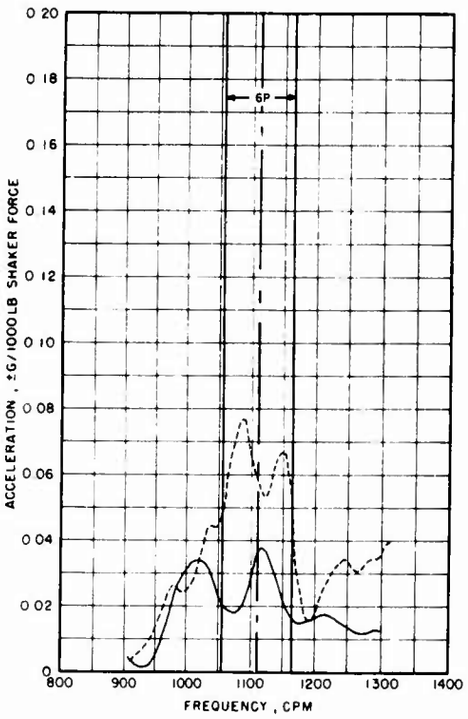

(b) Amplified Response

Figure 15. Pilot Vertical Isolated/Hard Response to Vertical Excitation.

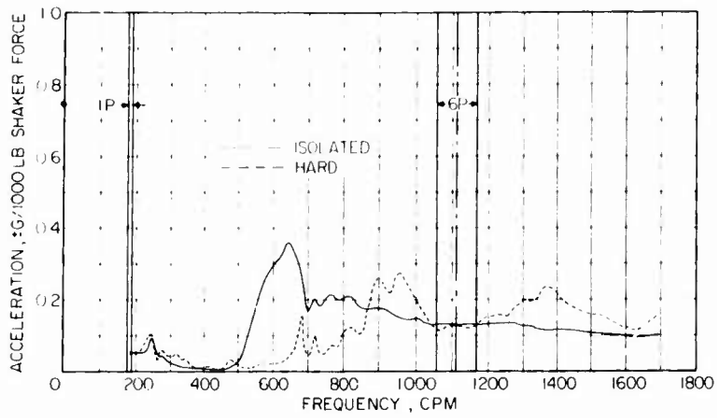

(a) Main Rotor Vertical

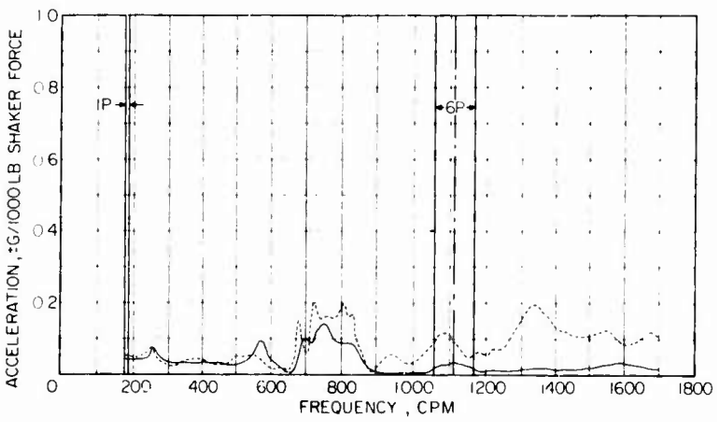

(b) Center of Gravity

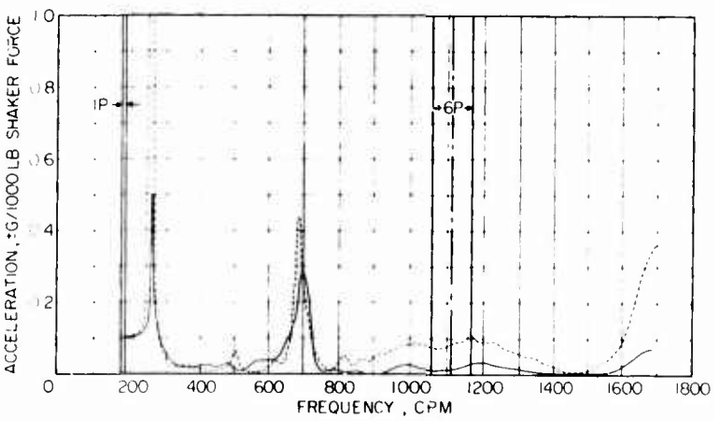

(c) Tail Rotor Gearbox Vertical

Figure 16. Representative Isolated/Hard Response to Vertical Excitation.

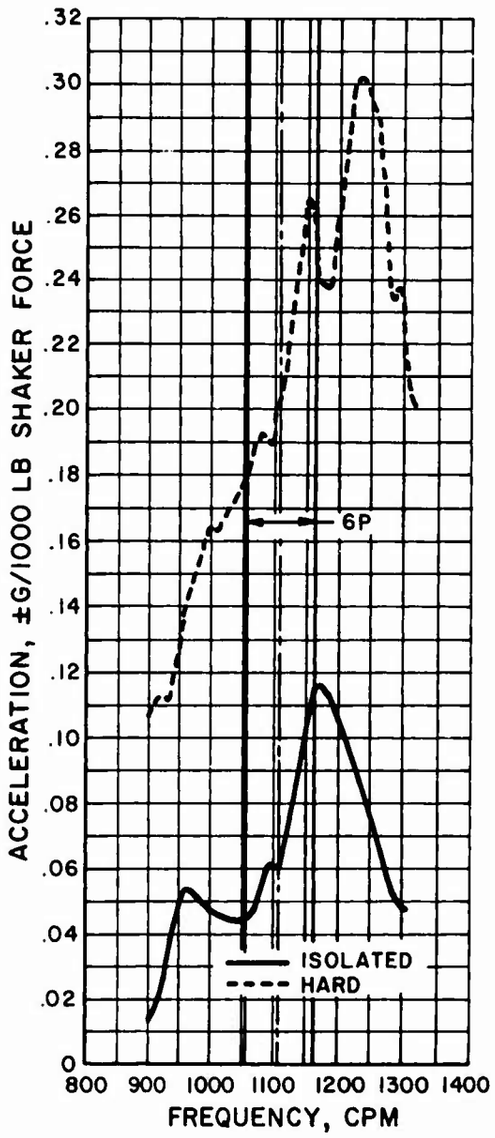

(d) Aft Cabin Vertical Amplified

Figure 16. Concluded.

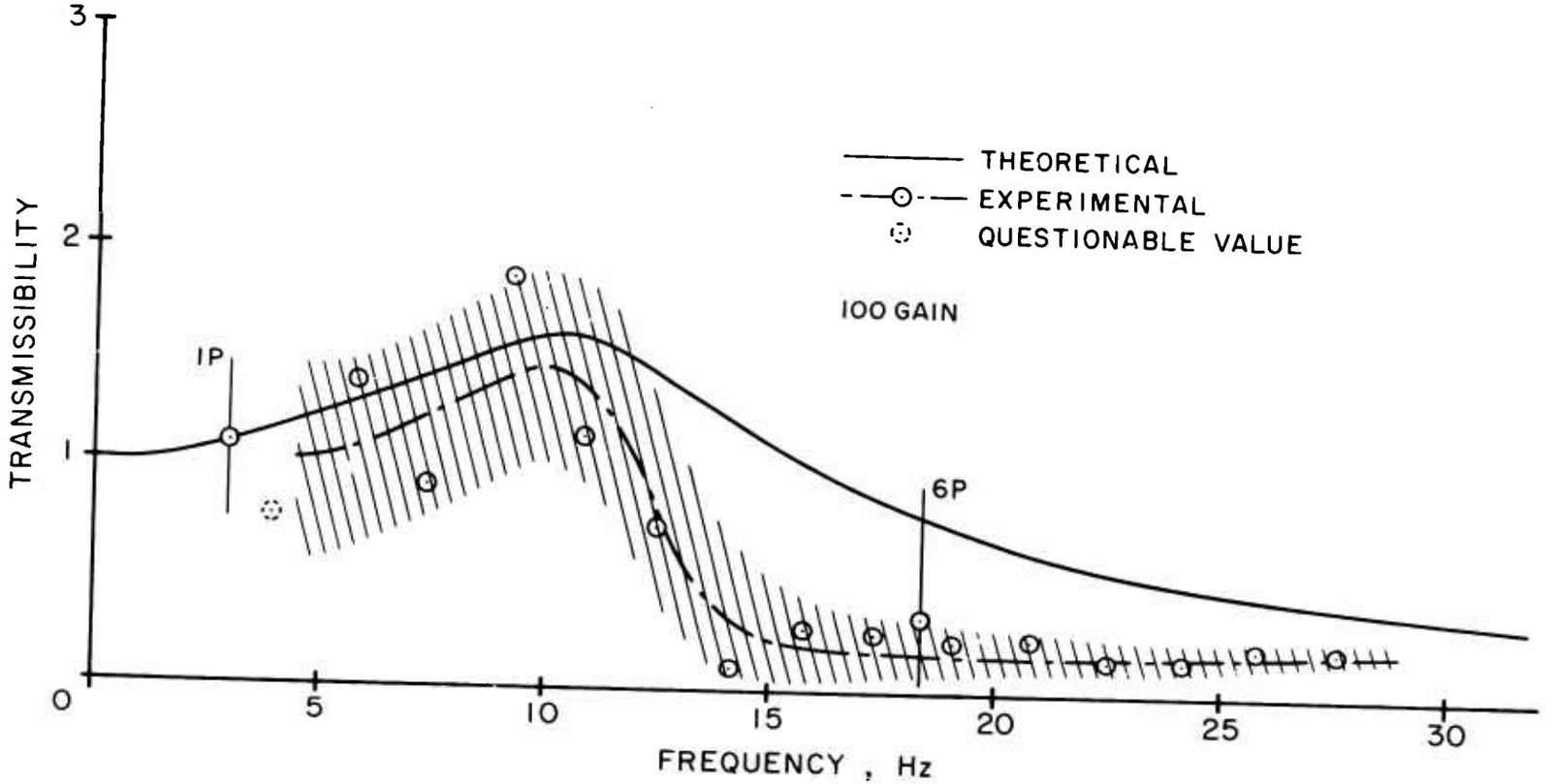

Figure 17. Analytical/Experimental Transmissibility to Vertical Excitation.

Fuselage Isolation to In-plane Excitation

Lateral and longitudinal isolation characteristics and results are very similar. Fuselage isolation to in-plane excitation using only the three vertical isolators is substantiated, and the results are compared to the analysis. Lateral results are correlated over the entire frequency range tested; longitudinal results are correlated at 1p and 6p frequencies only.

Lateral Excitation

Frequency sweeps of the pilot lateral response to lateral excitation at normal and amplified output sensitivities are shown in Figure 18. This location shows attenuation in response from approximately 500 cpm through the higher frequencies. Locations in the cabin and at the tail, shown in Figure 19, demonstrate that similar reductions are obtained throughout the test vehicle.

The main rotor-head and transmission base responses are of particular interest. The main rotor-head sweep indicates the characteristic hard-mounted test vehicle lateral transmission mode in the 700- to 900- cpm region, which is the most significant contributor to 6p response. Also note that no increase in rotor-head response is observed upon activating the isolation system and that, as shown in Figure 20, the response at the base of the transmission has been substantially reduced. This changes the motion of the upper body to a rotation about the base of the transmission, demonstrating the validity of the basic concept of providing isolation to in-plane rotor-head excitation with vertically oriented isolators and rigid in-plane restraints.

The transmission base response, Figure 20(b), shows the presence of a mode for the isolated configuration just above 200 cpm, which is not evident in the other sweeps. This response is lateral motion of the upper body relative to the fuselage. It apparently is the result of some in-plane rigid restraint attachment flexibility which was not noticed during the preliminary system checkout.

Experimental fuselage transmissibilities compared to analytical predictions are shown in Figure 21. The analytic curve corresponds to the actual isolation system gain and pressures tested. The experimental points are averages of fuselage values which were obtained using 100-cpm bandwidth evaluations. The lowest frequency value is questionable due to high response gradients.

Figure 21 shows that the line through the experimental transmissibilities has characteristic trends with little scatter. Experimental values are less than the analytic curve from 9 to 18 Hz, 550 to 1100 cpm, corresponding to the high hard-mounted test vehicle response in this region. At higher frequencies, the experimental values exceed the analytic curve, but the values are low. Also, the experimental curve might be approaching the analytical curve at the highest frequencies. Therefore, the deviations

noted may be the result of noise in the low isolated fuselage data. The 1p experimental value is shown to be lower than the analytical curve. It is concluded that the two mass analysis reasonably predicts experimental results.

Longitudinal Excitation

Frequency sweeps of the pilot vertical response to longitudinal excitation at normal and amplified output sensitivities are shown in Figure 22. The characteristic attenuation is evident in these sweeps as well as in other representative fuselage locations, shown together with the rotor-head response in Figure 23. These sweeps show fuselage response reductions from approximately 400 cpm and above.

The 6p experimental value is compared to its corresponding analytical curve in Figure 24 . A brief check was made at several other frequencies. It was noted that a complete frequency evaluation would show considerably more scatter than was shown for the lateral evaluation since longitudinal sensitivities were in general lower. However, the 6p output was sufficiently large and the transmissibility determined is considered representative.

The longitudinal rotor-head response sweep, Figure 23(a), confirms that the first test vehicle elastic mode frequency (240 cpm) is not significantly affected by activating the isolation system. Further, Table IV and Figure 24 indicate that only a small increase in 1p experimental fuselage sensitivity is experienced, and that the analytical results are substantially higher. The two-mass mathematical model might not be adequate in the low frequency region,but it is at least conservative.

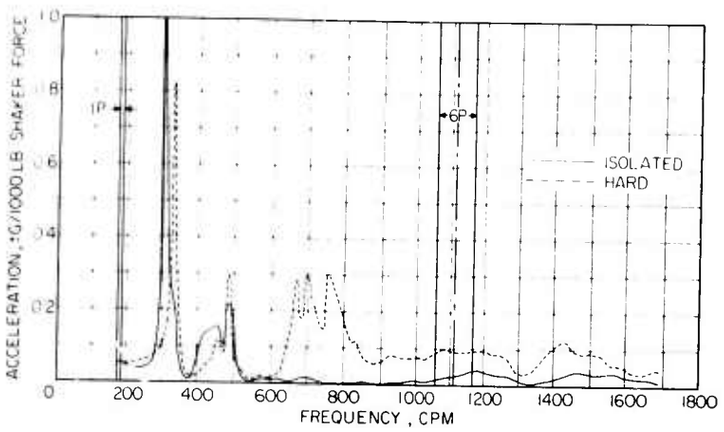

(a) Complete Sweep

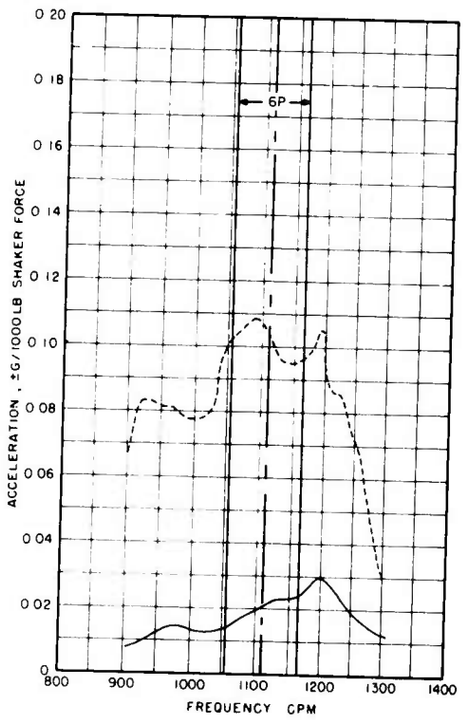

(b) Amplified Response

Figure 18. Pilot Lateral Isolated/Hard Response to Lateral Excitation.

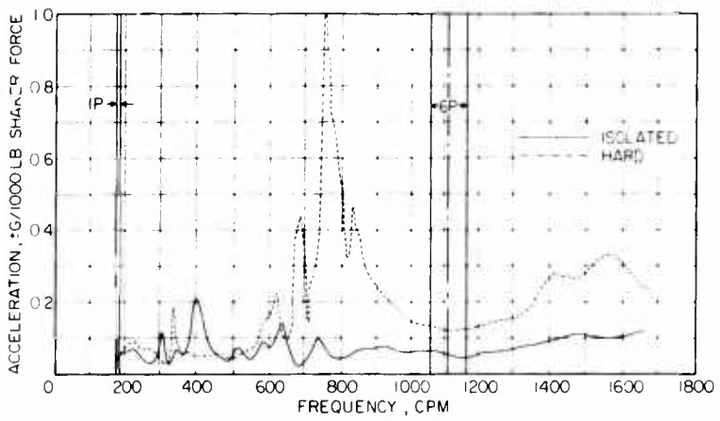

(a) Center of Gravity Lateral

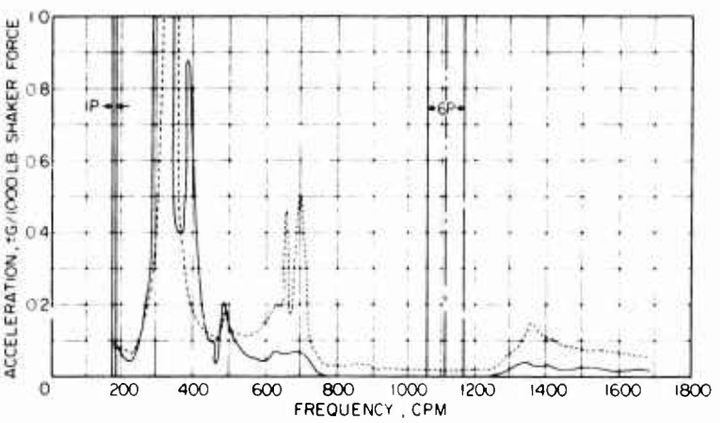

(b) Tail Rotor Gearbox Lateral

Figure 19. Representative Isolated/Hard Response to Lateral Excitation.

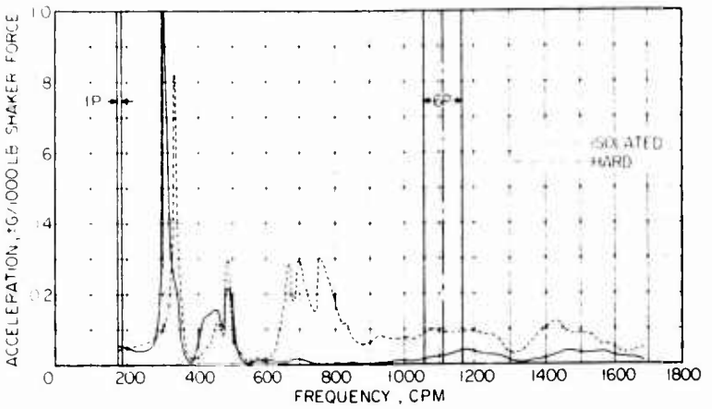

(a) Complete Sweep

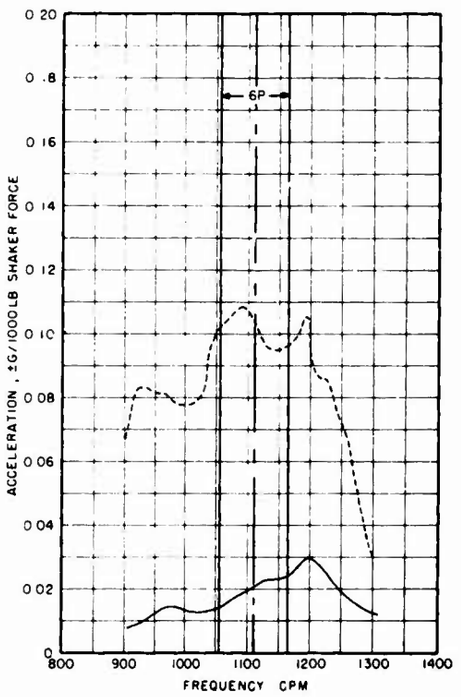

(b) Amplified Response

Figure 18. Pilot Lateral Isolated/Hard Response to Lateral Excitation.

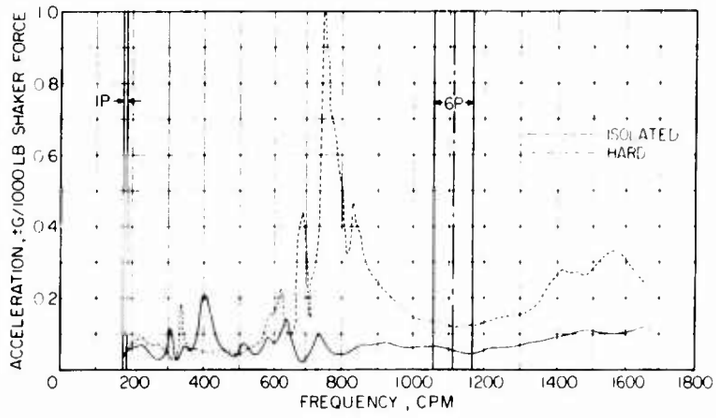

(a) Center of Gravity Lateral

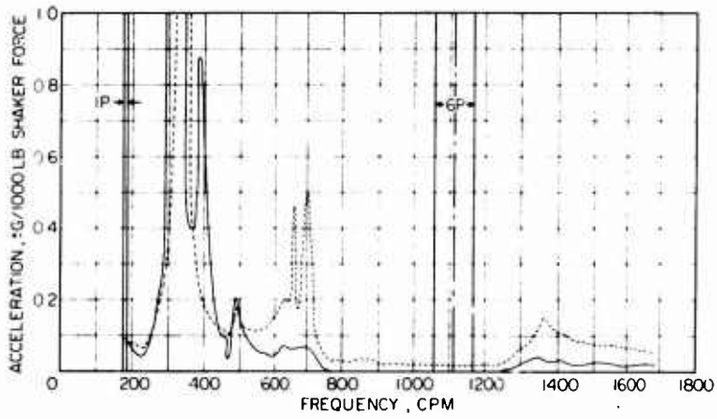

(b) Tail Rotor Gearbox Lateral

Figure 19. Representative Isolated/Hard Response to Lateral Excitation.

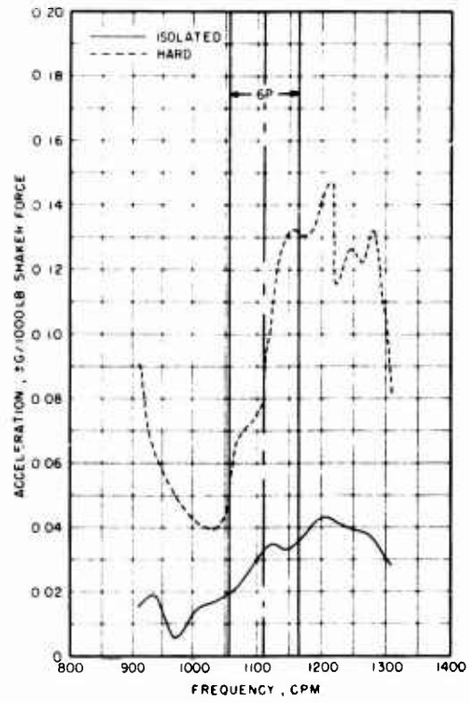

(c) Aft Cabin Lateral Amplified

Figure 19. Concluded.

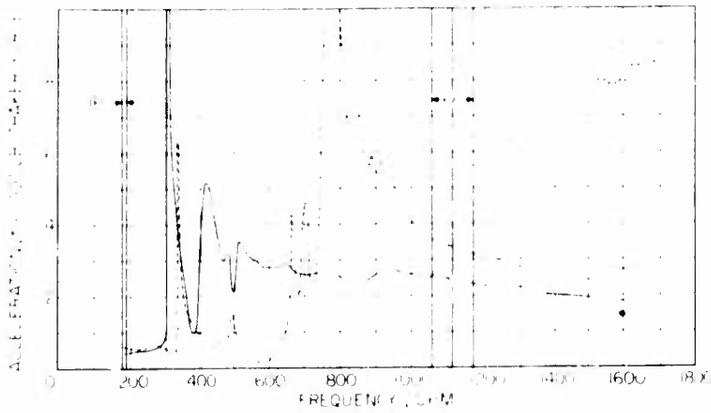

(a) Main Potor Lateral

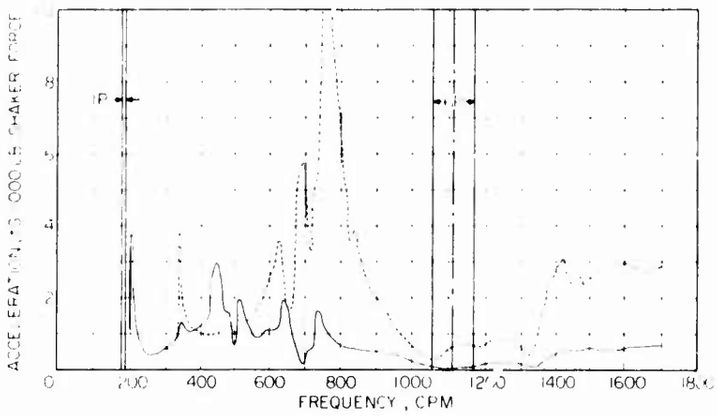

(b) Transmission Base Lateral

Figure 20. Main Rotor and Transmission Base Response to Lateral Excitation.

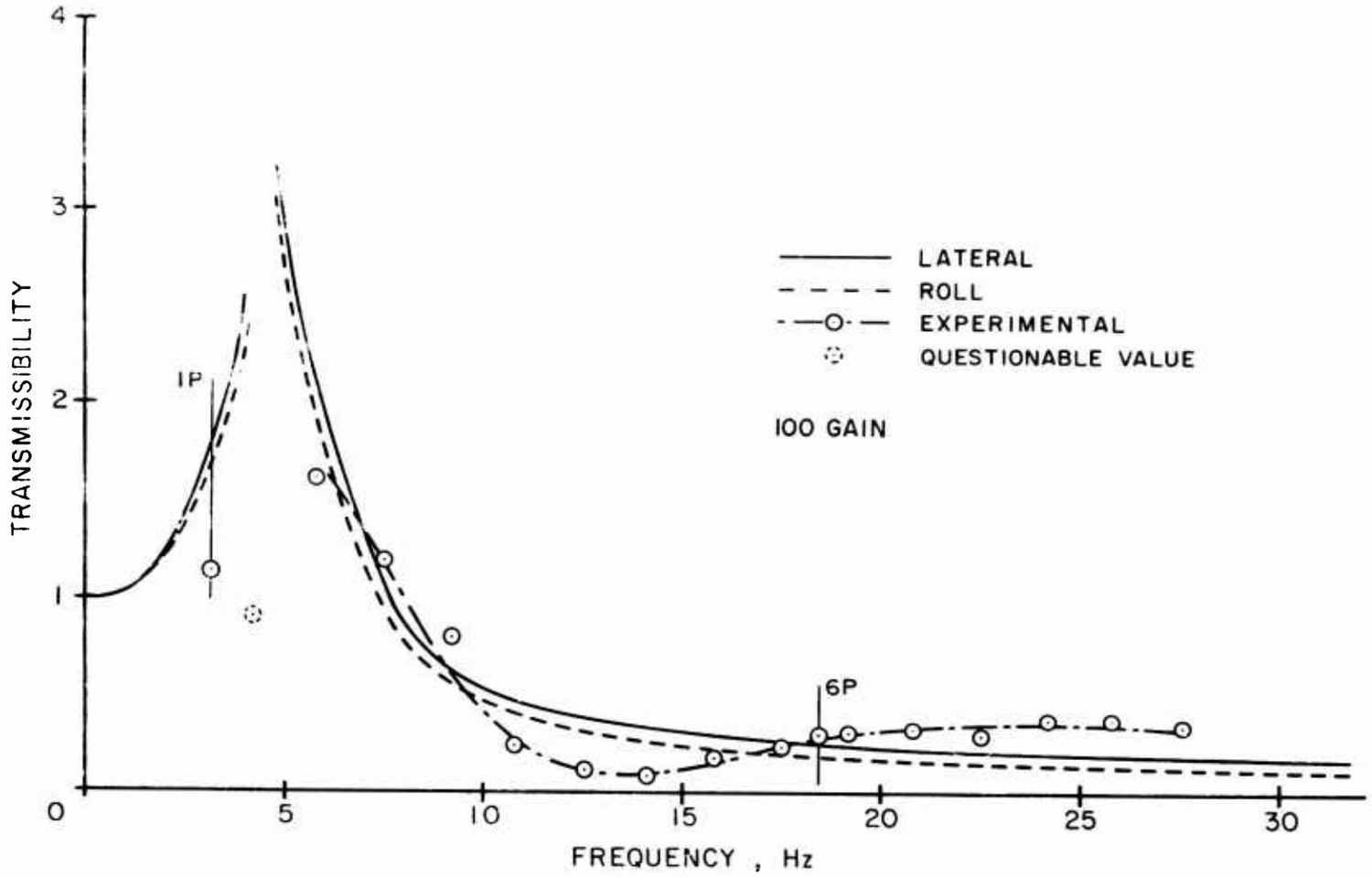

Figure 21. Analytical/Experimental Transmissibility to Lateral Excitation.

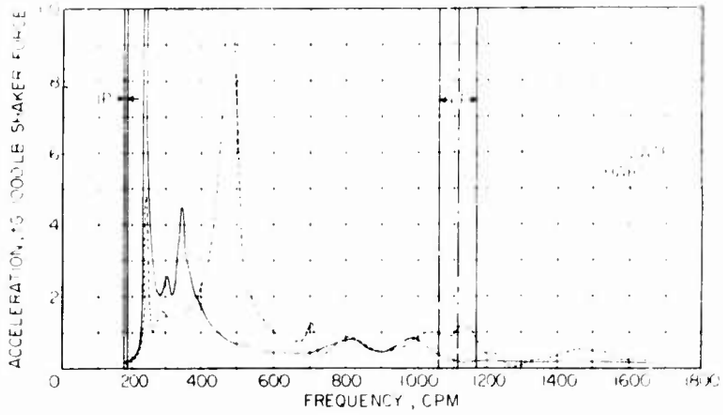

(a) Complete Sweep

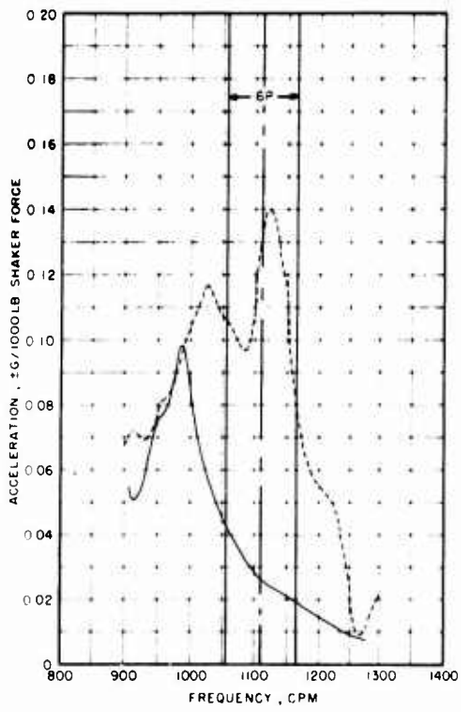

(b) Amplified Response

Figure 22. Pilot Vertical Isolated/Hard Response to Longitudinal Excitation.

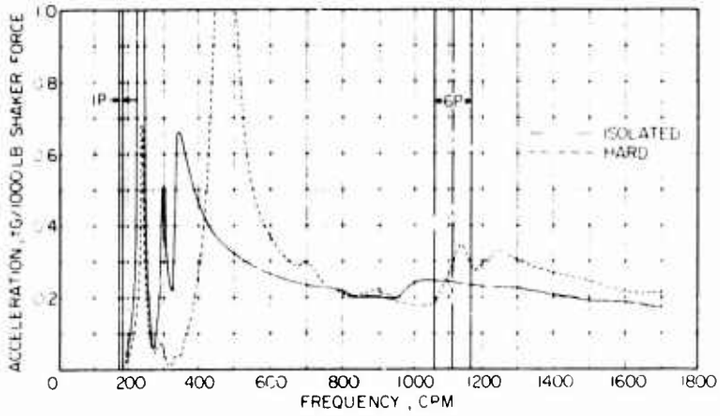

(a) Main Rotor Longitudinal

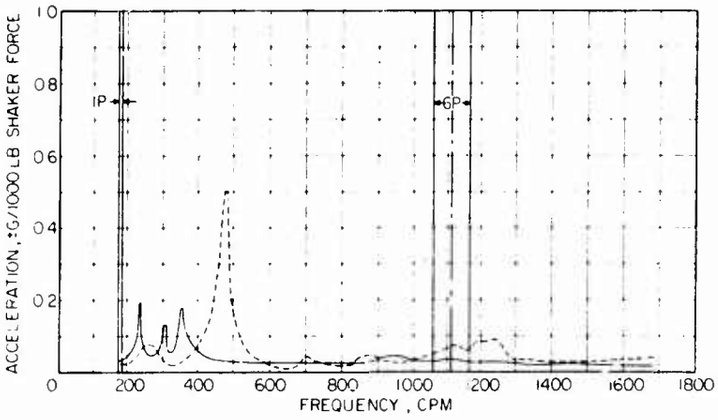

(b) Center of Gravity Longitudinal

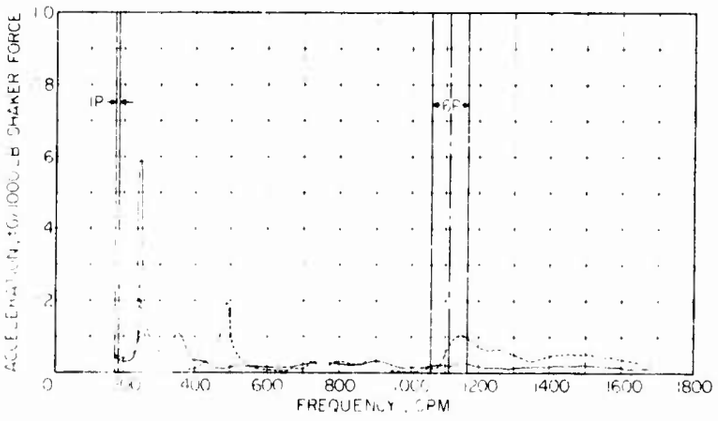

(c) Center of Gravity Vertical

Figure 23. Representative Isolated/Hard Response to Longitudinal Excitation.

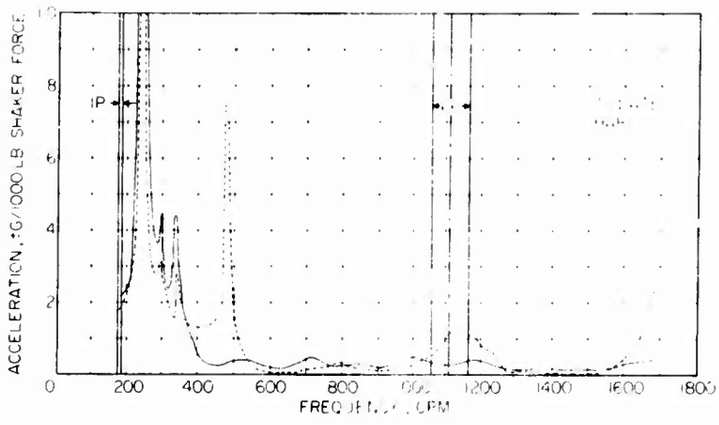

(d) Tail Rotor Gearbox Vertical

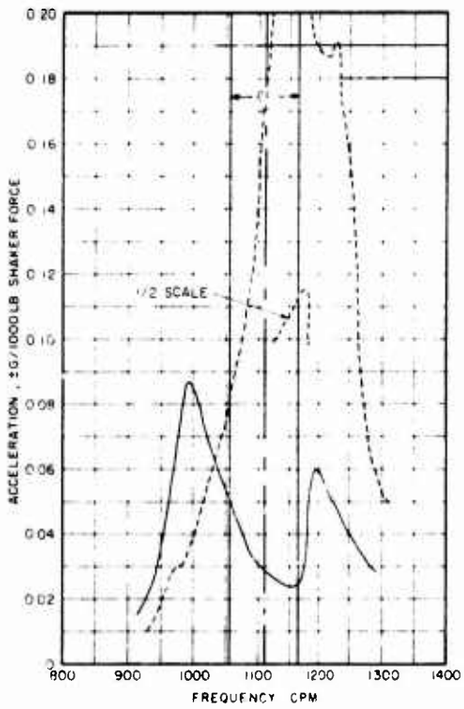

(e) Aft Cabin Vertical Amplified

Figure 23. Concluded.

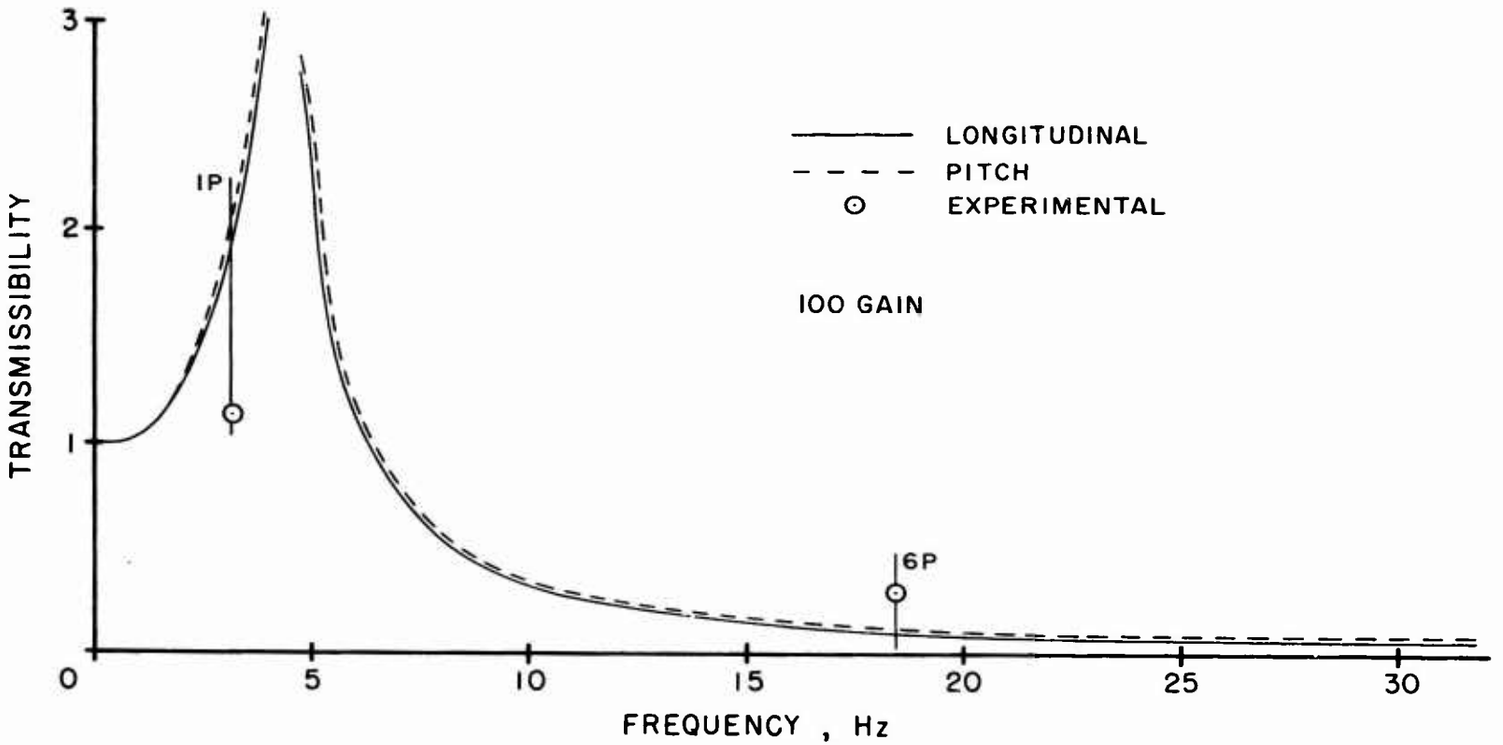

Figure 24. Analytical/Experimental Transmissibility to Longitudinal Excitation.

ISOLATOR MEASUREMENTS

Isolator parameters were measured while the test vehicle was constantly excited at the 6p and 1p frequencies. At both frequencies of excitation, in all three directions, the total flow required, as well as the mean isolator operating pressures, remained constant. The flow rate of 0.97 gpm at the system supply pressure of 3000 psi results in a constant power requirement of 1.7 horsepower obtained from the relationship

$$hp = \frac{1}{1720} P_h Q$$

where P_h = supply pressure, psi

Q = total flow rate, gpm

A check made during no excitation also resulted in a continuous 0.97-gpm requirement. It is concluded that this power requirement is associated with piston and/or servo spool leakages.

Vibratory pressures and displacements at the 6p frequency are presented in Table V together with the resultant force calculated from the pressures and associated piston areas. Limitations in reading oscillograph traces limit the resolution of these measurements to ±0.002 inch for the displacements and ±0.15 psi and ±0.45 psi for the low and high vibratory pressures based on distinguishing a 0.010 variation in the traces. This results in a ±6-pound uncertainty in vibratory force. For all directions of excitation, the port and starboard isolators should experience the same forces; however, the table indicates that it definitely was not responding in the same manner as the port isolator. Disassembly after the test indicated that the starboard isolator had a higher friction level due to scoring of the piston sleeve.

Table VI presents the 1p vibratory measurements. The vertical excitation was not sufficient to produce any readable output; most of the excitation was transferred by isolator friction rather than through the fluid. In the longitudinal and lateral directions, amplifications are indicated, again with the starboard isolator showing less response than the port.

A comparison of the vibratory displacements obtained and those predicted by the linear rigid-body analysis is presented in Table VII. As shown, when relative angular motions are computed from the previous tables, the pitch and roll displacements compare favorably with analysis. However, the vertical displacements are much smaller than predicted. Damping as well as gain nonlinearities might be factors accounting for the deviations of these results.

TABLE V. 6P ISOLATOR MEASUREMENTS

Measurement		Vertical Excitation ±850 lb			Longitudinal Excitation ±850 lb			Lateral Excitation ±850 lb		
		Port Isolator	Forward Isolator	Starboard Isolator	Port Isolator	Forward Isolator	Starboard Isolator	Port Isolator	Forward Isolator	Starboard Isolator
Displacement (in.)		±.0023	±.0013	±.0022	±.0015	±.0025	±.0011	±.0021	±.000	±.0013
Pressures* (psi)	High	±6.9	±2.7	±4.1	±4.3	±4.5	±1.4	±5.9	±0.0	±4.1
	Low	±5.1	±6.9	±3.0	±2.7	±2.1	±1.8	±4.2	±1.2	±2.3
Transmitted Vibratory Force (lb)		±78.	±65.	±46.	±45.	±42.	±21.	±65.	±9.	±41

*Shown are vibratory levels measured during shake testing. Steady pressures were set according to design values shown in Table I.

TABLE VI. 1P ISOLATOR MEASUREMENTS

Measurement	Vertical Excitation ±32.4 lb			Longitudinal Excitation ±32.4 lb			Lateral Excitation ±32.4 lb		
	Port Isolator	Forward Isolator	Starboard Isolator	Port Isolator	Forward Isolator	Starboard Isolator	Port Isolator	Forward Isolator	Starboard Isolator
Displacement(in.)	±.000	±.000	±.000	±.0015	±.0025	±.0017	±.0015	±.000	±.0008
Pressures (psi) High	±0.0	±0.0	±0.0	±4.5	±3.6	±4.1	±5.6	±0.0	±3.1
Low	±0.0	±0.0	±0.0	±3.3	±16.2	±1.8	±3.6	±4.3	±1.9
Transmitted Vibratory Force (lb)	±0.0	±0.0	±0.0	±50.0	±137.	±37.	±61.0	±30.2	±32.7

TABLE VII. COMPARISON OF TEST AND ANALYSIS - 1P AND 6P ISOLATOR DISPLACEMENTS

Relative Motion/Excitation	6P ±850 lb		1P ±32.4 lb	
	Test	Analysis	Test	Analysis
Vertical/Vertical (in.)	.0019	.0060	.000	.011
Pitch/Longitudinal (rad X 10^{-3})	.0768	.0714	.0830	.0880
Roll/Lateral (rad X 10^{-3})	.0630	.0800	.0425	.0704

PARAMETRIC VARIATION

Several changes in isolator damping, stiffness, and gain were investigated to verify that 6p transmissibilities were unaffected. Isolation system modes were stable, as predicted by analysis. However, two unstable modes involving the rigid-body modes of the test vehicle on the suspension system were observed.

No significant change in isolation was observed for changes in isolation damping and stiffness. Frequency sweeps of the pilot vertical-to-longitudinal excitation are shown in Figure 25(a). These three sweeps indicate that no significant change in 6p isolation occurred when air damping was eliminated and when the spring rate was also decreased by 32% at the 6p frequency. Air damping was eliminated by blocking off the capillary air flow restrictions. Spring rate was altered by changing the internal air volume. It was not possible to observe the change in frequency of the isolation mode because simultaneously blocking off the air damping restriction results in a compensating increase in stiffness at low frequencies. Orifice fluid damping was not varied, since the system performed as predicted and this change would have required disassembly of the isolators. The two-mass linear analysis has shown that a 12% increase in equivalent viscous damping would result in a 6% increase in vertical transmissibility and a 3% increase in in-plane transmissibility.

Figure 25(b) presents sweeps of the pilot vertical to longitudinal response for all three isolator gain settings of 50, 100, and 200. Gain was varied by changing C_2, the feedback element linkage ratio (see Figure 11). As expected, no significant change in isolation is observed. By comparing previously presented analytical transmissibility plots for gains of 200 and 100 (Figures 9 and 24 respectively), it is shown that no change in isolation was predicted. These results indicate that isolation damping, stiffness, and gain may be substantially altered from their design values without degrading 6p isolation.

Analysis showed that isolation gain has a significant effect on system stability and transient response characteristics (results of a cursory transient evaluation are presented in the next section). The effect of gain changes on stability is best illustrated by analytic root locus plots. Stability is indicated by the presence of negative real parts of the transfer function roots. Increased stability is indicated by an increase in the angle made by a line drawn through the root and the plot's origin, and the corresponding imaginary ordinate (positive ordinate for a positive root), when a system variable is changed (see Figure 25(c)). Each plot shows a pair of complex roots with increasing angles as gain is changed from 200 to 100, thus indicating increased stability. Further, these pairs of complex roots can easily be identified as the isolator rigid body modes since their circular frequency vector magnitudes correspond to the mode frequencies evident in their associated transmissibility plots. During test, stability was confirmed when no corresponding isolator mode instabilities were observed for all three gain settings.

However, the isolation system did interact with two of the rigid-body modes

of the test vehicle on the suspension system. One involved the entire test vehicle pitching about its rotor-head attachment to the bungee system at 0.5 Hz. This oscillation, once excited, was sustained by the isolation system in all three gain settings of 50, 100, and 200. The second oscillation observed was a vertical response of the entire test vehicle on its suspension system at approximately 1 0 Hz, occurring during longitudinal excitation sweeps. This oscillation was evidenced only at the 200 gain setting.

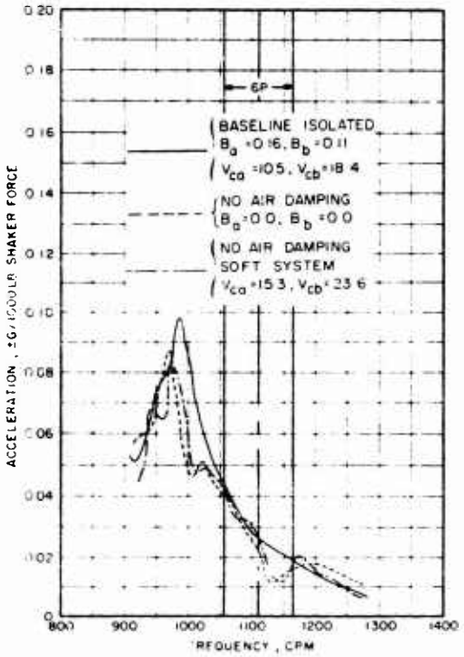

(a) Effect of Change in Damping and Stiffness on Pilot Vertical to Longitudinal Excitation.

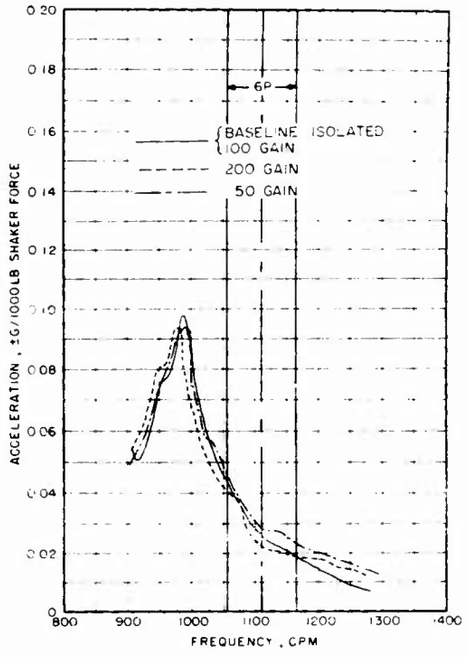

(b) Effect of Change in Gain on Pilot Vertical to Longitudinal Excitation.

Figure 25. Effect of Changes in Damping, Stiffness, and Gain.

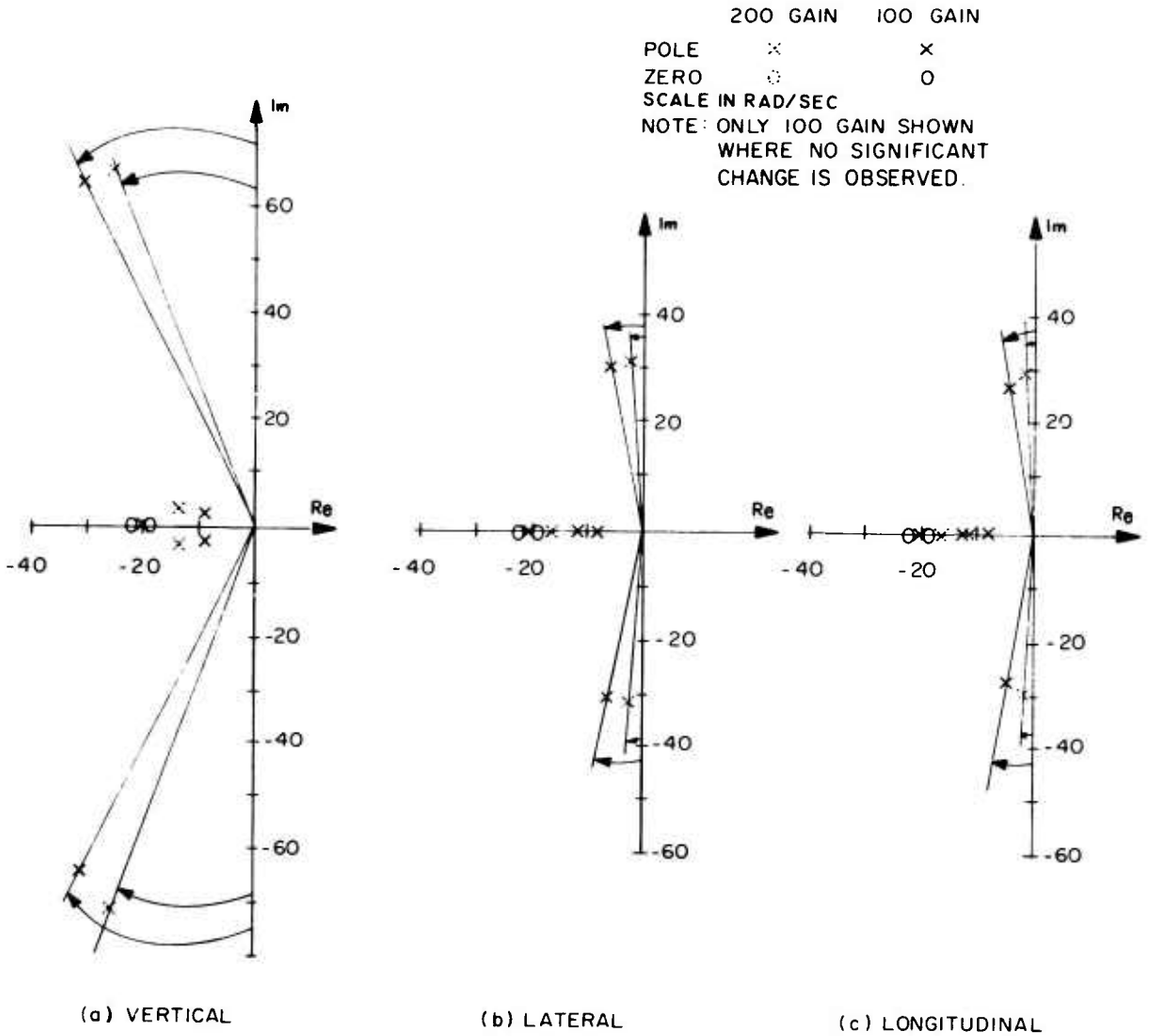

(a) VERTICAL (b) LATERAL (c) LONGITUDINAL

(c) Effect of Change in Gain on System Stability

Figure 25. Concluded.

TRANSIENT TEST

A cursory test was conducted to evaluate the transient response of the active system. Longitudinal step input loads were applied to the main rotor head while the relative isolator displacements were measured.

The test setup is shown in Figure 26. A cable was preloaded between the rotor head and the aircraft for the purpose of applying an instantaneous change in horizontal force upon release. By attaching to the base of the tail pylon, a nearly horizontal location was obtained. Attaching at the base avoided significant tail deflections or stored potential energy, which would have upon release caused undesired excitation, particularly to the aircraft's first mode. Further, although an equal and opposite force was applied to the lower body or fuselage, its inertia is an order of magnitude larger than the transmission and rotor head, making the response due to the reaction force negligible. This loading can also be considered an instantaneous change in applied moment to the upper body. The couple distance is from the rotor head to the base of the transmission, where there is an internal equal and opposite reaction force to the fuselage. Again, this internal reaction force can be neglected.

A time history of the relative angular deflection of the transmission and fuselage to a step load of 1500 pounds is shown in Figure 27, together with the response predicted by the rigid-body analysis. This particular time history is with the isolation system at a gain of 100. As shown, the linear rigid-body response closely predicts the actual results.

The second order variations in the time history are attributed to system nonlinearities and the response of elastic fuselage modes. A detailed inspection of the waveform reveals at least the contribution of the aircraft's first mode at approximately 4 Hz in addition to the isolators' mode at approximately 5 Hz. Periods for these frequencies are 0.25 and 0.20 second, which can be observed in the time histories. The relative contribution of this airframe response and the system's nonlinearities to the noted variations has not been quantitatively determined.

Figure 28 is a plot of peak deflection versus force applied for all the test conditions. In all cases, the experimental overshoots were less than predicted, with the 200 gain analytic line closely fitting the 100 gain test points. This could be attributed to nonlinearities in the servovalve flow gain. If desired, nonlinearities could be tailored through detail design of the servo.

A CH-53A cyclic input of approximately 1 degree, 1/2 inch of stick travel would result in the same moment about the aircraft center of gravity as supplied by the maximum load tested. In flight, this input would take approximately 0.05 second to develop, so the actual response might be noticeably less. However, consideration of actual response is limited, since no extrapolation to maximum loads can be made; maximum loads, approximately five times greater, have decreasing rates of application. To accurately establish the isolators' response to maximum inputs, a time history of each load should be applied to a system model which includes the

more important isolator nonlinearities.

Another consideration is that maximum isolator loads resulting from flight maneuvers can exceed the +3G design load of the isolation system. For flight application, it might be desirable to let the isolators bottom for infrequently applied loads.

In summary, a critical maneuver was selected and the vehicle was tested to approximately 20% of its range at a more severe rate of application. Measurements confirmed analytical response remarkably well and demonstrated that the system deflections are within the established design allowables. However, during the cursory investigation of maneuver loads, it was concluded that a more comprehensive load spectrum should be established and evaluated.

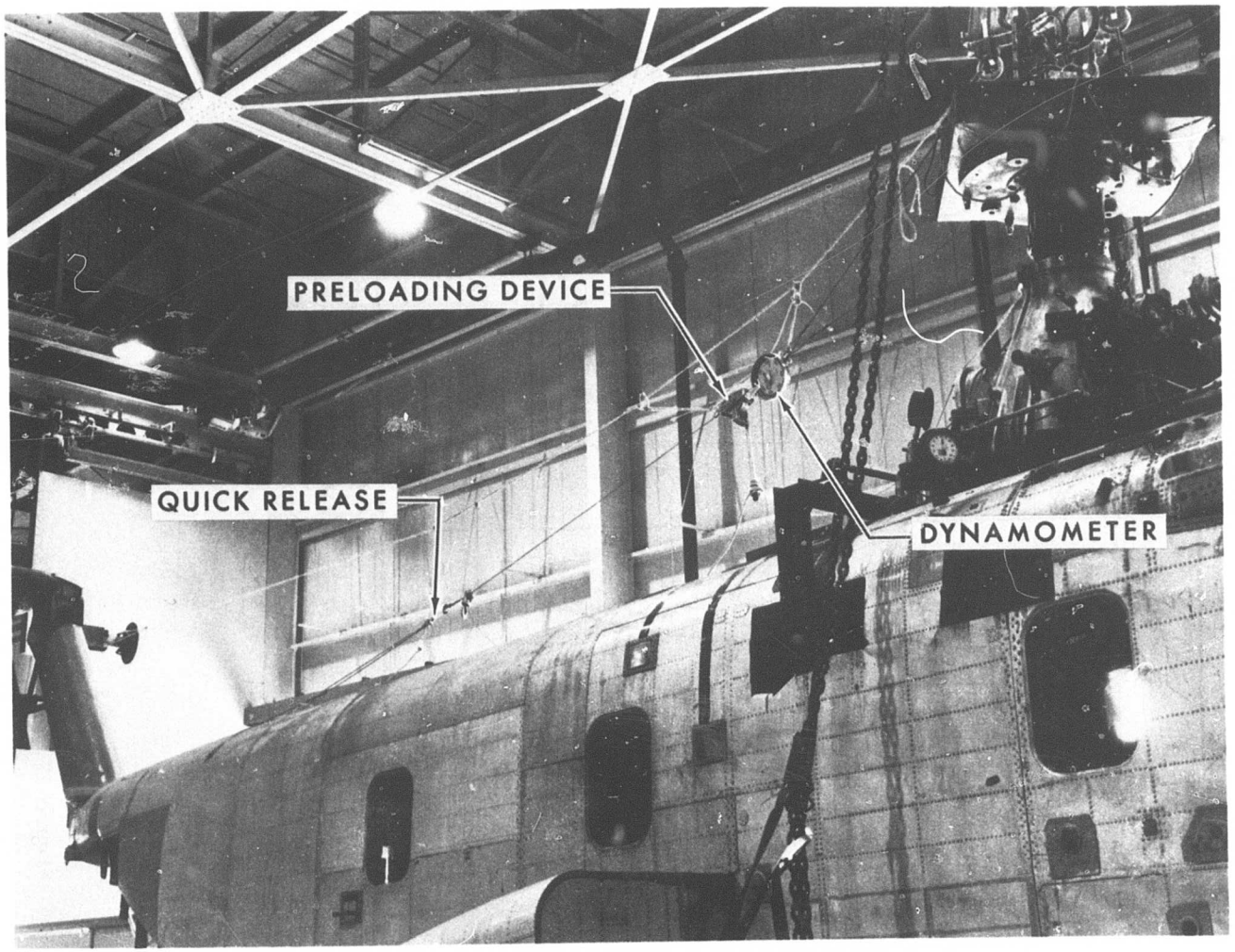

Figure 26. Transient Test Apparatus.

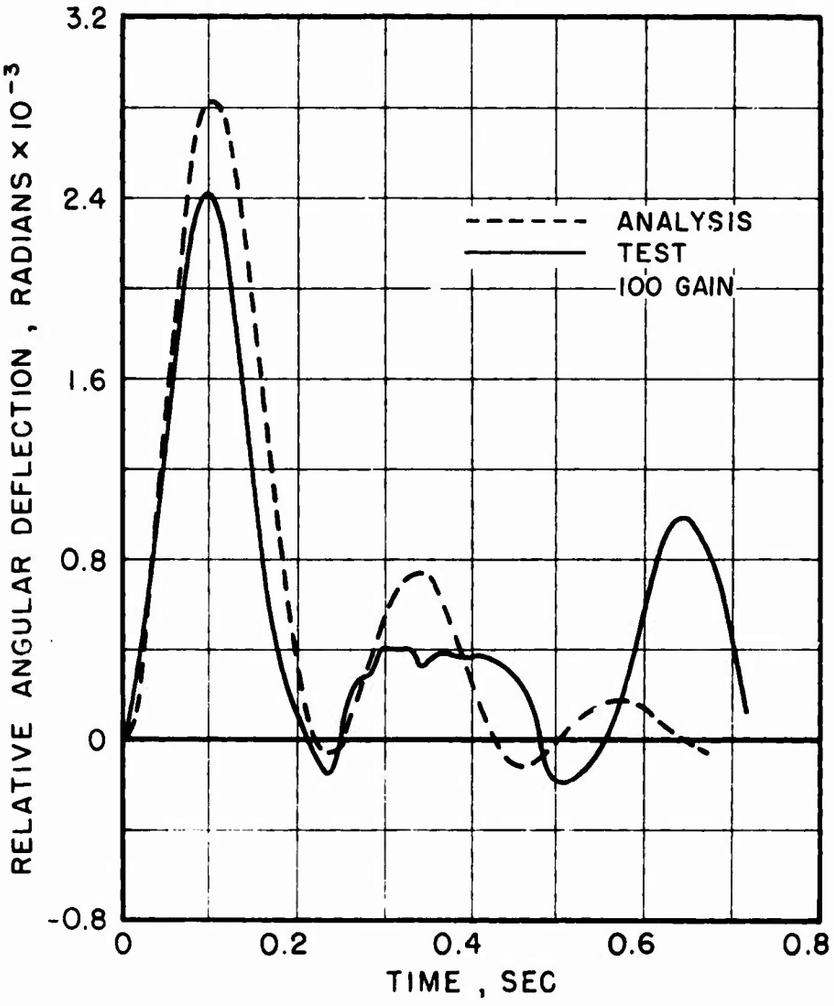

Figure 27. Analytical/Experimental Transient Response Time History.

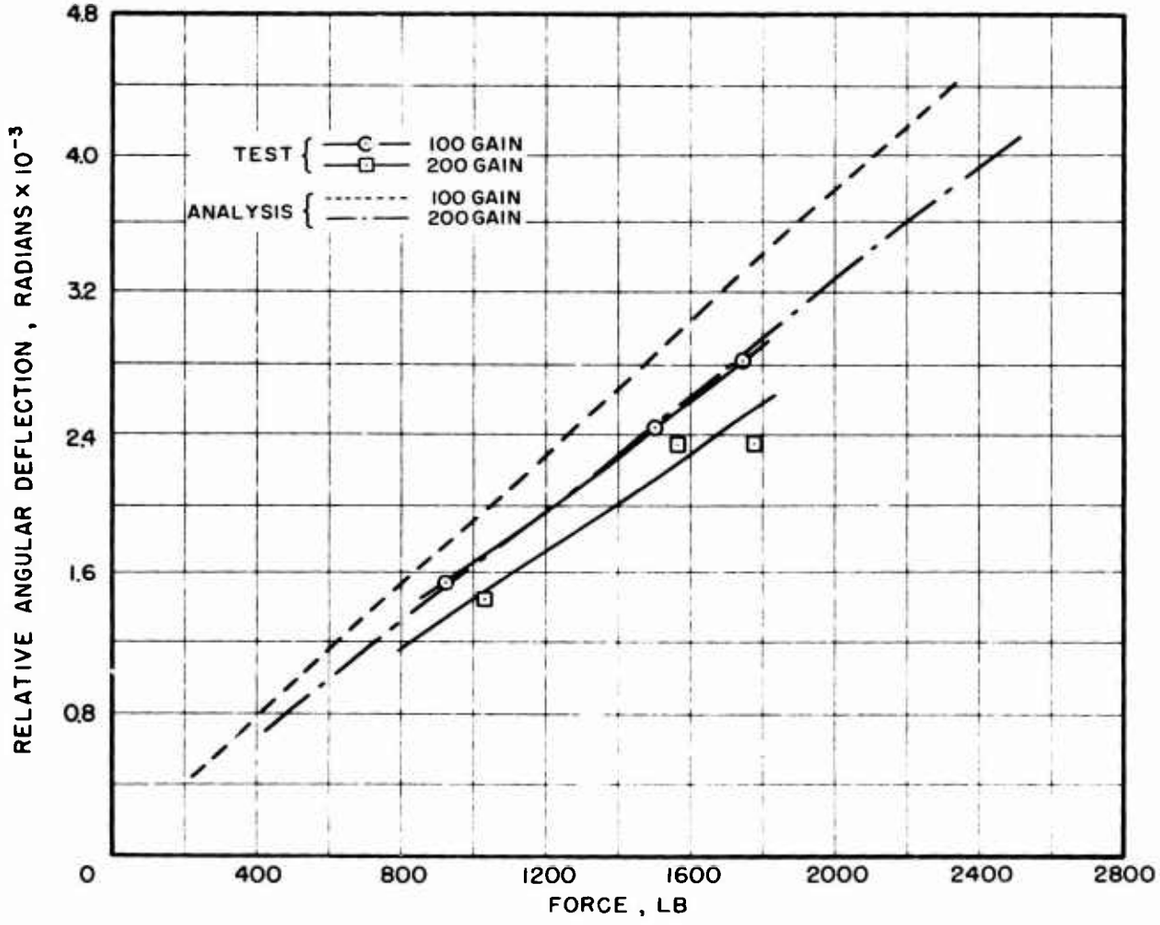

Figure 28. Peak Deflection Versus Step Load Applied for All Test Conditions.

MECHANICAL STABILITY

Classical theory can be used to show that the active isolation system tested does not affect the mechanical stability of the test vehicle (stability involving coupling between the in-plane rotor hub and blade motions). Substantiation is primarily based on the fact that all isolator mode frequencies are well above the rotor rotational frequency. Further, the isolator installation does not significantly change aircraft mode frequencies that are considered in stability investigations.

A complete substantiation of the CH-53A aircraft, or the nonisolated test vehicle, is provided in Reference 1. It includes effects of aircraft loading, locked/unlocked wheels, flat tires, operation on a 15-degree slope, operation on ice, altitude, and temperature. The methods of References 2 and 3 were applied to estimate the range of rotor speeds for which instability could occur. Reference 3 provided a chart for estimating the range of rotor speeds over which instability can occur if damping is sufficiently small. This range becomes smaller as damping is provided, or as the generalized mass of an in-plane vibration mode increases.

As part of the current investigation, mechanical stability boundaries were determined. A conservative result is obtained if the generalized mass of the mode is considered to be the rotor alone. Using the results of Reference 1, based on the methods of Reference 3, instability is predicted if the hub natural frequency is between .518 and 1.000 times the rotor rotational frequency when no damping is present. Since all isolation system hub modes are above the rotor rotational frequency, the test vehicle is mechanically stable.

WEIGHT, POWER, AND FAIL-SAFE REQUIREMENTS

A production isolation system for a 35,000-pound aircraft with CH-53A dynamic characteristics would weigh approximately 370 pounds or 1.1% of gross weight. This weight is based on a more compact isolator configuration utilizing a steel forged housing built to present isolator design parameters. Each isolator would weigh approximately 37 pounds. Consistent with primary hydraulic controls, the isolators would be designed for 5,000 hours between overhauls. Incorporation of isolator power supply requirements into the existing CH-53A utility hydraulic system to increase capabilities and add lines and fittings would result in an additional 10 pounds.

A triangular base structured of aluminum alloy forgings bolted to the transmission would pick up the upper isolator attachments. The longitudinal beams would be repositioned as shown in Figure 29. Also, the forward main transmission frame would be effectively interchanged with the existing secondary frame shown. Together with the horizontal torque struts, 230 pounds would be required. Stringers would be designed to accommodate loads from the horizontal struts. Approximately 20 pounds would be required for this rearrangement. These weights, together with estimates for a prototype installation, are presented in Table VIII.

Prototype installation hardware would be conceptually similar to the ground test installation and approximately double the production weight. The prototype isolator would increase in weight to approximately 47 pounds without the benefit of steel forgings,while an independent isolator power supply would weigh 30 pounds. An additional 20 pounds is estimated for the independent power supply to account for separate supporting structure, pump, reservoir, and oil cooler. A built-up aluminum alloy triangular base and rods would increase in weight to 300 pounds, with an equal amount required in the airframe to distribute the loads into existing structure.

Level-flight isolator operation at normal hydraulic system operating temperature of 160°F is estimated to require approximately 0.75 gpm at 3000 psi, or approximately 1.4 horsepower, to supply internal leakage requirements. This reduction in leakage flow from the test isolation system would result from improved piston design for the lapped piston/sleeve assembly. The design transient maneuver of ±1G to ±3G in 0.6 second is estimated to require 6 to 9 gpm or 11 to 16 horsepower to supply servovalve flow requirements at peak transient deflections. The maximum value was used to size isolator power supply weight in Table VIII. This peak power requirement represents only 0.25% of the 6400 horsepower available in a CH-53A aircraft and would have no effect on its operational capability.

Fail-safe aspects and requirements for a prototype and production installation would include the possibility of hydraulic or structural failure of an isolator. For the production installation, the utility hydraulic supply would be employed so that a system failure would not jeopardize safety of flight. Structurally, the prototype and production installation would be similar, both incorporating redundant load paths. Torque struts would be designed assuming one failed. The airframe itself would be designed to

provide suitable hard points for the isolator attachments and at least three additional redundant stops. These additional stops would likely be located as shown in Figure 29. Isolator malfunction, or failure, probably would be communicated to the pilot's instrument panel, possibly resulting in shutdown of the system. This implies that dynamic investigations ultimately should include one or more isolators against stops. In addition, consideration would be given to automatically inserting shims to remove stop clearance upon system shutdown.

TABLE VIII. ESTIMATED WEIGHT FOR TEST, PROTOTYPE, AND PRODUCTION SYSTEM

System	Test Weight (lb)	Prototype Weight (lb)	Production Weight (lb)
Isolators (3)	290	140	110
Transmission	0*	300	230
Airframe	700	300	20
Power Supply	- **	30	10
Total	-	770	370

* Transmission attachment weight less gears removed from transmission resulted in no net weight change.

** External ground power supply facilities were employed.

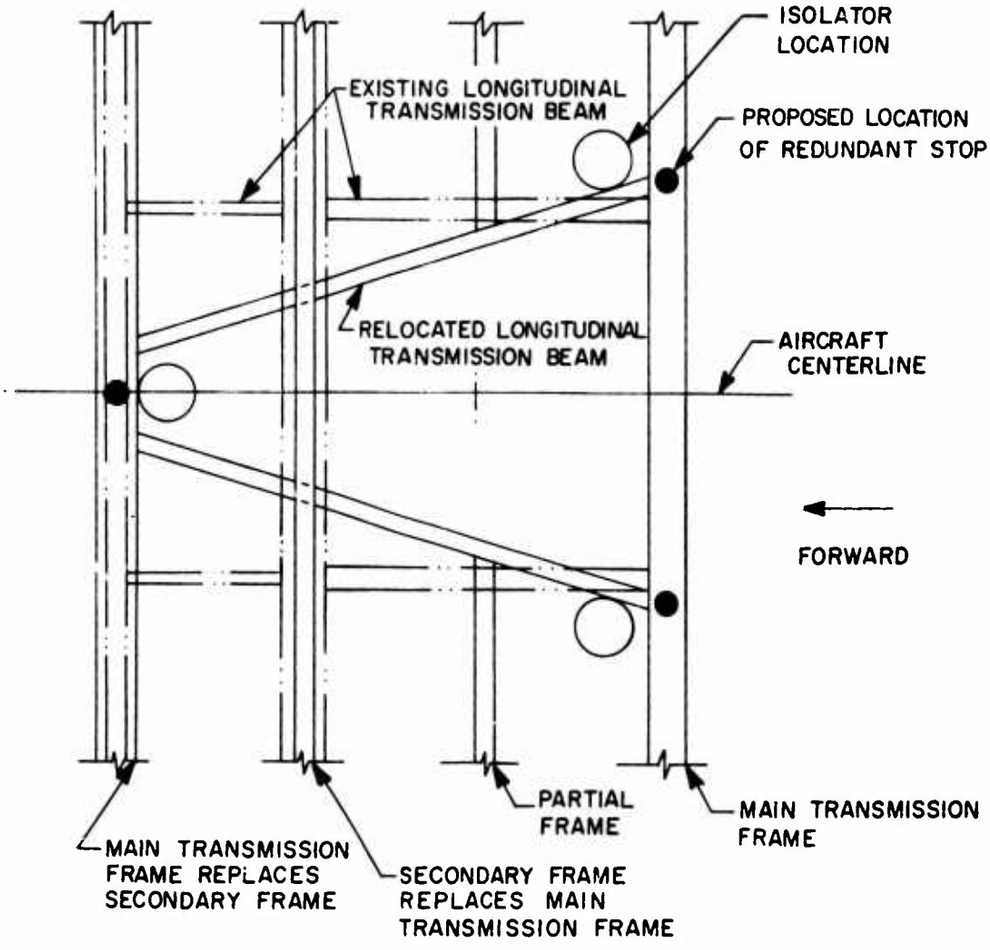

Figure 29. Top View of Production and Prototype Frame and Beam Rearrangement.

SEMIRIGID AND RIGID ROTOR CONSIDERATIONS

The active isolation system was contractually designed and tested to demonstrate fuselage isolation from CH-53A vertical and in-plane main rotor 6p excitation forces. These forces are the only significant source of rotor induced vibration for an aircraft configured with an articulated rotor. However, for semirigid or rigid rotor configurations, rotor mount excitations are of concern. Therefore, the simple rigid body analysis was extended to provide insight into the effects of pitch and roll moments on the isolated response.

Transmissibilities are dependent upon geometric and inertia properties of the rotor head, transmission, and fuselage, as well as the waterline location of the isolation system. Figure 29 presents 6p transmissibilities for the rotor-head forces and moments versus the isolator waterline location between the upper- and lower-body centers of gravity. (Isolator impedance was set equal to zero to simplify curve calculations. This does not significantly change results at 6p). Improvement in these rotational transmissibilities can be achieved by lowering the position of the isolators, but only by compromising the lateral response to lateral excitation and the longitudinal response to longitudinal excitation. By contrast, translational transmissibilities to pitch and roll moment excitations cannot be effectively reduced by isolator waterline placement alone. Isolator focusing, possibly including kinematic linkages, may be required.

The transmissibilities to pitch and roll moments generated from the rigid body analytical model are illustrated in Figures 31 and 32 respectively. The system parameters utilized in the analysis correspond to the baseline configuration tested. As shown, the isolated rigid body translational responses to moments are amplified, particularly in the case of longitudinal to pitch excitation. It should be noted that even though the rigid body longitudinal to pitch amplification at 6p is significantly higher than lateral to roll, it is not anticipated that the actual flexible longitudinal response will exhibit a similar relationship. This hypothesis is based upon the low elastic airframe amplification which can be expected in the longitudinal direction. In addition, the rotational transmissibilities indicate some 1p amplification while the 6p transmissibility remains near unity.

If, in the case of a semirigid or rigid rotor, isolation to rotor moments is required, the geometry of the system should first be investigated. These investigations should include isolation system waterline location for np isolation and isolator spacing for 1p tuning.

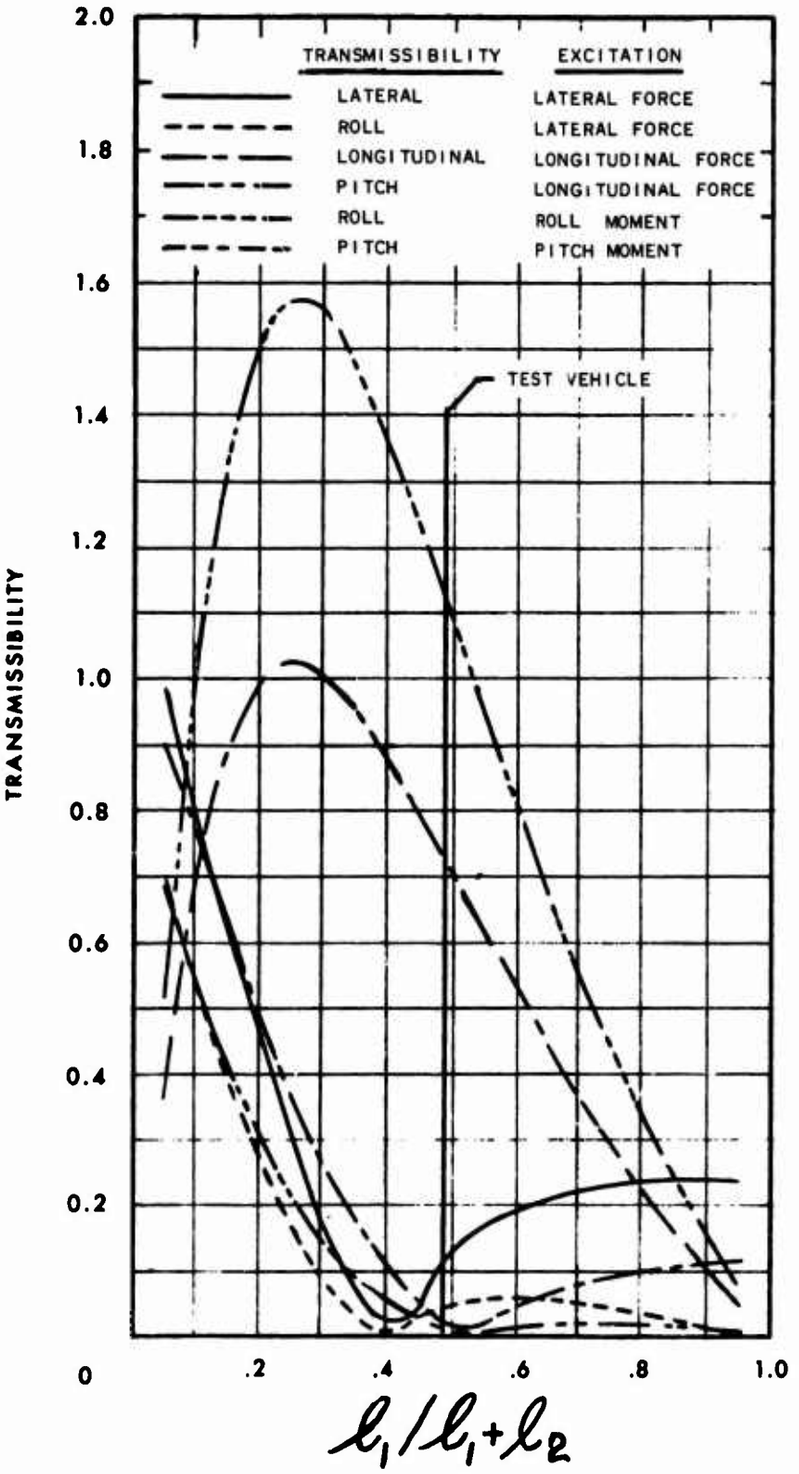

Figure 30. Effect of Isolator Waterline Location on Transmissibilities.

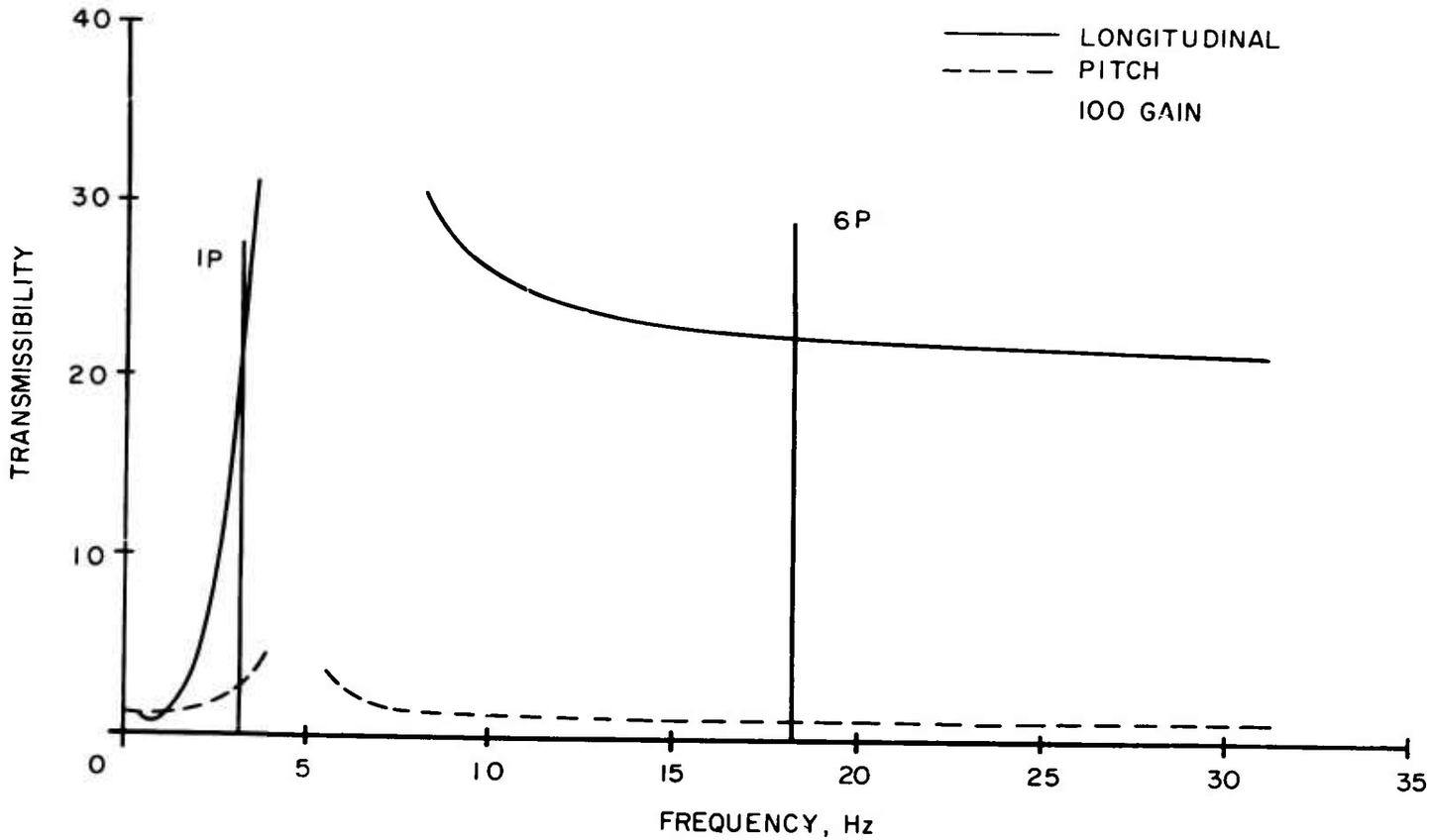

Figure 31. Longitudinal and Pitch Transmissibilities to Pitch Excitation.

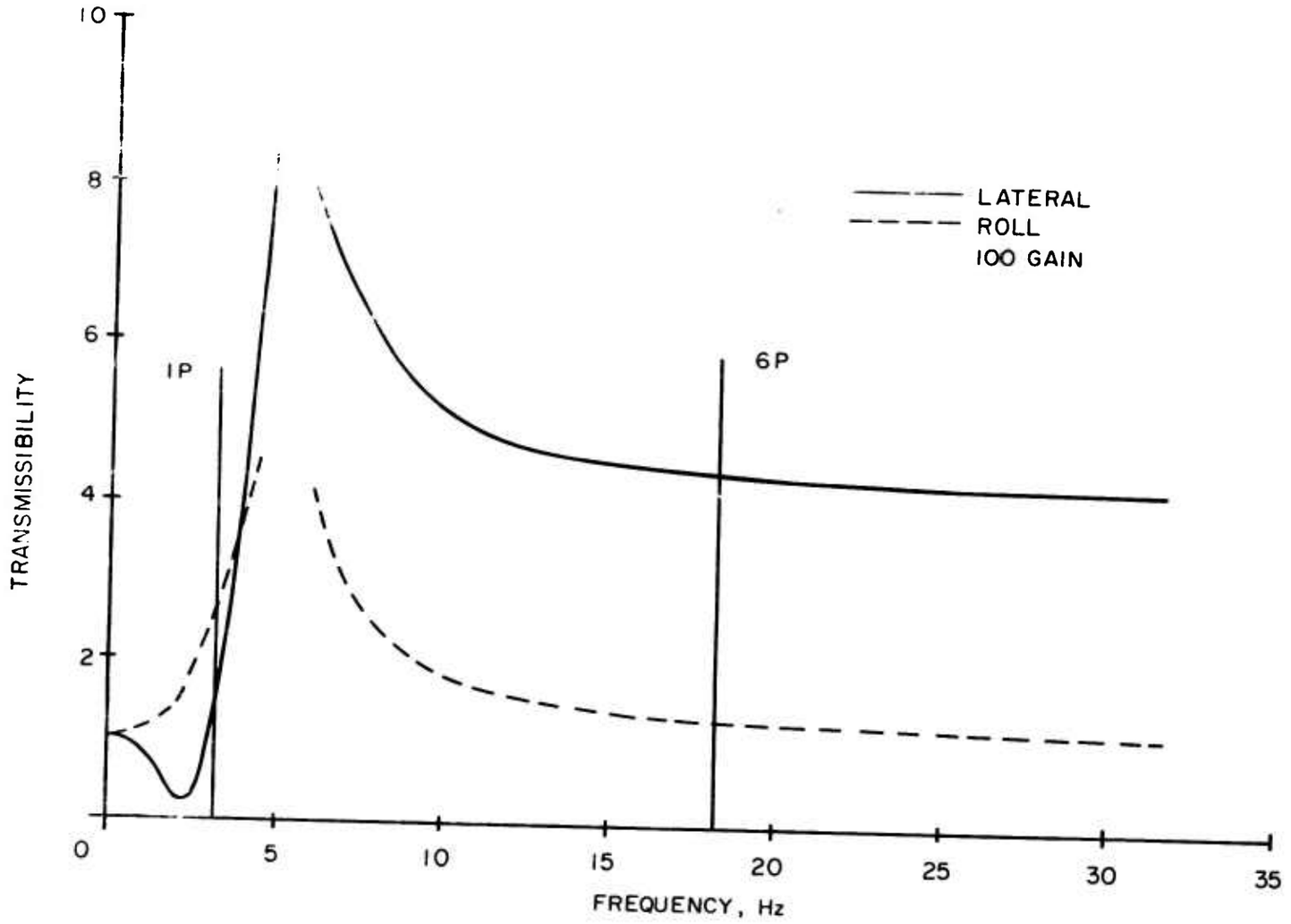

Figure 32. Lateral and Roll Transmissibilities to Roll Excitation.

CONCLUSIONS

Successful active isolation of a full-scale CH-53A helicopter fuselage was demonstrated by ground shake test. As a result of the testing and analytical investigations, the following conclusions are drawn:

1. Overall fuselage sensitivity reductions to main rotor 6p in-plane and vertical force excitations are 72% and 65% respectively with the system tested.

2. Vibration reduction potential is dependent upon geometrical location of the isolation system with respect to the isolated and non-isolated bodies.

3. Significant vibration reductions are achievable over the entire frequency range above the isolator resonances.

4. Test and analytical results show that isolator damping, stiffness, and gain may be substantially altered from their design values without significantly degrading 6p isolation.

5. Fuselage sensitivity to main rotor in-plane 1p excitation has increased only 13%, attributable to the active elements in the system.

6. Results of a transient response test indicate that maximum allowable deflection design goals for control systems and engine installations can be met.

7. Test results correlated reasonably well with the simplified analytical model describing the unisolated and isolated portions of the aircraft each as a single rigid mass.

8. Mechanical stability of the CH-53A aircraft remains virtually unchanged by incorporation of the isolation system.

9. Isolation system modes are stable, as shown by analysis and confirmed by test.

10. Isolation system size is of reasonable proportion to the test vehicle.

11. Weight of a production CH-53A isolation system is estimated at 1.1% of aircraft weight.

12. Hydraulic power requirements of a production isolation system are negligible.

RECOMMENDATIONS

It is recommended that the active isolator program be continued with the design, fabrication, and test of a flight demonstration vehicle. The recommended steps for this further development are:

1. Design analysis of overall flight-vehicle dynamic characteristics, including:

   a. Rotor stability
   b. Aircraft control
   c. Flight load spectrum to evaluate effects on isolation and transient response characteristics

2. Determination of hardware, including physical configuration of isolator hardware, torsional and in-plane restraint, and control linkages

3. Fabrication and installation in a CH-53A aircraft

4. Ground testing, including:

   a. Structural proof tests
   b. Tie-down tests to evaluate compatibility of all dynamic components

5. Flight testing to evaluate:

   a. Handling qualities
   b. Mechanical stability characteristics
   c. Isolation system performance
   d. Transient response characteristics

LITERATURE CITED

1. Gockel, M. A., STRUCTURAL DYNAMIC ANALYSIS REPORT, SER 65176, Sikorsky Aircraft Division, United Aircraft Corporation; Prepared under Contract NOw 63-0150f, June 1964.

2. Coleman, R. P., THEORY OF SELF-EXCITED MECHANICAL OSCILLATIONS OF HELICOPTER ROTORS WITH HINGED BLADES, NACA Report 1351.

3. Deutsch, M.L., GROUND VIBRATIONS OF HELICOPTERS, Journal of the Aeronautical Sciences, May 1946.

4. Paglino, Vincent M., AN EXPERIMENTAL STUDY OF THE PERFORMANCE AND STRUCTURAL LOADS OF A FULL-SCALE ROTOR AT EXTREME OPERATING CONDITIONS, Sikorsky Aircraft Division of United Aircraft Corporation; USAAVLABS Technical Report 68-3, U. S. Army Aviation Materiel Laboratories, Fort Eustis, Virginia, July 1968, AD 674187.

5. Soliman, J. I., SELF-DAMPED PNEUMATIC ISOLATOR FOR VARIABLE FREQUENCY EXCITATION, J. of Mech Eng Sciences, Vol. 8, No. 3, Sept. 1966, pp. 284-293.

6. Shearer, J. L., STUDY OF PNEUMATIC PROCESSES IN THE CONTINUOUS CONTROL OF MOTION WITH COMPRESSED AIR-I, Trans. ASME 78, 1956, pp. 233-242.

7. Shearer, J. L., STUDY OF PNEUMATIC PROCESSES IN THE CONTINUOUS CONTROL OF MOTION WITH COMPRESSED AIR-II, Trans. ASME 79, 1957, pp. 243-249.

8. Harris and Crede, SHOCK AND VIBRATION HANDBOOK, New York, McGraw Hill, 1961, Section 33.

9. Kuzma, T. A., CH-53A HELICOPTER DEMONSTRATION DATA TEST REPORT, SER-65254, Sikorsky Aircraft Division, United Aircraft Corporation, Prepared under contract NOw 63-0150f, December 1964.

10. Schuett, Erich P., PASSIVE HELICOPTER ROTOR ISOLATION USING THE KAMAN DYNAMIC ANTIRESONANT VIBRATION ISOLATOR (DAVI), Kaman Aircraft Corporation; USAAVLABS Technical Report 68-46, U. S. Army Aviation Materiel Laboratories, Fort Eustis, Virginia, December 1968, AD 687324.

APPENDIX
PRELIMINARY DESIGN ANALYSIS

PART I - DESIGN ANALYSIS DEVELOPMENT

The objective of this effort was to set up an analysis to establish analytical feasibility and to provide CH-53A design data for a self-contained isolation system capable of providing both fuselage vibration and acoustic isolation from main rotor and transmission excitations. The active transmission isolation system must be capable of providing fuselage vibration attenuation to vertical and in-plane excitation forces at CH-53A 6p frequencies and above, while maintaining stability and controlling static and vertical transient displacements.

The isolation system devised is a modification of the existing hydropneumatic Ames active isolation system, employed for wind-tunnel testing reported in Reference 4. The Ames system has the basic desirable features of utilizing only hydraulic power for operation and entrapped air volumes for achieving a low spring rate necessary for isolation. Although the Ames system is capable of isolating at np frequencies and reacting transient loads, it is inherently frequency limited due to its geometric configuration with external air-oil accumulators necessitating the flow of hydraulic fluid through long lines. The new concept shown in Figure 33 differs from the previous concepts only in the placement of the pneumatic isolation bags inside the isolator cylinder.

Steady and transient loads applied to the isolator through its housing are reacted by differential hydraulic pressure across the isolator piston supplied by the servovalve. The linkage and servovalve spool shown provide a flow of hydraulic fluid altering pressures to oppose piston motion for steady and transient loads. Isolator piston area is determined by the hydraulic supply pressure and the maximum load the isolator is required to center. Air volumes, separated by diaphragms from the hydraulic fluid, provide the resilience required for isolation and are determined by the piston area and steady operating pressures. Isolator gain is determined by the flow of fluid required to compress the air volumes during transient load conditions. For a given servovalve, gain can be adjusted by varying the feedback linkage ratio. Damping is employed to maintain stability and dampen response to transient excitations.

The isolator's characteristics are most easily explained in terms of its impedance, or resistance to motion, as a function of frequency (see Figure 33(b)). For a qualitative illustration of the effect of isolator parameters on the isolator's impedance, Figure 33(b) can be broken up into four separate curves, Figure 34, which combine to give the total impedance.

1. Curve 1 is the basic spring rate determined by the total air volumes and operating pressures. This curve is a constant independent of frequency.

2. Curve 2 is the air spring rate associated with the air volume above the air dampers. It is independent of frequency. The value of air damping determines the transition from curve 1 to curve 2 since, at high frequencies the air damping effectively cuts off the volume below the damper.

3. Curve 3 shows the effect of the servovalve. This value is proportional to the reciprocal of frequency and is essentially zero at np.

4. Curve 4 corresponds to the impedance due to viscous fluid and piston damping, which is proportional to frequency.

5. For the Ames isolator, another curve would be required showing an increase in impedance with frequency squared due to mass effects of fluid in the lines.

Additional statements may be made describing the isolator's characteristics:

1. Valve gain controls displacements, has no effect on isolation, determines amplitude of resonance peaks and their frequency, and determines stability.

2. Air damping provides increased stability and lowers peaks with little effect on np isolation.

3. Piston and fluid damping determines stability and lowers amplitude of peaks and the frequency at which they occur.

Integration of the dynamics of the isolation system into the dynamics of the helicopter is now required. The mathematical model used is shown in Figure 35. This model consists of two rigid bodies attached by means of the isolation system consisting of three identical isolator elements mounted in a vertical orientation between the transmission and the helicopter transmission support frames. Supplementary degrees of freedom are controlled by the use of additional attachment elements.

The values of the isolator design parameters obtained for a helicopter configuration were determined by the method of successive approximations. Preliminary calculations were performed to determine the first trial values of the isolator design parameters. These values were then used in a computer program written to evaluate the dynamic characteristics of the helicopter/isolator from the associated equations of motion. The values of the design parameters were successively altered until satisfactory performance of the isolation system was obtained.

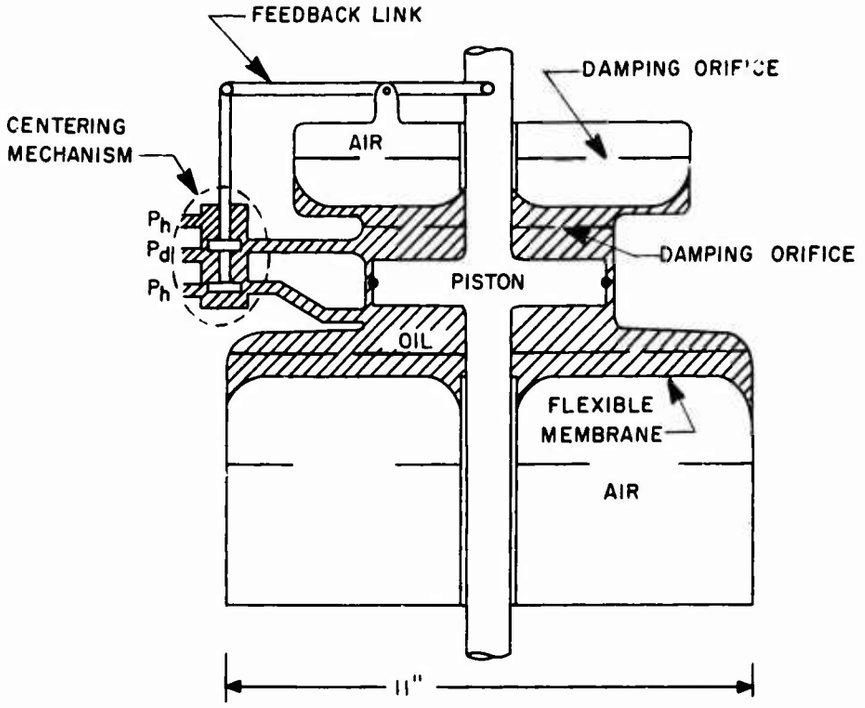

(a) ISOLATOR SCHEMATIC

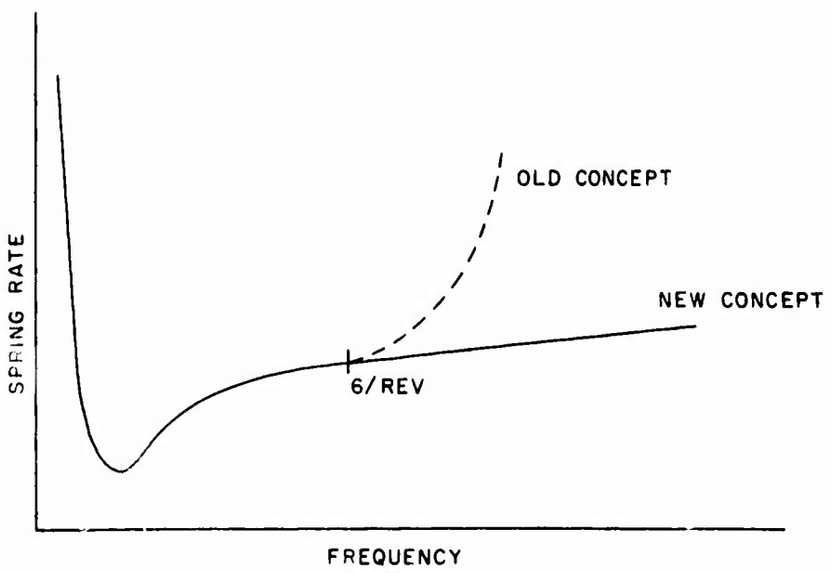

(b) SPRING RATE VS. FREQUENCY

Figure 33. Active Transmission Isolator Concept Shown Qualitatively.

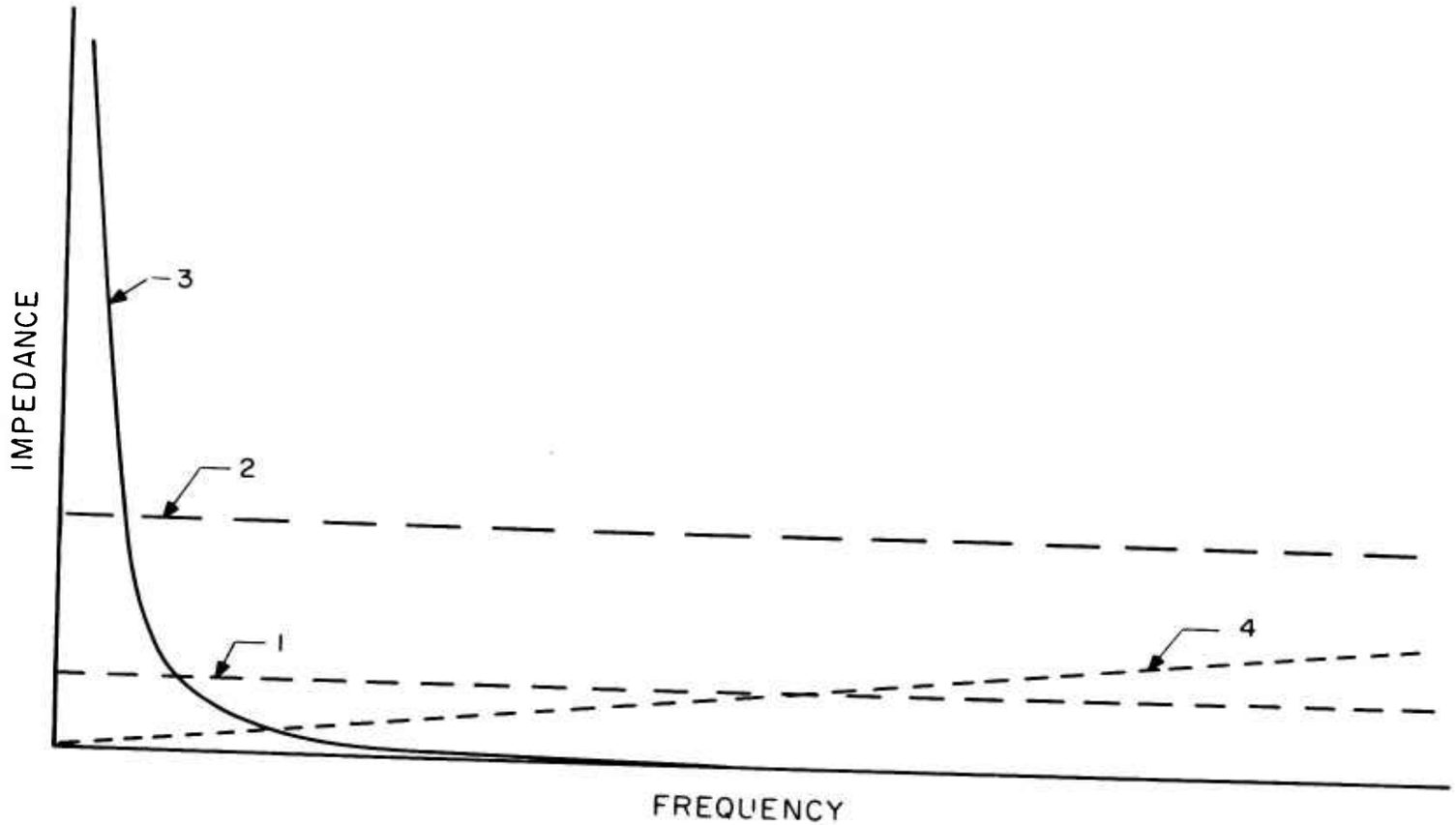

Figure 34. Illustrative Breakdown of Isolator Impedance Components.

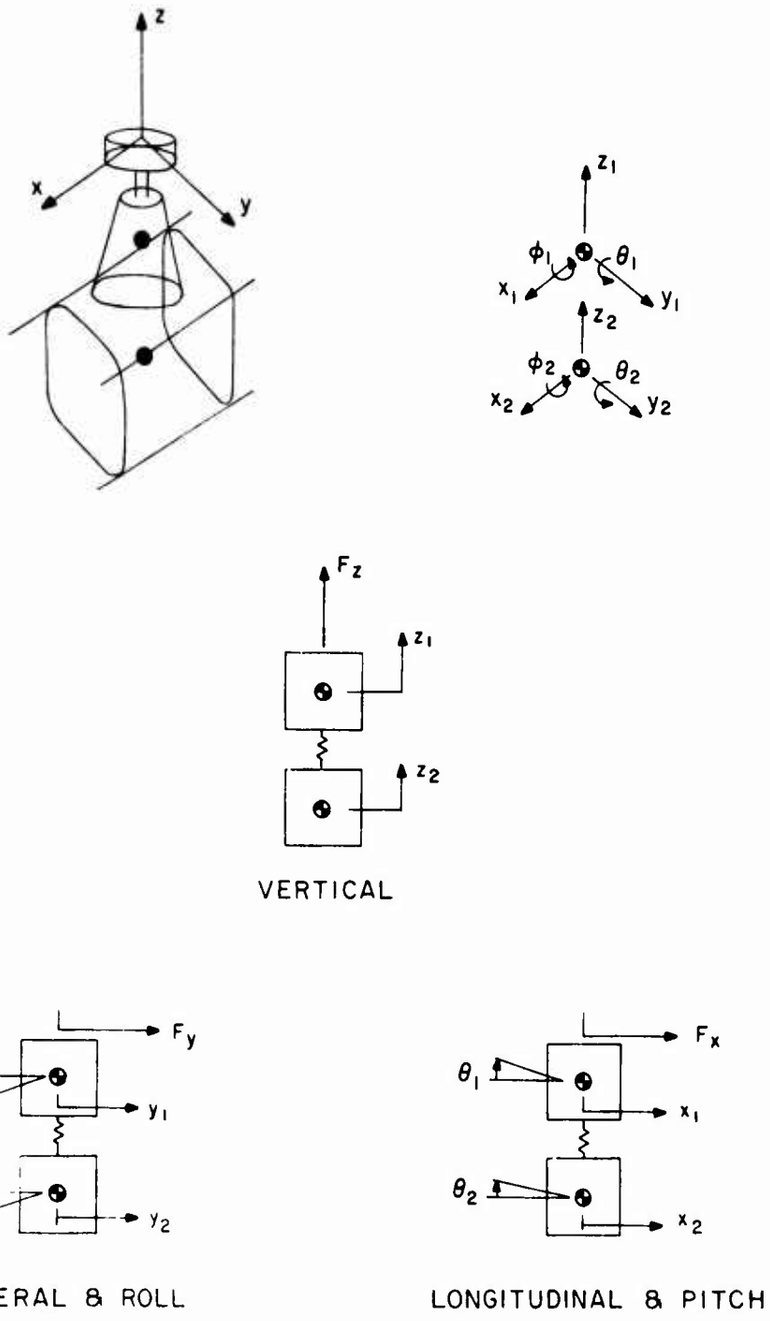

Figure 35. Description of Coordinate System and Mathematical Models.

List of Assumptions

The following assumptions are used in the analysis which follows:

1. Isolator element

   a. Variations about operating pressures are small.

   b. All processes are adiabatic.

   c. Air behaves as an ideal gas.

   d. Air damping is viscous.

   e. Fluid and piston damping is viscous.

   f. Flow through the servovalve is proportional to valve displacement.

For vibratory inputs, the above assumptions are applicable and result in a linear analytic model. Transient inputs result in nonlinear isolator characteristics since assumptions (a) and (d) no longer give an accurate description of the system. However, these assumptions result in conservative values of transient response.

2. Mathematical model of helicopter

   a. All three isolators are equally statically loaded.

   b. Inertias and masses of upper body are based on rigid blades.

   c. No mass or spring coupling exists between in-plane rotor head forces and vertical motion of the fuselage center of gravity.

   d. Small angles are assumed.

   e. Transverse spring-rate effects due to axial loading of link type elements are neglected.

   f. All forces are considered as being applied at the rotor head location.

Equations of Motion

The equations of motion describing the performance of the isolation system were developed by determining the expression for the impedance of each isolator and substituting these impedance expressions into the helicopter's vertical and in-plane dynamic equilibrium equations.

1. Isolator Impedance

   Figure 33(a) is a functional schematic of an isolator element. The

isolator element impedance, denoted by K_I, is defined as the magnitude ratio of the piston input force F_I and the associated piston displacement across the isolator element, X_I. The impedance K_I was determined in the form of a polynomial expression in powers of s, the derivative operator ($s = \frac{d}{dt}$). The polynomial coefficients of the powers of s are functions of the isolator design parameters consisting of volumes, pressures, gains, and damping. A schematic of a typical air spring part of an isolator element is shown in Figure 36. Equation 1 is the impedance expressions for the air spring adapted from the derivations performed in References 5, 6, 7 and 8. The subscripts a and b are used to distinguish between the two air springs associated with each isolator element, where the subscript b refers to the high pressure side when the isolator is reacting a suspension load. Referring to the functional schematic shown in Figure 37, the isolator element impedance expressions shown in Equation (6) were obtained by execution of the following steps:

a. Determining the upper and lower air volume reaction forces in terms of $X_I(s)$, by substituting the continuity of flow expressions, Equation (2), into Equation (1) together with the linear valve feedback flow relations, Equations (3).

b. Determining the total isolator element reaction force in terms of $X_I(s)$ by summing the air volume reaction forces, Equation (1), with the viscous damping expression, Equation (4).

c. Equating the piston applied force to the total isolator reaction force as shown in Equation (5).

In the resulting isolator impedance expression Equation (6b), $K_I(s)$ is a polynomial expression in which the numerator coefficients n_i and the denominator coefficients d_j are functions of the isolator design parameters.

2. Vertical Equation of Motion

Using K_I to represent the isolator impedance, Equations (8a) are the vertical dynamic equilibrium equations associated with the isolated helicopter model shown in Figure 38(a), and Equation (8b) is the equation associated with the rigid configuration shown in Figure 38(b). Reduction of Equations (7) and (8) yields expressions for Δz, the relative displacement across the isolation system, and T_{mz}, the vertical transmissibility defined as the magnitude ratio of the fuselage displacements in the isolated and unisolated configurations. The form of these expressions is shown in Equations (9). The coefficients a_i, b_j, c_i and d_j are functions of the isolator design parameters and the helicopter masses m_1 and m_2. The roots of the denominator polynomial, $D_z(s)$, of the vertical transfer function, T_z, determine the stability characteristics of the isolation system in the vertical direction. The existence of a positive real part for any of the roots

would indicate instability, while the absence of a positive real part would indicate stability.

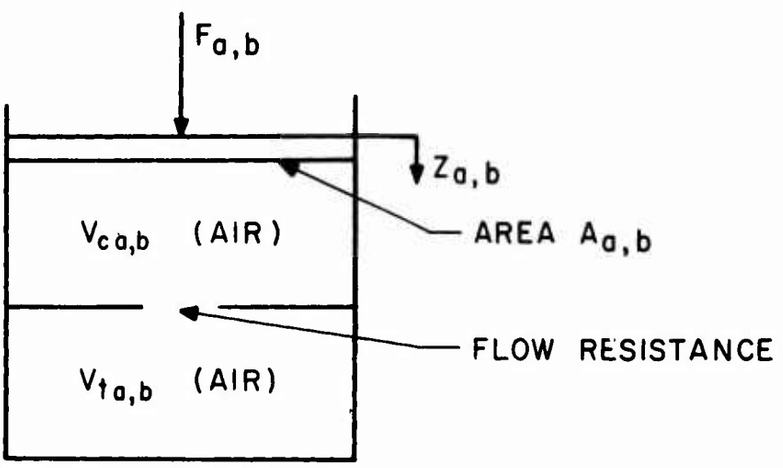

Figure 36. Air Spring With Damping.

Air Spring Impedance (1)

$$F_{a,b} = K_{a,b}(s)\ Z_{a,b}(s)$$

where

$$K_{a,b}(s) = \frac{\gamma P_{a,b} A_{a,b}^2}{V_{ca,b} + V_{ta,b}} \cdot \frac{1 + \dfrac{V_{ta,b}}{\gamma B_{a,b} P_{a,b}} s}{1 + \dfrac{V_{ca,b} V_{ta,b}}{(V_{ca,b} + V_{ta,b}) \gamma B_{a,b} P_{a,b}} s}$$

Continuity of Flow

$$\text{a.)}\ q_a - S_a s\, X_I + A_a s\, Z_a = 0 \qquad (2)$$

$$\text{b.)}\ q_b - S_b s\, X_I - A_b s\, Z_b = 0$$

Valve Feedback Flow

$$\text{a.)}\ q_a = -G_a C_2\, X_I \qquad (3)$$

$$\text{b.)}\ q_b = +G_b C_2\, X_I$$

Viscous Damping

$$F_{vd} = C_v s\, X_I \qquad (4)$$

Piston Force Summation

$$F_I = F_a + F_b + F_{vd} \qquad (5)$$

Isolator Element Impedance

$$\text{a.)}\ F_I(s) = K_I(s)\, X_I(s) \qquad (6)$$

$$\text{b.)}\ K_I(s) = \frac{N(s)}{D(s)}$$

where

$$N(s) \equiv \Sigma_{i=0}^{4}\, n_i s^i$$

$$D(s) \equiv \Sigma_{i=0}^{3}\, d_j s^i$$

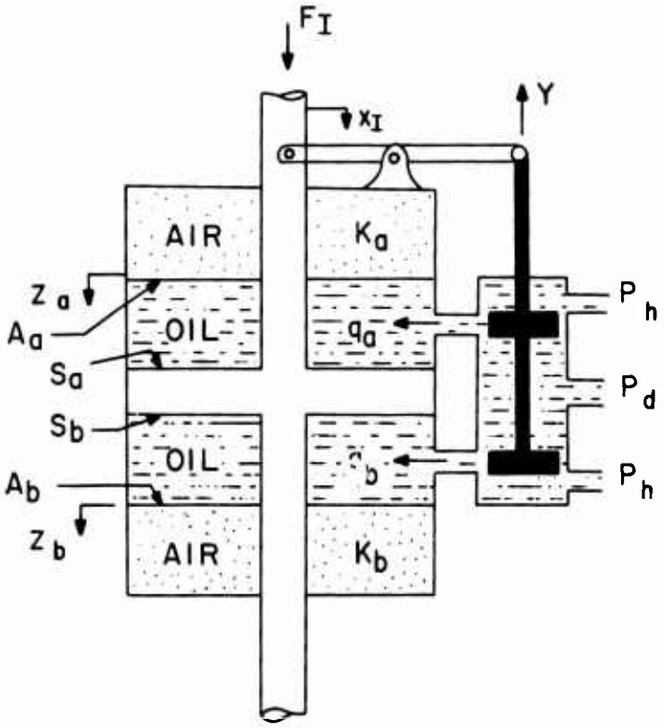

Figure 37. Functional Schematic With Notation .

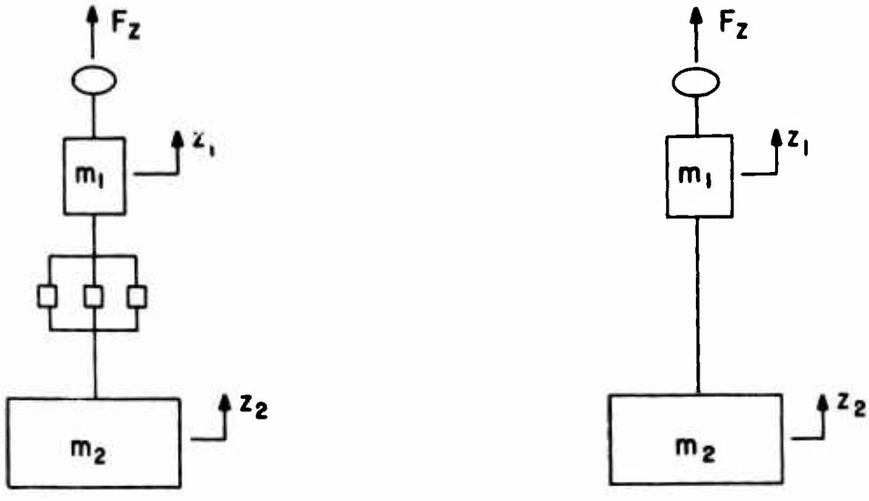

(a) ISOLATED (b) RIGID

Figure 38. Vertical Rigid-Body Model.

Vertical Relative Displacement (7)

$$\Delta z = z_1 - z_2$$

Vertical Rigid-Body Model Equation of Motion (8)

a.) Isolated

$$F_z = m_1 s^2 z_1 + 3K_I z_1 - 3K_I z_2$$

$$0 = m_2 s^2 z_2 + 3K_I z_2 - 3K_I z_1$$

b.) Rigid

$$F_z = (m_1 + m_2) s^2 z_2$$

Vertical Transfer Function & Transmissibility (9)

a.) Transfer Function

$$\Delta z(s) = T_z(s)\, F_z(s)$$

where

$$T_z = \frac{N_z(s)}{D_z(s)} = \frac{\Sigma_{i=0}^{3} a_i s^i}{\Sigma_{j=0}^{5} b_j s^j}$$

b.) Transmissibility

$$T_{mz} = \frac{z_2(s)}{z_{2r}(s)} = \frac{N_{mz}(s)}{D_{mz}(s)} = \frac{\Sigma_{i=0}^{4} c_i s^i}{\Sigma_{j=0}^{5} d_j s^j}$$

3. In-Plane Analysis

The development of the in-plane equations of motion in the roll-lateral direction was very similar to the development in the pitch-longitudinal directions. For brevity, only the pitch-longitudinal development is presented.

Equations (10) are the dynamic equilibrium equations associated with the isolated longitudinal mathematical model shown in Figure 39(a). Reduction of Equations (10) yields expressions for x_2, θ_2, or θ_r in the form of polynomials in the powers of s, the derivative operator, multiplied by the longitudinal input force, F_x. Reduction of the equilibrium equations associated with the rigid configuration shown in Figure 39(b) yields expressions for x_{2r} and θ_{2r}. Equations (11a) show the form of the expressions for longitudinal and pitch transmissibilities, T_{mx} and $T_{m\theta}$. Equation (11b) shows the form of the expression for θ_r, the rotational motion across the isolation system. The polynomial coefficients e_i, f_j, g_i, h_j, r_i, and s_j are functions of the isolator design parameters and the helicopter properties ℓ_1, ℓ_2, ℓ_3, m_1, m_2, I_{1y}, and I_{2y}. The roots of the denominator polynomial D of the transfer function $T_{\theta r}$ indicate the stability or instability of the isolation system.

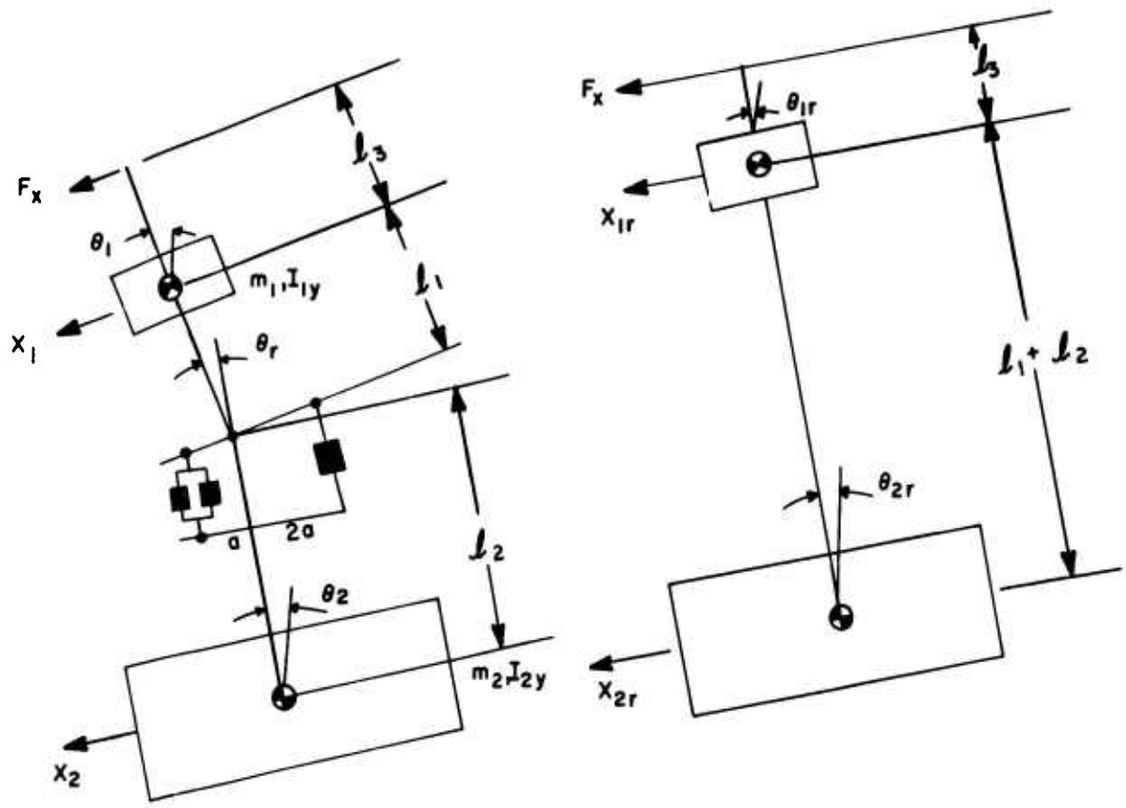

(a) ISOLATED

(b) RIGID

Figure 39. In-Plane Mathematical Model (Longitudinal Pitch).

Isolated Longitudinal Equilibrium Equations (10)

$$F_x(\ell_1 + \ell_3) = m_1\ell_1 s^2 x_1 - I_{1y} s^2 \theta_1 - 6\ K_I a^2 \theta_r$$

$$0 = m_2\ell_2 s^2 x_2 - I_{2y} s^2 \theta_2 + 6\ K_I a^2 \theta_r$$

$$F_x = m_1 s^2 x_1 + m_2 s^2 x_2$$

Longitudinal Transmissibilities and Transfer Function (11)

a.) $$T_{mx} = \frac{x_2(s)}{x_{2r}(s)} = \frac{\Sigma_{i=0}^{5} e_i s^i}{\Sigma_{j=0}^{5} f_j s^j}$$

$$T_{m\theta} = \frac{\theta_2(s)}{\theta_{2r}(s)} = \frac{\Sigma_{i=0}^{5} g_i s^i}{\Sigma_{j=0}^{5} h_j s^j}$$

b.) $$\theta_r(s) = T_{\theta r}(s)\ F_x(s)$$

$$T_{\theta r} = \frac{N_\theta(s)}{D_\theta(s)} = \frac{\Sigma_{i=0}^{5} r_i s^i}{\Sigma_{i=0}^{5} s_j s^j}$$

Performance Criteria

The criteria established for the performance of the isolation system governed the selection of the isolator design parameters.

The performance criteria established in the design analysis program are as follows:

1. The design parameters shall be selected such that normal aircraft

hydraulic pressure (3000 psi) is sufficient to center the isolator to zero displacement for loads of less than +3.0G.

2. The isolator system shall be stable.

3. The transmissibilities in the vertical and in-plane directions shall exhibit vibration reduction at frequencies of np and higher and shall not be excessive at 1p.

4. The displacement across the isolator system shall be contained to acceptable levels for all steady loads and for a vertical ramp force going from +1G to +3G in a period of 0.6 second.

5. The isolator size and weight shall be of acceptable proportion to the aircraft.

Computer Operation

Sikorsky Aircraft has developed digital computer programs to expedite a rapid numerical solution to the equations of motion and the establishment of isolator design parameters for a given helicopter.

The flow of execution of the computer programs is as follows:

1. Run Computer Deck E959CA to establish the optimum waterline (W.L.) position for the isolator installation. Figure 40 demonstrates the effect that various values of ℓ_1, the length which defines the isolator W.L. position, have on the transmissibility of the isolator system. For various values of ℓ_1, deck E959CA solves T_∞ from Equation (12), obtained from Equation (11a) as excitation frequencies approach infinity.

2. Run Computer Deck E959. It performs, for a given set of helicopter properties and a set of isolator design parameters, the following operations:

   a. Determines the polynomial coefficients of the isolator impedance K_I.

   b. Determines the polynomial coefficients of the transfer functions associated with the vertical, lateral and longitudinal directions.

   c. Calls subprogram POLRT in which the roots of the denominators of the transfer functions are determined.

   d. Determines stability of the isolator system by searching for a positive real part in any of the denominator roots.

e. Depending on the results of step d, performs one of the following operations:

(1) If a positive real part is found, the isolator system is unstable and the computer reexecutes steps a,b,c, and d with a new set of design parameters.

(2) If no positive real part exists, the isolator system is stable and the polynomial coefficients associated with the transmissibilities in the vertical, lateral, and longitudinal directions are determined.

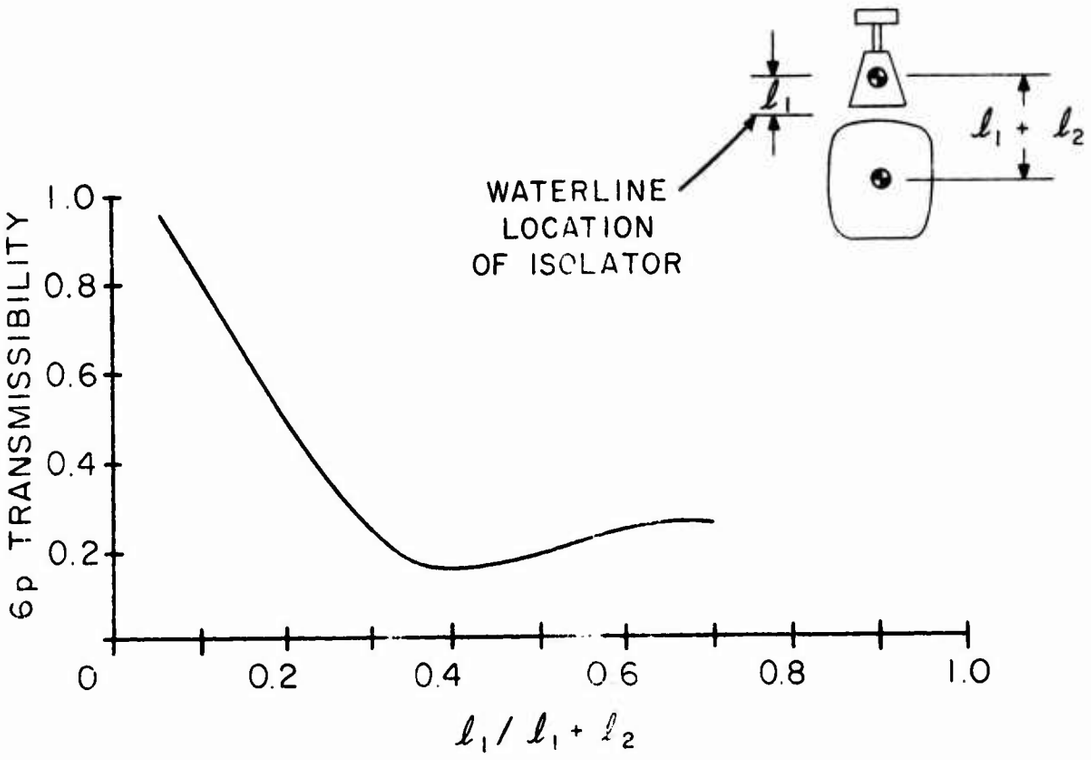

Figure 40. Effect of Isolator Waterline Location on Lateral Isolation.

In-plane Transmissibility Asymptote (12)

$$T_\infty = \frac{I_{2x}(I_{1x}-m_1\ell_1\ell_3)\left[m_A I_A + m_1 m_2 (\ell_1+\ell_2)^2\right]}{\left[m_1(\ell_1+\ell_2)\ell_3 - I_A\right]\left[m_A I_{1x} I_{2x} + m_1 m_2 (I_{2x}\ell_1^2 + I_{1x}\ell_2^2)\right]}$$

where $I_A = I_{1x} + I_{2x}$

$m_A = m_1 + m_2$

f. Calls subroutine Bode which determines the steady-state transmissibilities over a frequency range from 0.1 to 160 Hz.

g. Switches back to step 1 and repeats the operation with a new set of design parameters.

3. Run ROOT LOCUS and TIME HISTORY computer program which, using the vertical transfer function polynomial coefficients found from E959, determines the time history response for prescribed vertical transient loads.

PART II - AIRCRAFT ANALYSES

Sikorsky Aircraft has performed analytical studies on three helicopter gross weight classes to demonstrate the feasibility and the versatility of the vibro/acoustic active transmission isolator concept. The method of successive approximation was utilized to attain the goals of the three helicopter studies. The primary analysis was performed on a 35,000-pound CH-53A helicopter. This analysis was conducted to completion of design data for a ground shake test isolation system. Cursory analyses were performed on a 7,000-pound UH-1D and a 147,000-pound heavy-lift helicopter to demonstrate the feasibility of the active isolation system concept.

CH-53A Analysis

The design data for the CH-53A ground test isolation system is presented in Table IX, together with the geometric and inertia properties used. The total air volume for each isolator is 200 $in.^3$, and the isolator piston area is 16.4 $in.^2$ Figures 41 through 45 contain plots of the helicopter/isolation system performance data.

The time response of the vertical deflection across the isolation system for a vertical ramp loading going from +1G to +3G in a period of 0.6 second is shown in Figure 41. This corresponds to a rate of loading of 3.3 G per second. The maximum deflection has a magnitude of 0.8 inch and occurs after 0.45 second.

Transient deflections encountered in an actual application of this isolation system would be significantly less for two major reasons. First, actual aircraft transient inputs are less severe. Figure 41(c) shows the most rapid load application encountered in the CH-53A Structural Demonstration Flight Test Report (Reference 9). This input corresponds to a jump takeoff with the load going from +1G to +2.1G in 0.4 second. This rate of loading is 2.7G per second, or approximately 20 percent less than the design input. The second reason is that the amplitudes associated with the air spring and air damping result in a substantially stiffer system than represented by the linearized model.

Plots of the vertical, lateral, and longitudinal transmissibilities versus frequency are shown in Figures 42 through 44. The vertical transmissibility at 6p (18.5 Hz) is 0.6. The lateral translation and rotational 6p transmissibilities are 0.17 and 0.12 respectively. For the longitudinal direction, the 6p transmissibilities are both 0.06. Note that all transmissibilities decrease asymptotically to low values at infinity for all frequencies above 6p. The isolation system is stable. Figure 45 shows plots of the denominator roots of the vertical, lateral and longitudinal transfer functions. The absence of a positive real part for any of the roots verifies the system stability.

A conceptual hardware sketch of the CH-53A isolator element is shown in Figure 46; Figure 47 is a schematic of the isolation system mounted on the transmission of the CH-53A helicopter.

TABLE IX. CH-53A DESIGN DATA, GEOMETRIC AND INERTIA PROPERTIES

Piston Area ($in.^2$)		16.4
Air Volumes ($in.^3$)	Total	200
	V_{cb}	70
	V_{ca}	24
	V_{tb}	80
	V_{ta}	26
Piston and Fluid Damping (lb sec/in.)	C_v	390
Air Damping ($in.^5$/lb sec)	B_a	.74
	B_b	.66
Operating Air Pressures (psi)	P_a	200
	P_b	750
Valve Feedback Gains ($in.^2$/sec)	G_a	190
	G_b	190
Masses (lb)	m_1	7,500
	m_2	27,090
Inertias (slug · ft^2)	I_{1x}	1,136
	I_{1y}	1,512
	I_{2x}	22,667
	I_{2y}	176,000
Lengths (in.)	ℓ_1	47
	ℓ_2	49
	ℓ_3	19
Isolator Spacing (in.)	a	16.7
	b	22.0

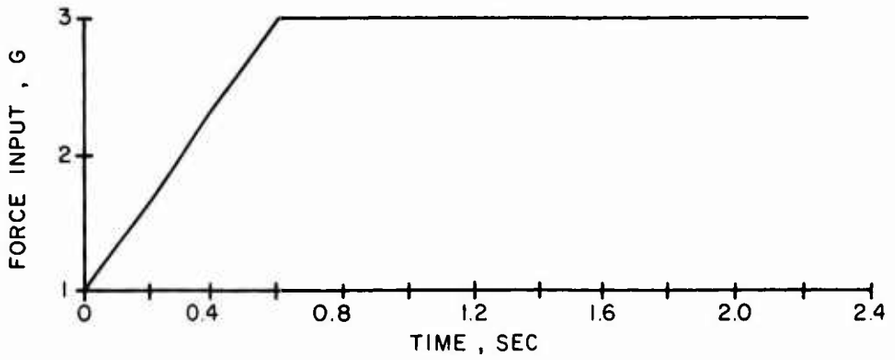

(a) DESIGN LOAD

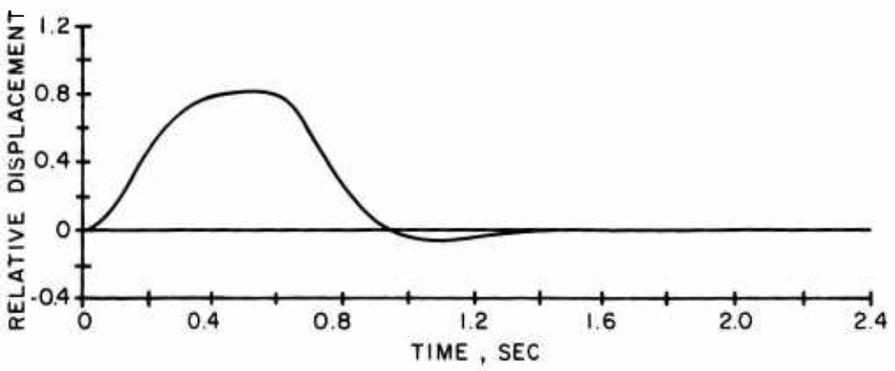

(b) RESPONSE

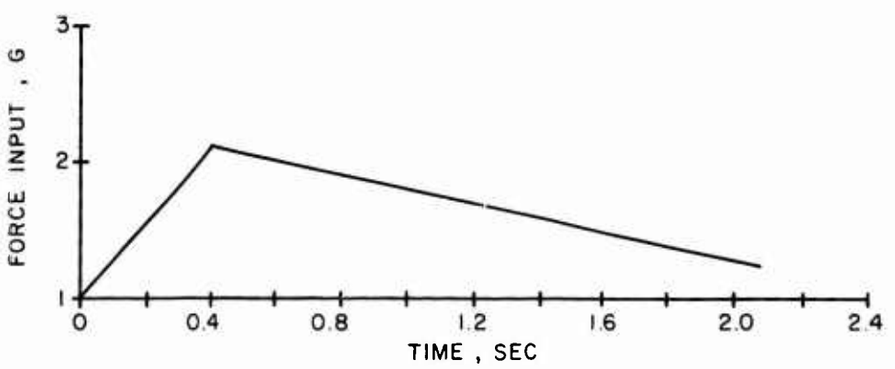

(c) ACTUAL JUMP TAKEOFF

Figure 41. CH-53A Vertical Transient Loads and Response.

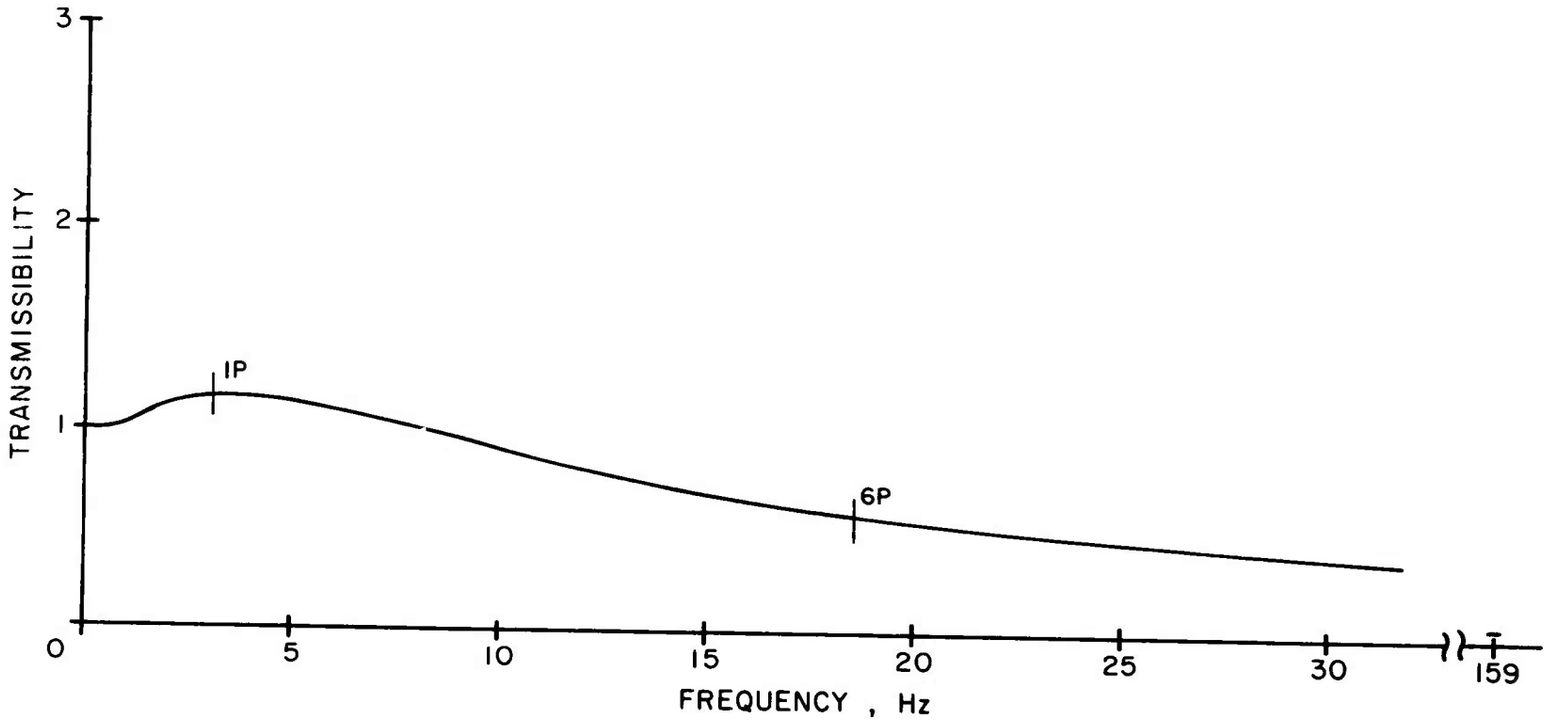

Figure 42. CH-53A Vertical Transmissibility.

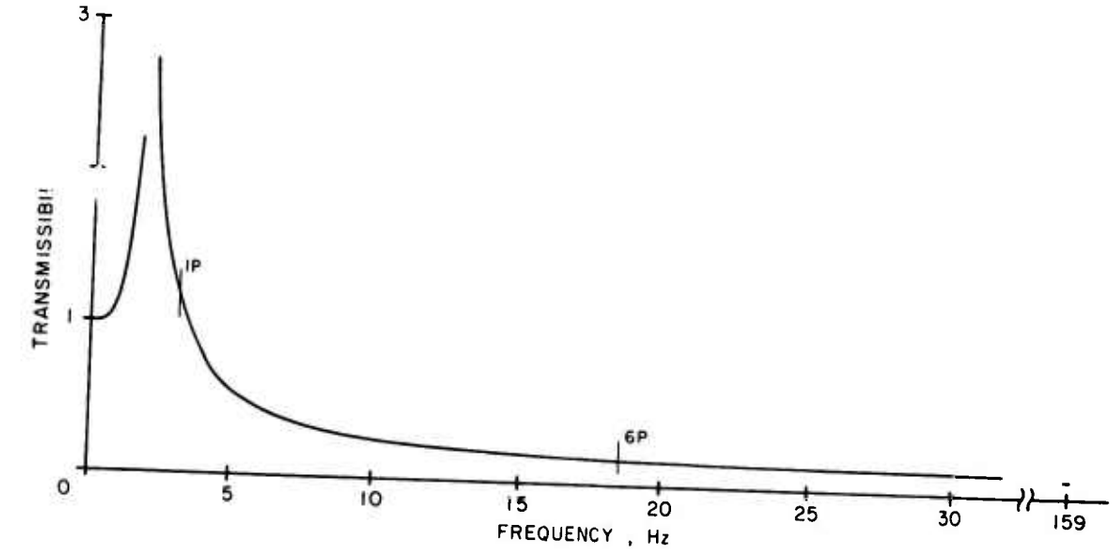

(a) LATERAL

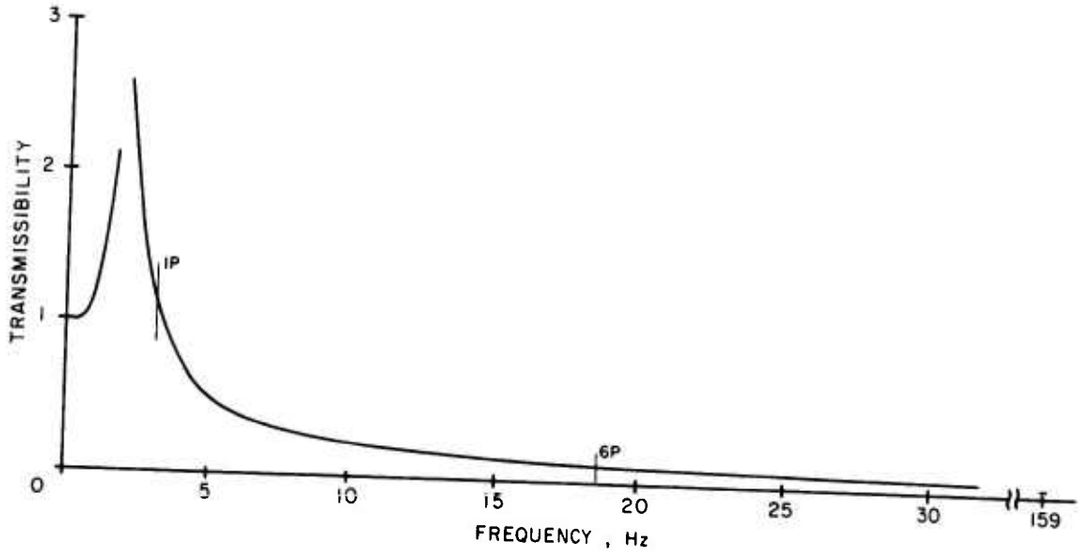

(b) ROLL

Figure 43. CH-53A Lateral and Roll Transmissibility.

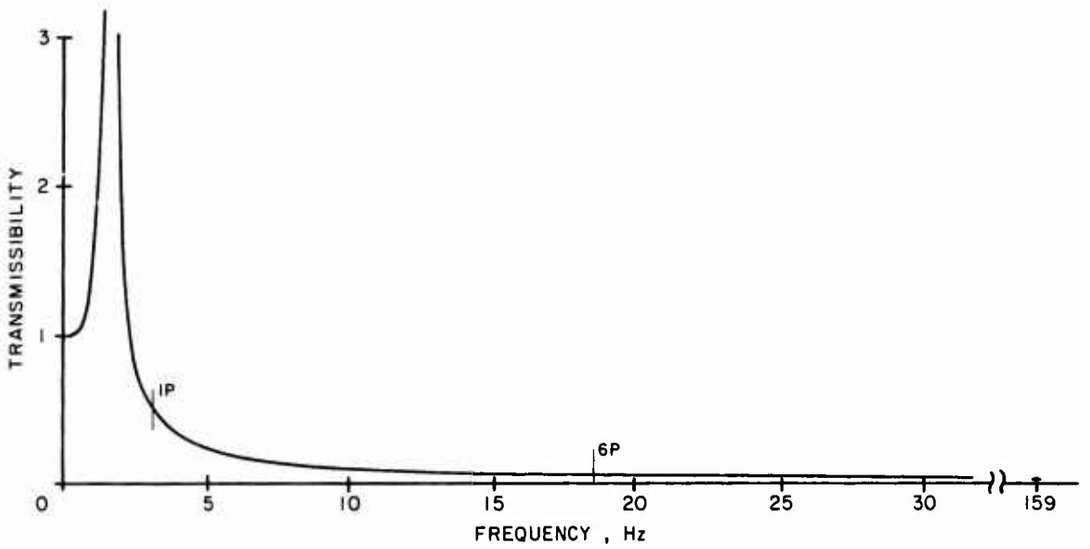

(a) LONGITUDINAL

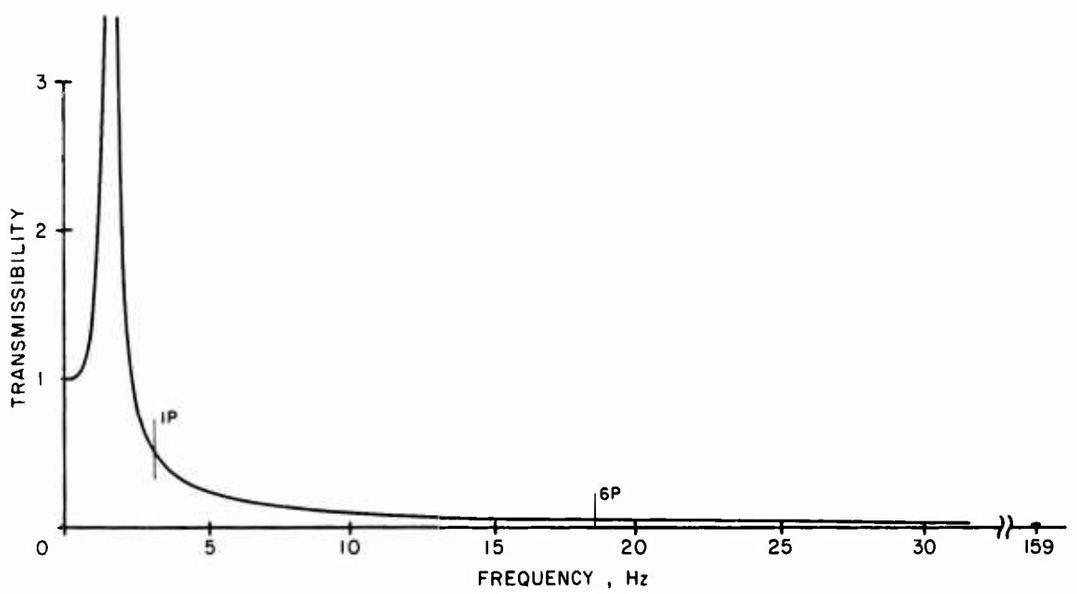

(b) PITCH

Figure 44. CH-53A Longitudinal and Pitch Transmissibilities.

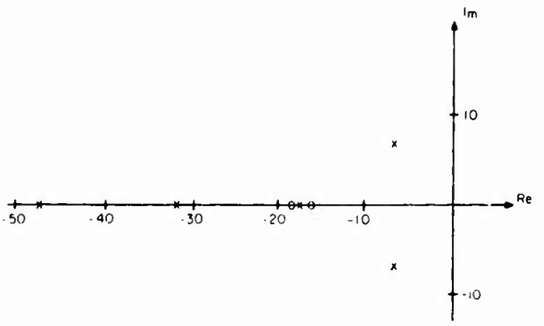

(a) VERTICAL

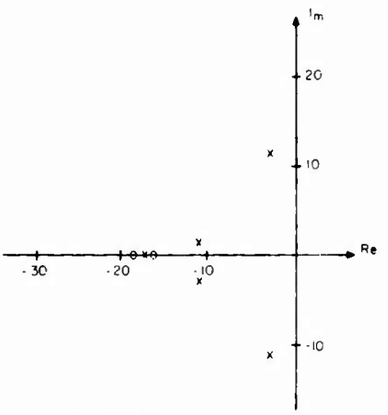

(b) LATERAL

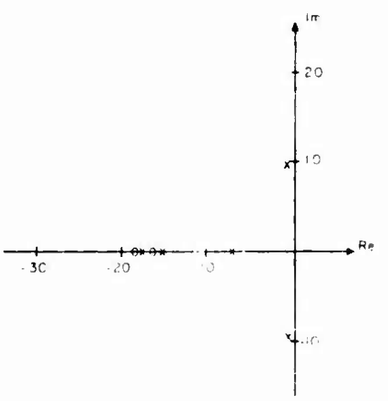

LONGITUDINAL

Figure 45. CH-53A Transfer Function Roots.

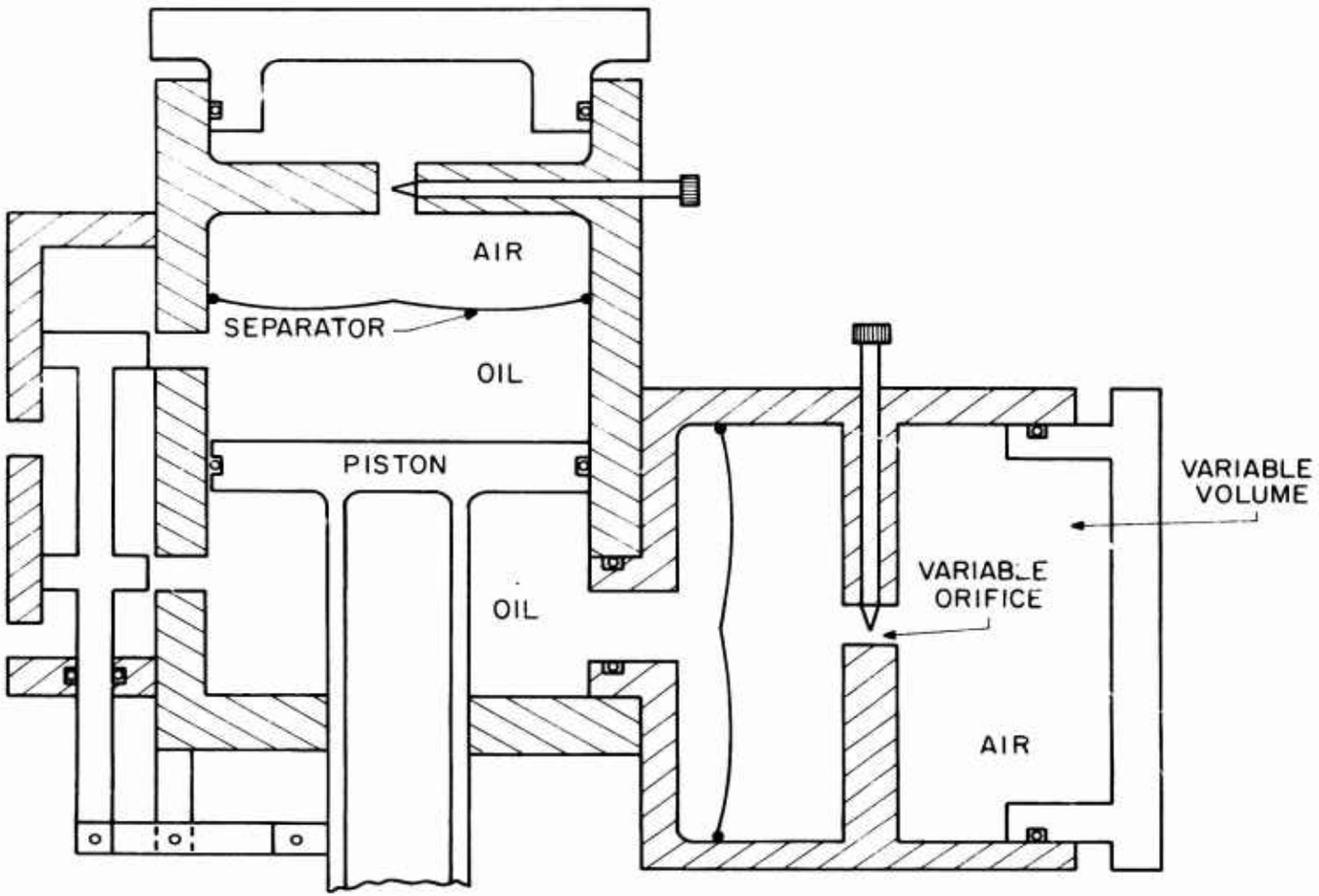

Figure 46. CH-53A Isolator Conceptual Hardware Sketch.

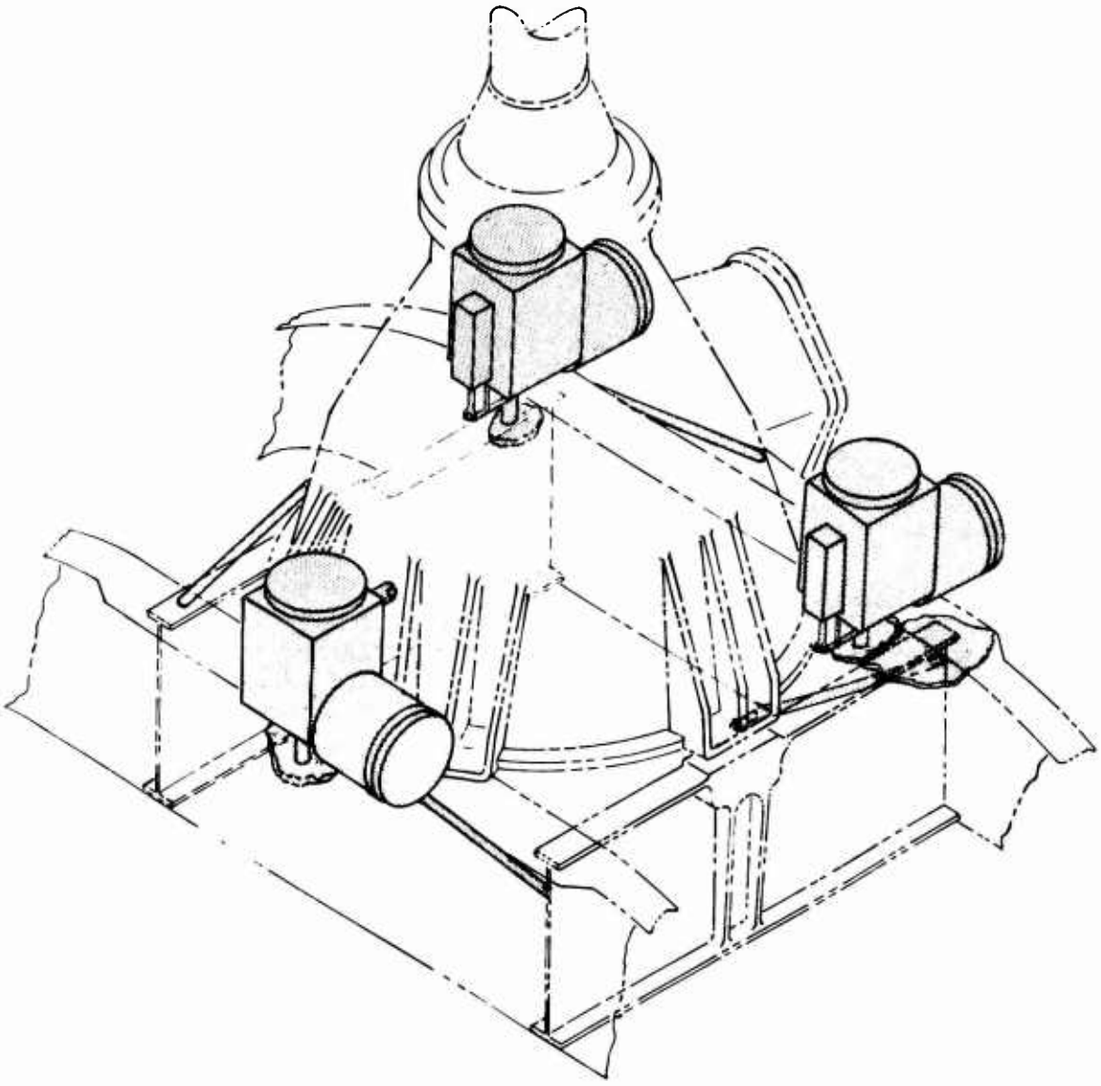

Figure 47. CH-53A Isolator Installation Sketch.

UH-1D Analysis

Table X contains the values of the isolator parameters obtained from the cursory feasibility analysis performed on the 7,000-pound UH-1D together with the geometric and inertia properties used. The isolation system is stable. Plots of the performance data are shown in Figures 47 through 50.

Each of the three isolator elements has an air volume of 265 $in.^3$ and a piston area of 2.8 $in.^2$ The 2p (10 HZ) and 4p (20 Hz) vertical vibratory transmissibilities are 0.45 and 0.24 respectively. The in-plane 2p transmissibilities vary from 0.26 to 0.40. The in-plane 4p transmissibilities vary from 0.12 to 0.28. All transmissibilities decrease asymptotically as the excitation frequency approaches infinity.

Figure 48 shows the time response of the vertical deflection across the isolation system under the prescribed transient load. The analytical deflections shown are conservative with respect to an actual system and have a maximum value of 1.6 inches occurring after 0.3 second. Reduced transient deflections could be obtained by performing further analytical iterations.

The upper body mass of the mathematical model used in the UH-1D analysis contained the engine in addition to the rotor head and transmission.

Heavy-Lift Helicopter Analysis

Table XI contains the values of the isolator parameters obtained from the cursory feasibility analysis performed on the 147,000-pound heavy lift helicopter configuration, together with the geometric and inertia properties used. The isolation system is stable,and plots of the performance data are shown in Figures 52 through 55.

Each of the three isolator elements has an air volume of 2,000 $in.^3$ and a piston area of 71 $in.^2$ The 6p (11 Hz) vertical vibratory transmissibility is 0.8, and the in-plane 6p transmissibilities vary from 0.08 to 0.10. All transmissibilities decrease to low asymptotes for all frequencies above 6p.

Figure 52 shows the time response of the vertical deflection across the isolation system under the prescribed transient load. The analytical deflections shown are conservative with respect to an actual system and have a maximum value of 2.0 inches occurring after 0.6 second.

The rotor excitation frequency, mass, and geometric properties were obtained from Sikorsky Aircraft's proposed heavy-lift-helicopter system as of April 1, 1969. The inertia properties were extrapolated from those presented in Reference 10.

TABLE X. UH-1D ISOLATOR PARAMETERS, GEOMETRIC AND INERTIA PROPERTIES		
Piston Area ($in.^2$)		2.8
Air Volumes ($in.^3$)	Total	265
	V_{cb}	94
	V_{ca}	31
	V_{tb}	106
	V_{ta}	34
Piston and Fluid Damping (lb-sec/in.)	C_v	43
Air Damping ($in.^5$/lb-sec)	B_a	.74
	B_b	.76
Steady Operating Air Pressures (psi)	P_a	293
	P_b	840
Valve Feedback Gains ($in.^2$/sec)	G_a	130
	G_b	130
Masses (lb)	m_1	2,400
	m_2	4,600
Inertias (slug-ft^2)	I_{1x}	130
	I_{1y}	100
	I_{2x}	825
	I_{2y}	6,000
Lengths (in.)	ℓ_1	6.3
	ℓ_2	57.0
	ℓ_3	37.0
Isolator Spacing (in.)	a	10.0
	b	16.5

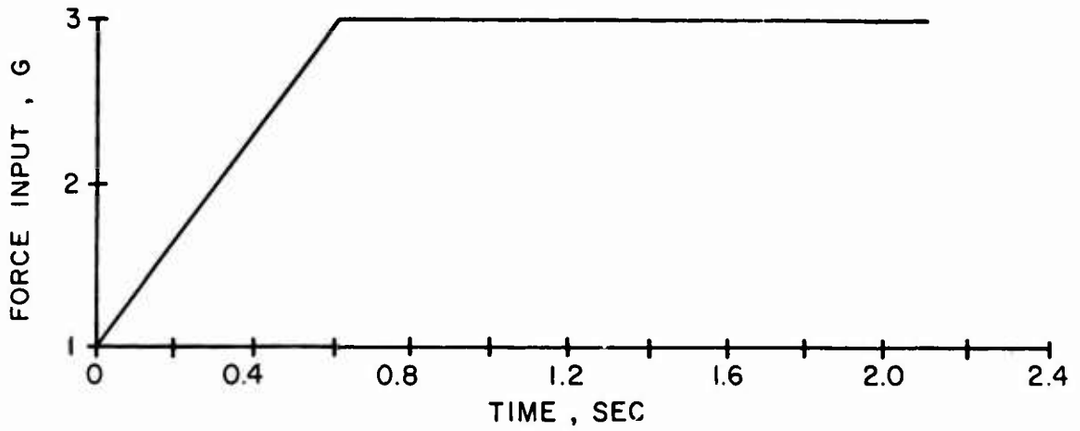

(a) DESIGN LOAD

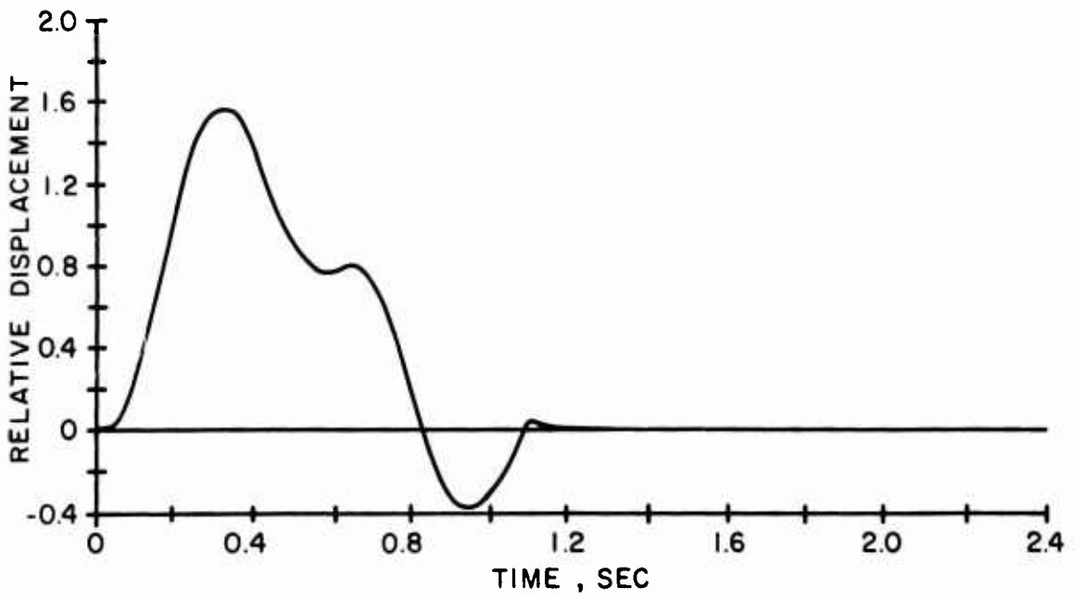

(b) RESPONSE

Figure 48. UH-1D Vertical Transient Load and Response.

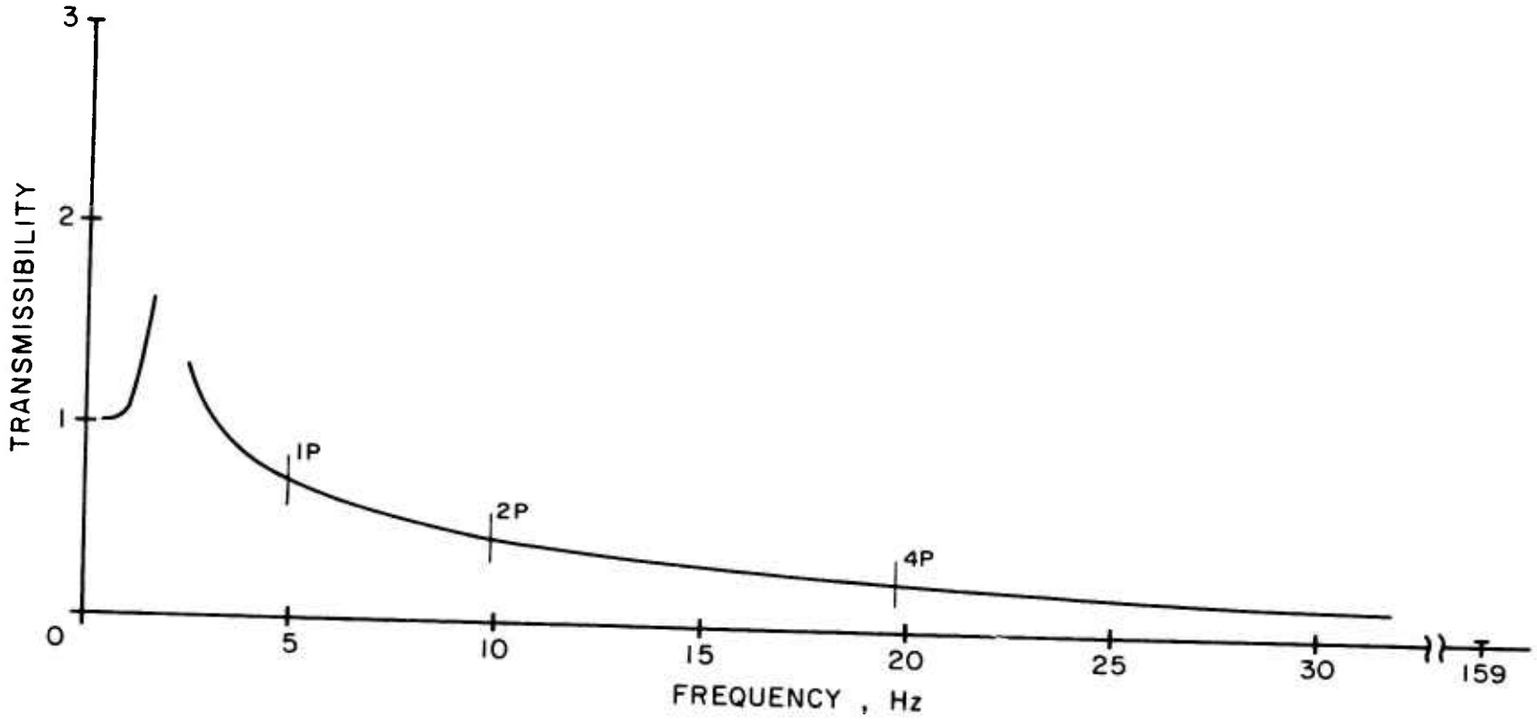

Figure 49. UH-1D Vertical Transmissibility.

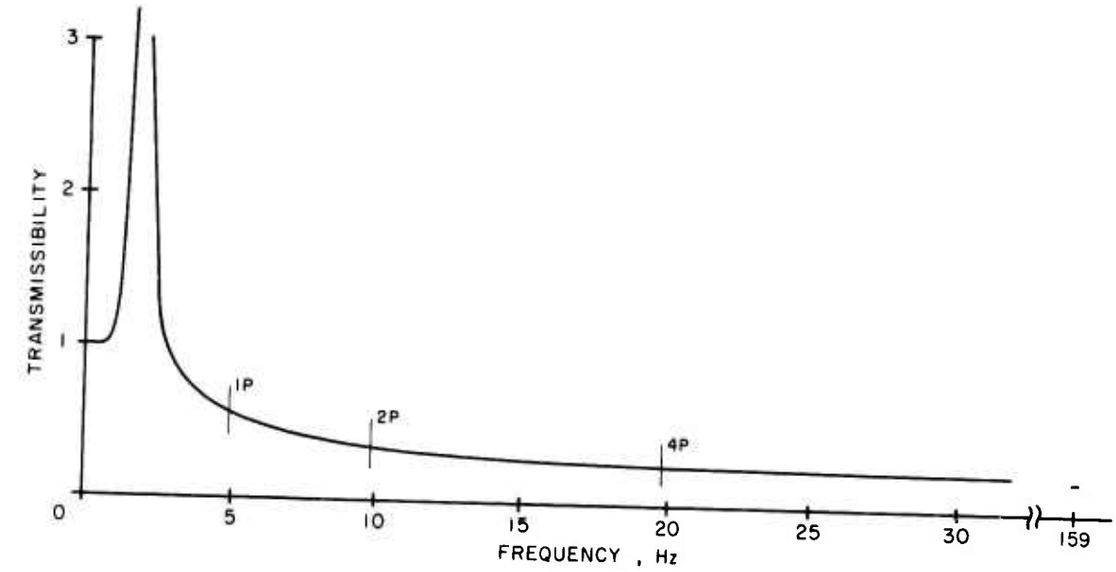

(a) LATERAL

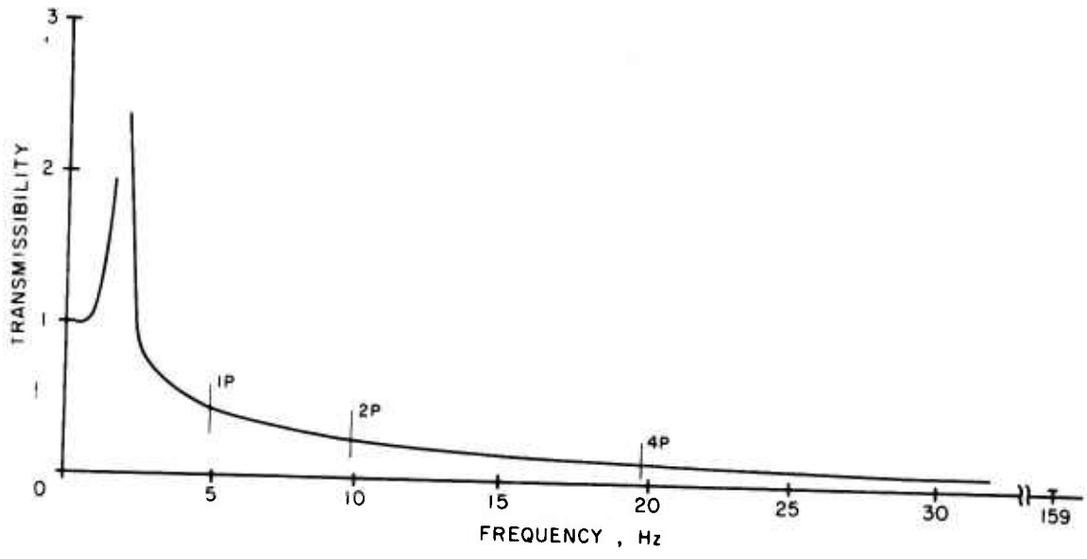

(b) ROLL

Figure 50. UH-1D Lateral and Roll Transmissibilities.

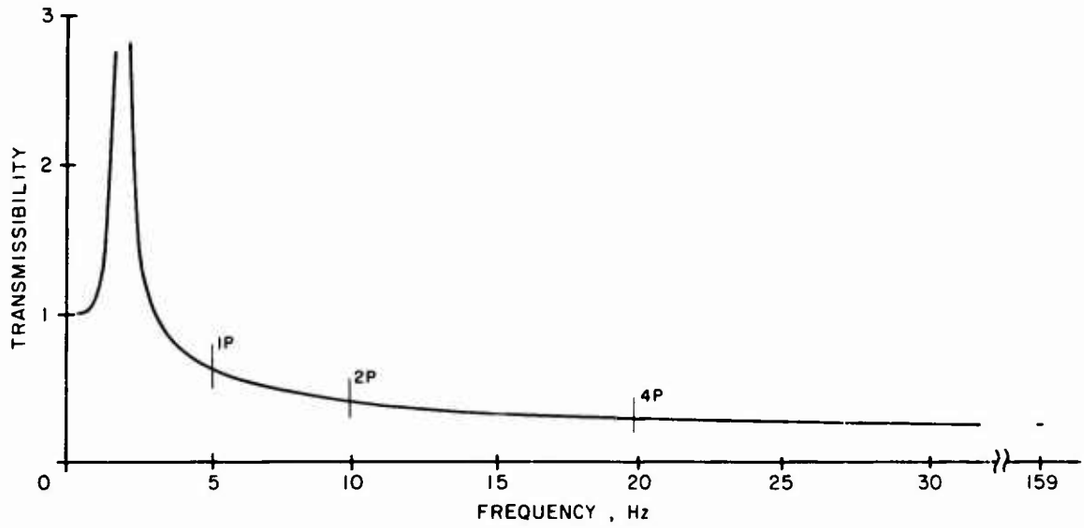

(a) LONGITUDINAL

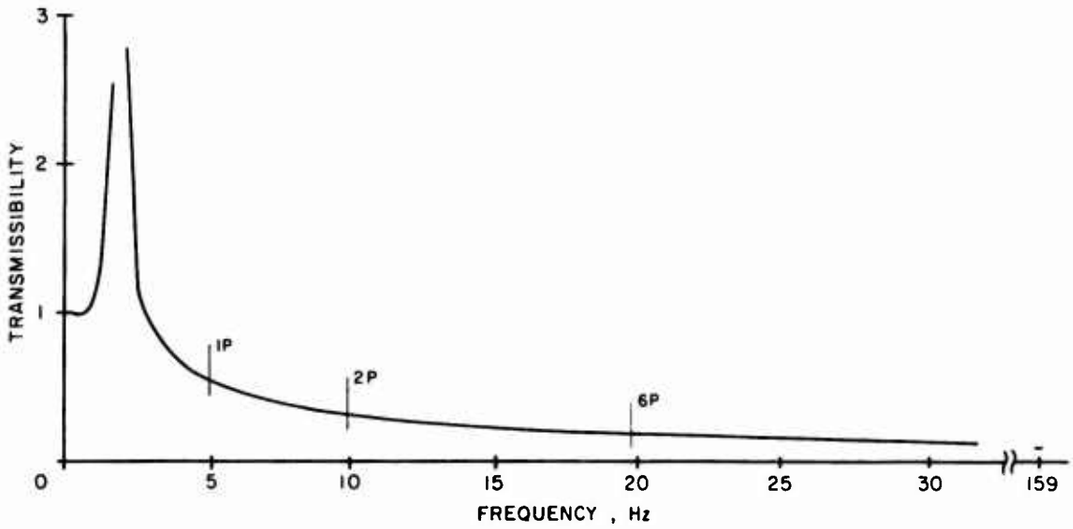

(b) PITCH

Figure 51. UH-1D Longitudinal and Pitch Transmissibilities.

TABLE XI. HLH ISOLATOR PARAMETERS, GEOMETRIC AND INERTIA PROPERTIES

Piston Area ($in.^2$)		71
Air Volumes ($in.^3$)	Total	2000
	V_{cb}	705
	V_{ca}	235
	V_{tb}	795
	V_{ta}	265
Piston and Fluid Damping (lb-sec/in.)	C_v	1318
Air Damping ($in.^5$/lb-sec)	B_a	4.11
	B_b	3.71
Operating Air Pressures (psi)	P_a	204
	P_b	750
Valve Feedback Gains ($in.^2$/sec)	G_a	750
	G_b	750
Masses (lb)	m_1	31,200
	m_2	116,300
Inertias (slug-ft^2)	I_{1x}	17,000
	I_{1y}	23,000
	I_{2x}	480,000
	I_{2y}	2,500,000
Lengths (in.)	ℓ_1	81
	ℓ_2	91
	ℓ_3	35
Isolator Spacing (in.)	a	26.5
	b	30.0

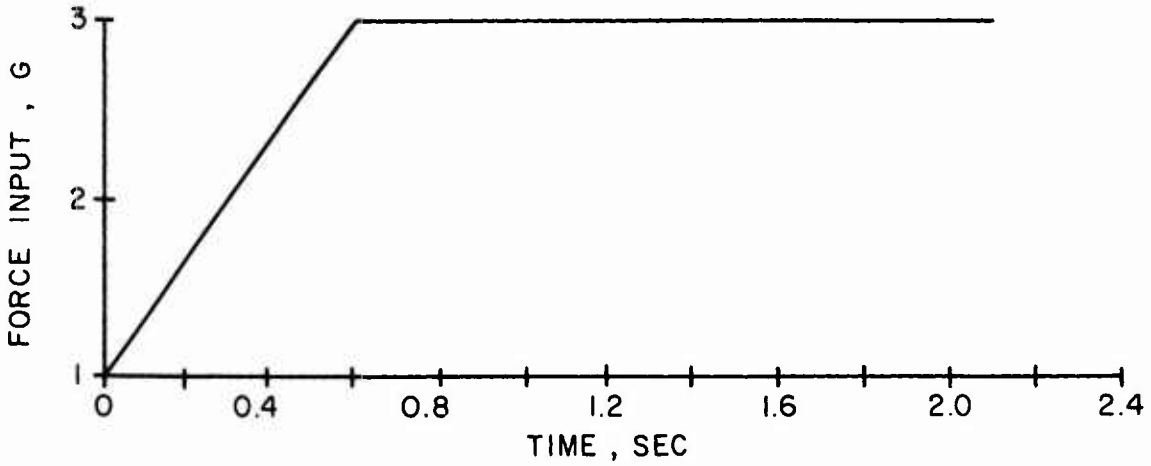

(a) DESIGN LOAD

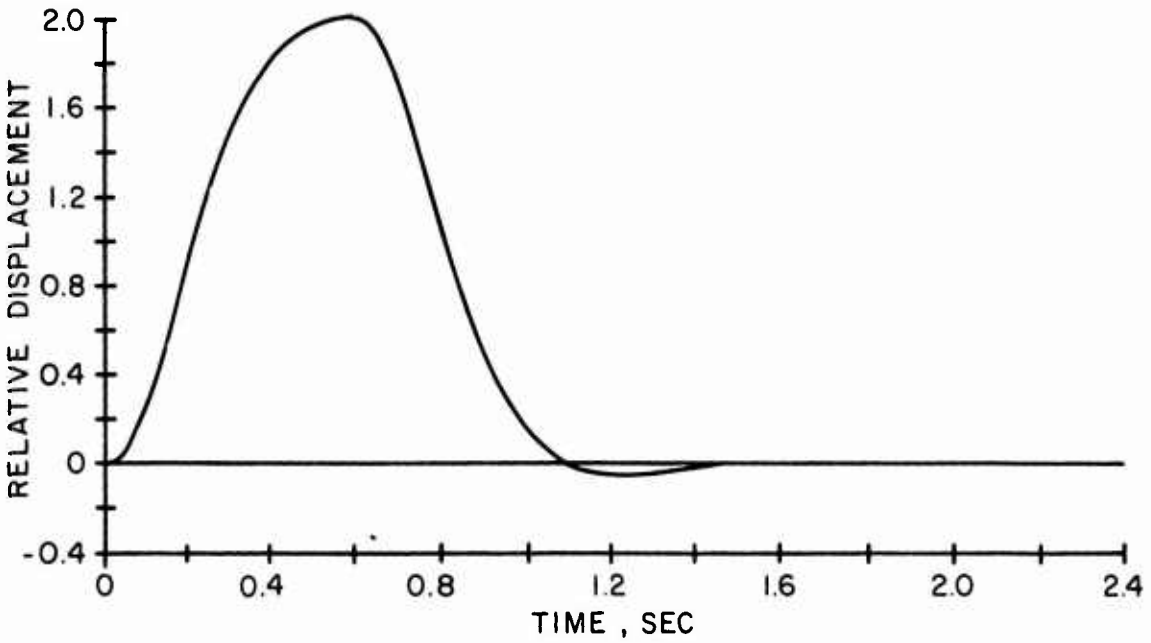

(b) RESPONSE

Figure 52. HLH Vertical Transient Load and Response.

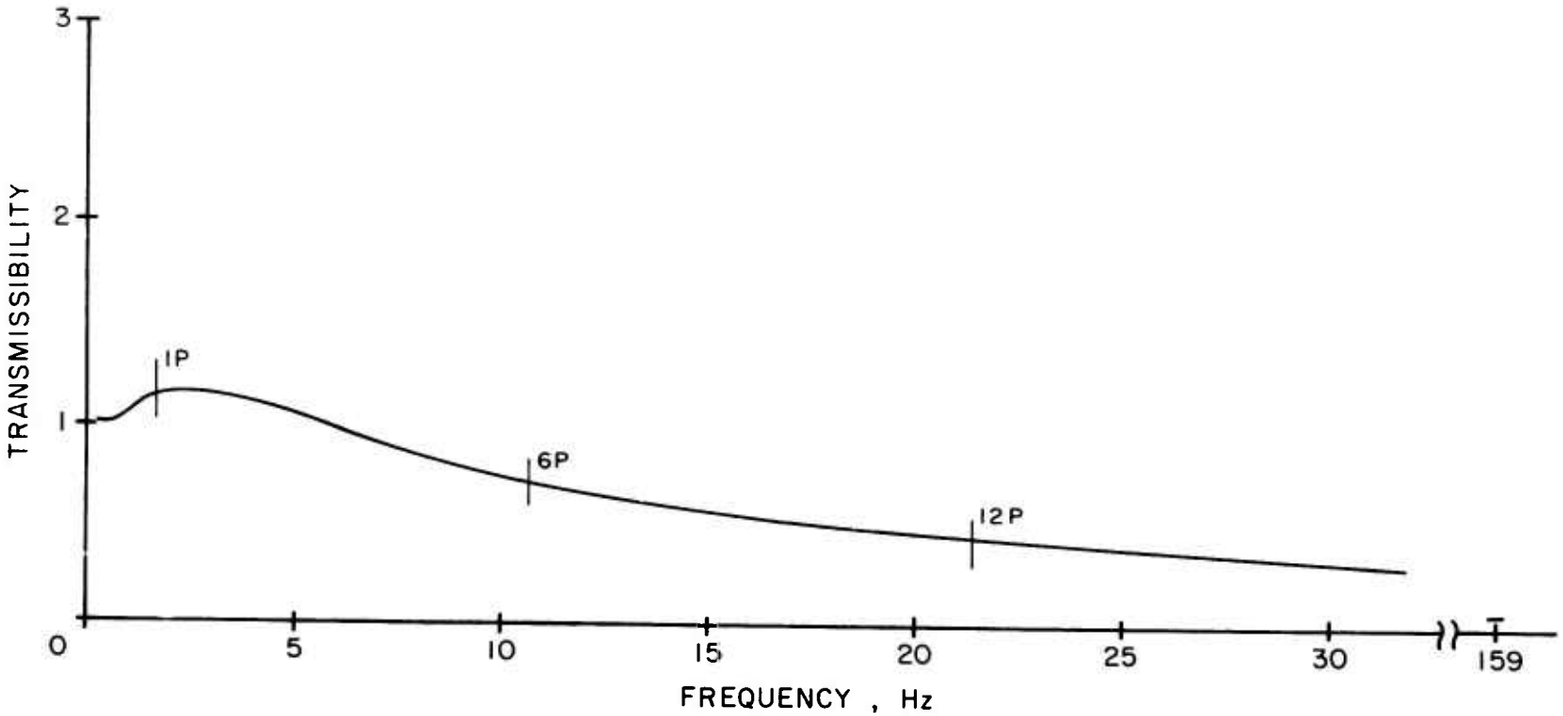

Figure 53. HLH Vertical Transmissibility.

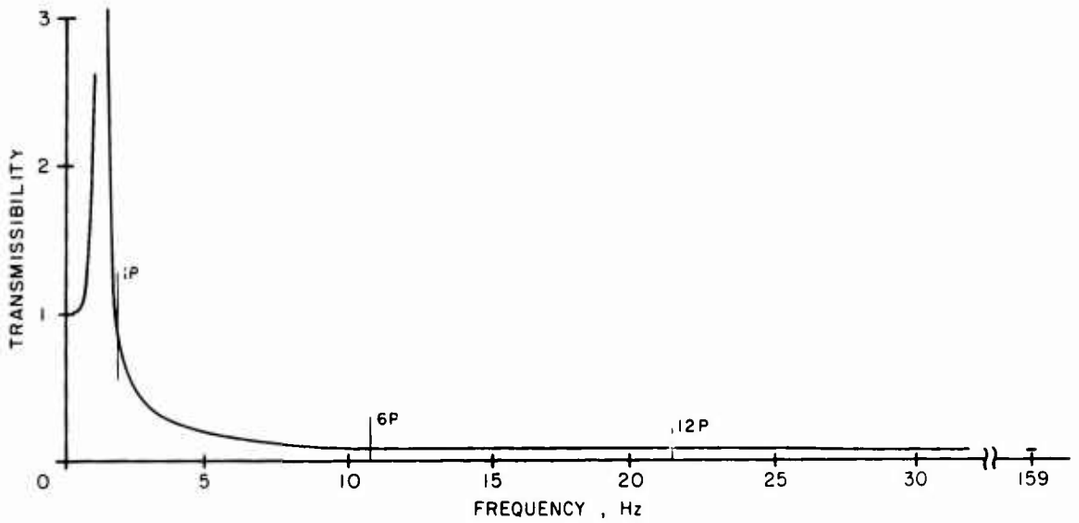

(a) LATERAL

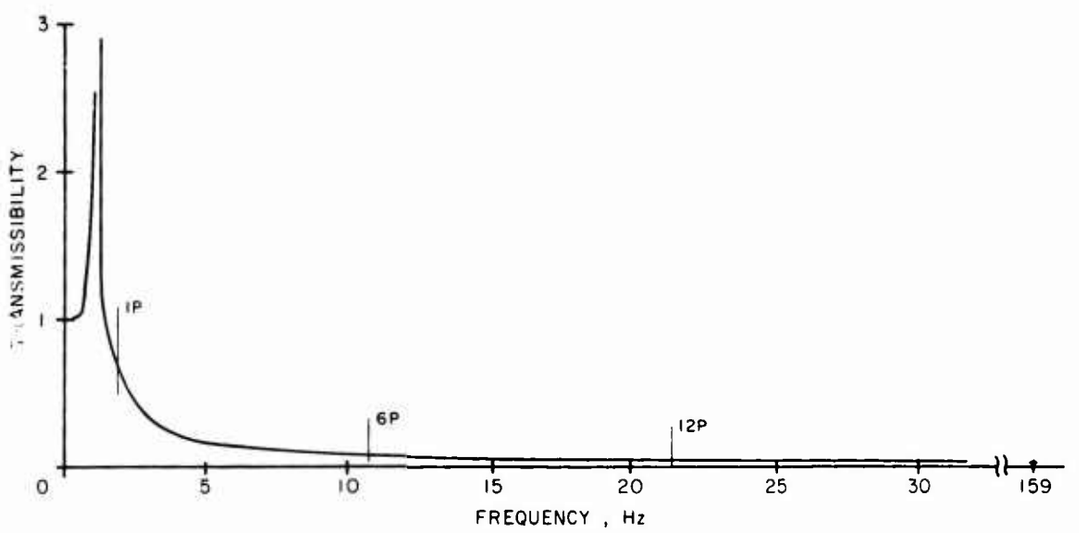

(b) ROLL

Figure 54. HLH Lateral and Roll Transmissibilities.

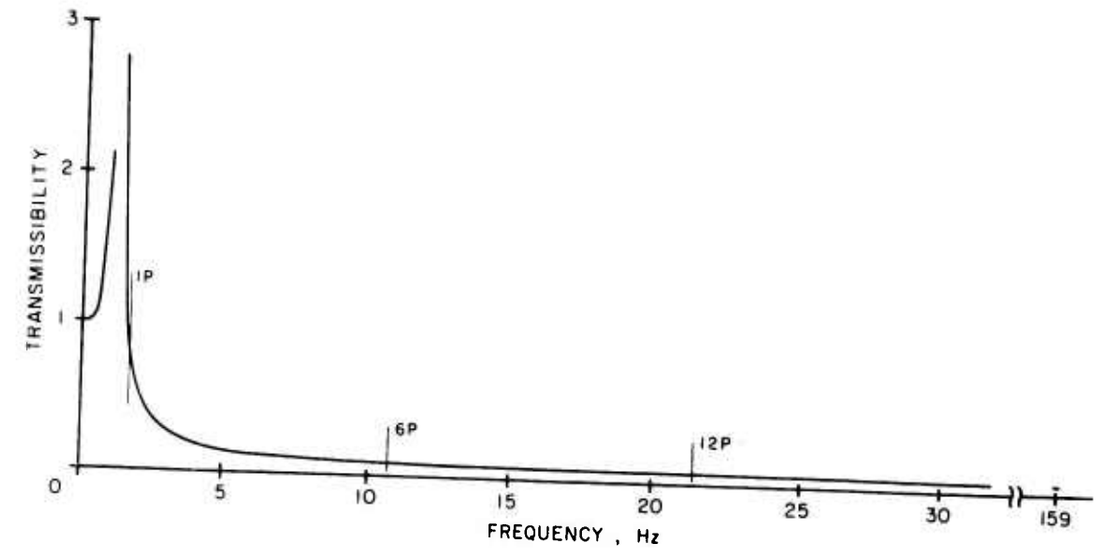

(a) LONGITUDINAL

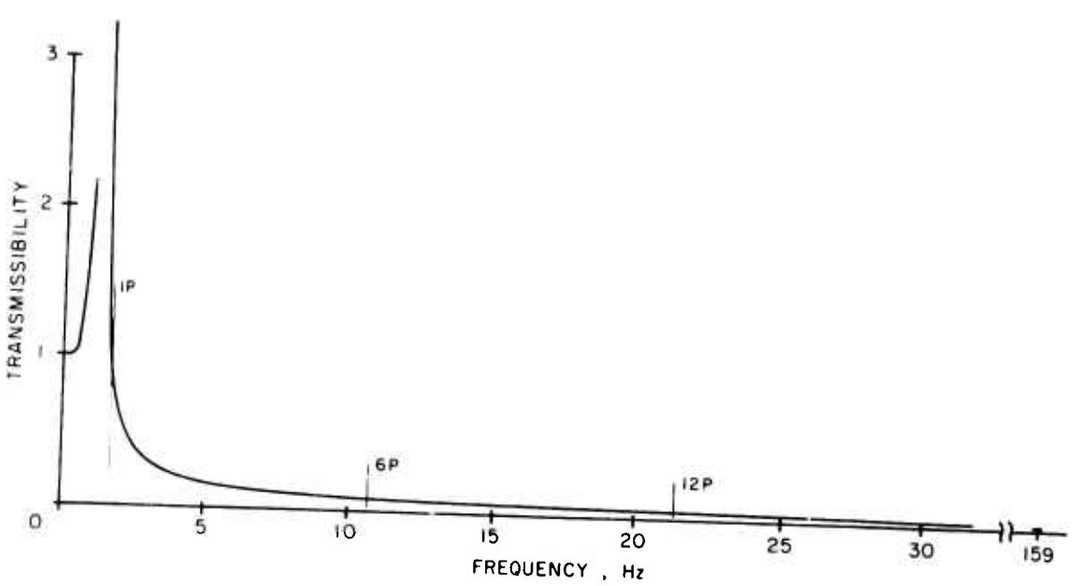

(b) PITCH

ure 55. HLH Longitudinal and Pitch Transmissibilities.